DYSREGULATION OF SIRT1 ACTIVITY IN THE PATHOGENESIS OF HUNTINGTON'S DISEASE

Tulino, Raffaella

Awarding institution:
King's College London

DYSREGULATION OF SIRT1 ACTIVITY IN THE PATHOGENESIS OF HUNTINGTON'S DISEASE

By

Raffaella Tulino

Neurogenetics Laboratory

Department of Medical and Molecular Genetics

Division of Genetics and Molecular Medicine

Guy's, King's and St. Thomas' School of Medicine

Guy's Campus, London

A dissertation presented in partial fulfilment for the degree of doctor of philosophy at

King's College London, University of London

January 2015

Declaration

I declare that I, Raffaella Tulino, performed all the experiment work presented in this thesis with the exception of:

*Sirt1*KO colony breeding, genotyping and subsequent tissue collection which was performed by Miss Agnesska C. Benjamin.

*Sirt1*Tg colony breeding, genotyping and subsequent tissue collection which was performed by Mrs Nelly Jolinon.

Abstract

Huntington's disease (HD) is a fatal neurodegenerative disorder for which there are no therapeutic treatments. Previous studies have suggested that an increase in SIRT1 activity might have a neuroprotective effect in mouse models of HD. SIRT1 is a NAD^+-dependent protein deacetylase and plays an important role in neuronal health during development, differentiation and ageing. However, the mechanisms controlling SIRT1 activity and the effect of HD progression on such processes are currently unknown. In this study we explored the impact of HD on SIRT1 function in different brain regions of the R6/2 (fragment transgenic) and *Hdh*Q150 (knock-in) HD mouse models. We show the existence of a striatum-specific age-dependent regulatory mechanism of SIRT1 activity and a down-regulation of SIRT1 function in the brains of both models. Interestingly, we did not detect a co-localization of SIRT1 with mHTT inclusions and to further support this finding, we did not observe any reduction of SIRT1 protein level in HD brains. In this study, we hypothesize that there is a link between SIRT1 activity and SIRT1 phosphorylation status and provide evidence of altered SIRT1 phosphorylation in the striatum and cerebellum of HD mice. DBC1 is a negative regulator of SIRT1. We found that the ablation of DBC1 did not improve behavioural impairments in R6/2 mice, suggesting that the mutant HTT-related reduction in SIRT1 activity might lie outside the inhibitory circuit controlled by DBC1. Taken together, these data show for the first time that there is a striatum-specific mechanism controlling SIRT1 activity via phosphorylation in an age-dependent manner and that the SIRT1 function is impaired in HD. This work provides insights into the mechanisms that regulate SIRT1 activity in the brain, confirms that SIRT1 plays a key role in both the normal and HD brain and opens new avenues for the development of therapeutic strategies.

Acknowledgements

First and foremost I would like to thank my supervisor Professor Gillian Bates for providing me with the opportunity to pursue this PhD project in your laboratory and all the support and motivation you have given me during the course of this project.

Thank you to my supervisor: Dr. Alisia Carnemolla. Thank you for providing me motivation, inspiration, and guidance throughout my PhD.

I would like to thank my husband, Antonio Masucci, for giving me all his loving support, having faith in me and for always being there when I needed him.

Thank you to my family: Francesco Tulino, Anna Liccardo, Sara Tulino, Antonino De Stefano, Raffaele Masucci, Rita Sorice, Gerardo Masucci e Lorenzo Masucci. You are a great family and I am grateful for all your support.

Thank you to the members of neurogenetics laboratory for helping me when I run into difficulties during my PhD, in particular to Dr. Alisia Carnemolla, Dr. Christian Landles, Dr. Michal Mielcarek, Dr. Kirupa Sathasivam and Miss Agnesska C. Benjamin.

Thank you to Ivan Rattray and Christian Landles for help in proof-reading of this thesis.

I would also like to express my gratitude to the European Commission and CHDI Foundation for providing the financial support without which this work could not have been undertaken.

Contents

List of figures

List of tables

List of abbreviations

aa	amino acid
Ac	acetylated
AD	Alzheimer's disease
ADP	adenosine diphosphate
ALS	amyotrophic lateral sclerosis
AMPK	adenosine monophosphate activated protein kinase
ANOVA	analysis of variance
APP	amyloid precursor protein
ATP	adenosine triphosphate
ATP5B	ATP synthase subunit beta
BAC	bacterial artificial chromosome
BCA	bicinchocinic acid
BDNF	brain-derived neurotrophic factor
BSA	bovine serum albumin
C	carboxy-
C. *elegans*	Caenorhabditis *elegans*
CA150	co-activator 150
CAG	cytosine adenine guanine
cAMP	cyclic adenosine monophosphate
Canx	calnexin
CB	cannabinoid
CBF	CBA/Ca x C57BL/6 F1
CBP	(c-AMP-response-element-binding protein) binding protein
CBP	CREB binding protein

CDK	cyclin dependent kinase
CHOP	C/EBP homologous protein
CNS	central nervous system
CoA	coenzyme A
Co-REST	co-repressor of REST
CREB	cAMP responsive element binding protein
CtBP	C-terminal binding protein
D.melanogaster	*Drosophila melanogaster*
DHCR7	dehyrocholesterol reductase 7
DMSO	di-methyl sulfoxide
DNA	deoxyribonucleic acid
ECL	enhanced chemi-luminescence
ER	endoplasmic reticulum
ERAD	ER activated degradation
FDFT1	farnesyl diphosphate farnesyl transferase 1
FDPS	farnesyl diphosphate synthase
FL	full-length
GABA	gamma-aminobutyric acid
GPe	external segment of the globus pallidus
GPi	internal segment of the globus pallidus
HAP1	huntingtin-associated protein 1
HAT	histone acetyltransferase
HD	Huntington’s disease
HDAC	histone deacetylase
Hdh	Huntington's disease homologue

HEAT	HTT, EF3, PP2a, TOR1
HIP1	huntingtin-interacting protein-1
Hippi	Hip-1 protein interactor
HMGCoA	4-hydroxy-4-methyl-glutaryl Coenzyme A
HMGCR	HMGCoA reductase
HMGCS1	HMGCoA synthase 1
HSF1	heat shock transcription factor 1
HSR	heat shock response
HTT	huntingtin
IDI1	isopentenyl diphsphate delta isomerase1
IF	immunofluorescence
K	lysine
kDa	kiloDalton
KI	Knock-in
KO	Knock-out
MEF	myocyte enhancer factor
mGluR	metabotropic glutamate receptor
mHTT	mutant huntingtin
mRNA	messenger RNA
MSNs	medium sized spiny neurons
N	amino-
NAD	nicotinamide adenine dinucleotide
NAM	nicotinamide
N-CoR	nuclear receptor co-repressor
NES	nuclear exclusion signal

NGF	nerve growth factor
NII	neuronal intranuclear inclusion
NLS	nuclear localisation signal
NMDA	N-methyl-D-aspartate
NMDAR	NMDA receptor
NRSF	neuronal restrictive silencing factor
NuRD	nuclear remodelling deacetylase
P/CAF	p300/CBP associated factor
PBS	phosphate buffered saline
PCR	polymerase chain reaction
PGC1α	PPARγ co-activator 1α
PMFS	phenylmethanesulfonylfluoride
polyQ	polyglutamine
PP2A	protein phosphatase 2 A
PSD-95	postsynaptic density-95
PTM	post-translational modification
Q	glutamine
qPCR	quantitative PCR
REST	repressor element 1 silencing transcription factor
RNA	ribonucleic acid
ROS	reactive oxygen species
RPL13A	ribosomal protein 13a
rpm	revolutions per minute
rRNA	ribosmal RNA
RT	real time

RT	Room Temperature
S	serine
SBMA	spinobulbar muscular atrophy
SCA	spinocerebellar ataxia
SDS-PAGE	SDS polyacrylamide gel electrophoresis
SEM	standard error of the mean
SMRT	silencing mediator for retinoic acid and thyroid hormone receptors
SP1	specificity protein 1
SQLE	squalene epoxidase
SREBP	sterol regulatory element binding protein
STN	subthalamic nucleus
T	threonine
TAFII130	TATA-binding protein (TBP)-associated factor
TBP	TATA box binding protein
TOR1	target of rapamycin 1
TSA	Trichostatin A
UBC	ubiquitin C
UPP	ubiquitin-proteasome pathway
UPS	ubiquitin proteasome system
v	volume
WB	western blot
wk	week
WT	wild-type
YAC	yeast artificial chromosome

Chapter 1 INTRODUCTION

In 1872 George Huntington described a condition that afflicted a group of his patients. He noted that this condition never skipped a generation, causing them to exhibit dance-like writhing motions (Huntington, 1872). More than a century on, despite the huge effort placed in understanding the pathology known now as Huntington's disease (HD), there are no effective treatments and a cure still remains elusive.

1.1 Huntington's Disease

HD is an inherited neurodegenerative disorder characterized by chorea, behavioural manifestations, and dementia (Warby et al., 2011). It is caused by a mutation in the huntingtin gene (*HTT*) and is transmitted in an autosomal dominant manner, thus offspring have a 50% chance of inheriting the disease-causing allele should one of their parents be HD-positive. Adult-onset HD is the most common form of this disorder with onset between 30 and 50 years for most patients and is characterised by a triad of psychiatric, cognitive and motor symptoms. Juvenile HD patients usually have a more rapid disease progression that is characterised by bradykinesia rather than the typical chorea observed in adult onset HD (Bates, Tabrizi and Jones, 2014; Walker, 2007). The only therapeutic options currently available to HD patients do not modify disease progression, but rather are directed against primary symptoms such as chorea or depression. The disease progresses to death 10-20 years after clinical diagnosis.

HD is the result of a mutation in *HTT* which is located within the 4p16.3 locus on the short arm of chromosome 4. The HD chromosome was found to contain an unstable polymorphic trinucleotide repeat. The polymorphic stretch of the CAG repeat resides in the 5' coding region of the gene and encodes an expanded polyglutamine

(polyQ) tract in the 348kD huntingtin protein (HTT) (Huntington's Disease Collaborative Research Group, 1993). In humans, the polyQ tract is encoded by a stretch of CAG codons that is followed by the sequence CAACAG that also encodes glutamine residues. It has been established that it is the length of the CAG repeat that defines whether the allele is considered to be in the normal range. In affected individuals the CAG repeat number expands from the normal population range (6-35 repeats) to greater than 36 repeats. 36–39 repeats result in incomplete penetrance of the disease, with a much later onset and slower progression of symptoms. With very large repeat counts (40 repeats), HD has full penetrance and can occur under the age of 20, when it is then referred to as juvenile (Bates et al., 2014).

Despite the fact that the huntingtin gene and protein are ubiquitously expressed in the human body, the well-described pathology of HD is largely restricted to the brain. Post mortem HD brains are characterized by atrophy of the cerebral cortex and basal ganglia followed by enlargement of the ventricular space as well as a loss of white matter (De la Monte et al., 1988). The cerebral cortex shows a progressive atrophy of grey matter, but it is well known that the region most affected by HD pathology is the striatum (comprising the caudate and putamen) (Fig. 1).

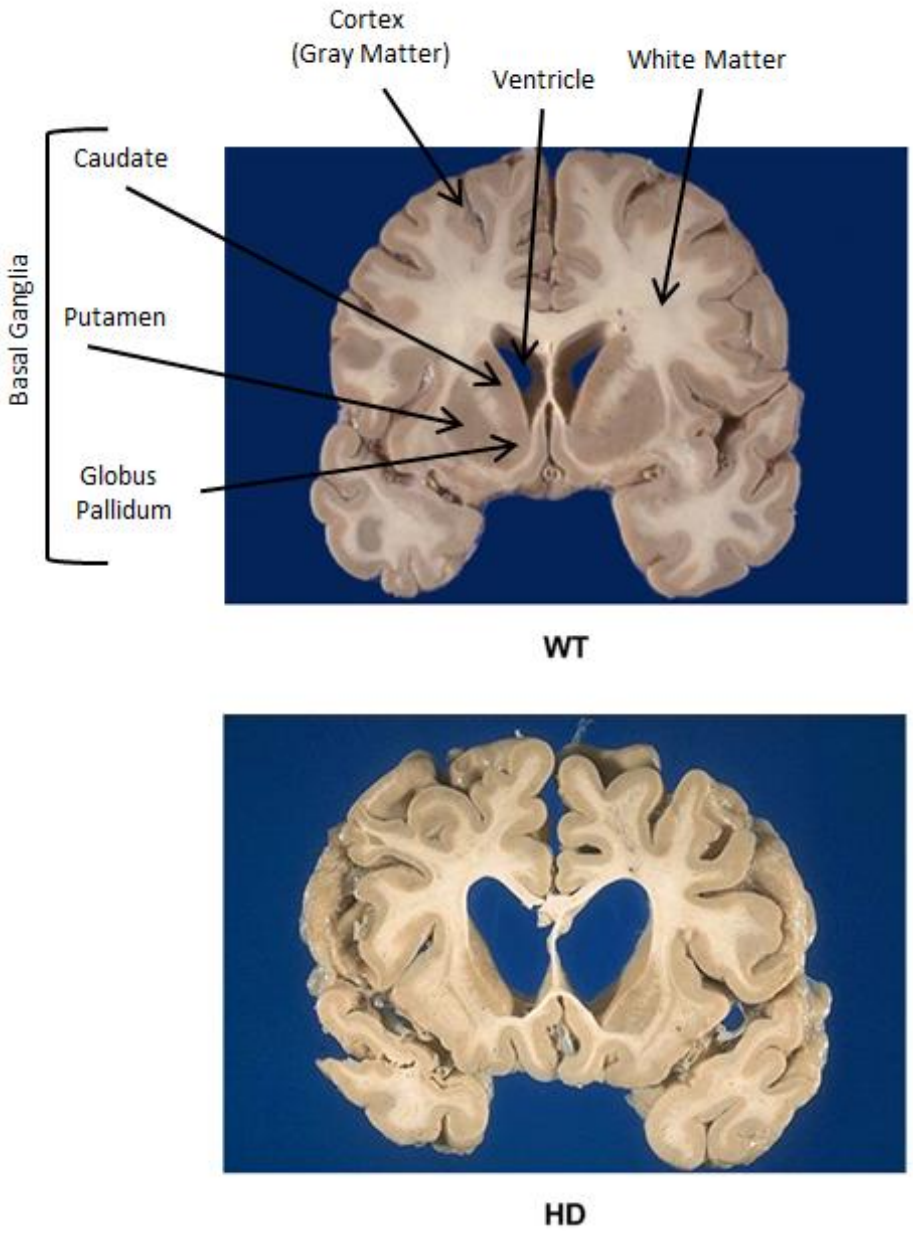

Figure 1. Comparison of coronal sections of brains from an end stage disease HD and unaffected individual. Note the pronounced atrophy of the cortex, caudate and putamen, enlargement of ventricles and white matter loss. Brain images courtesy of Edward C. Klatt.

The striatum is the main input compartment of the basal ganglia (Fig. 2), and comprises a collection of subcortical nuclei involved in the control of movement. The striatum receives glutamatergic and dopaminergic innervations from all regions of the cerebral cortex, as well as specific thalamic nuclei. The flow of information returns to the cortex through the thalamus, the major output structure. Principal motor dysfunctions in HD are due to the degeneration of the medium-sized spiny neurons (MSNs); these projection neurons represent more than 90% of the striatal cell population. Although all MSNs are GABAergic, they differ in a number of properties including the expression of dopamine and acetylcholine receptor subtypes, peptide content and projection targets.

A classical model describes two major neuronal motor pathways, referred to as direct and indirect pathways, which act in opposition, and predict the motor impairment in HD (Albin et al., 1989). GABAergic neurons at the origin of the direct pathway mainly express dopamine D1 and muscarinic M4 receptors, substance P, and project to the globus pallidus internal sigments (GPi). On the other hand, GABAergic neurons of the indirect pathway mainly express dopamine D2 receptors and enkephalin, and project to the globus pallidus external sigments (GPe) (Reiner et al., 1988; Albin et al., 1991; Richfield et al., 1995; Sapp et al., 1995). The first stage of HD is characterized by loss of the projection neurons of the indirect pathway causing an imbalance in favour of the direct pathway. Movements are therefore initiated, but can't be controlled (Albin, 1989). At later stages, the general loss of the MSNs, including those projecting through the direct pathway, induces a drastic motor dysfunction leading to bradykinesia.

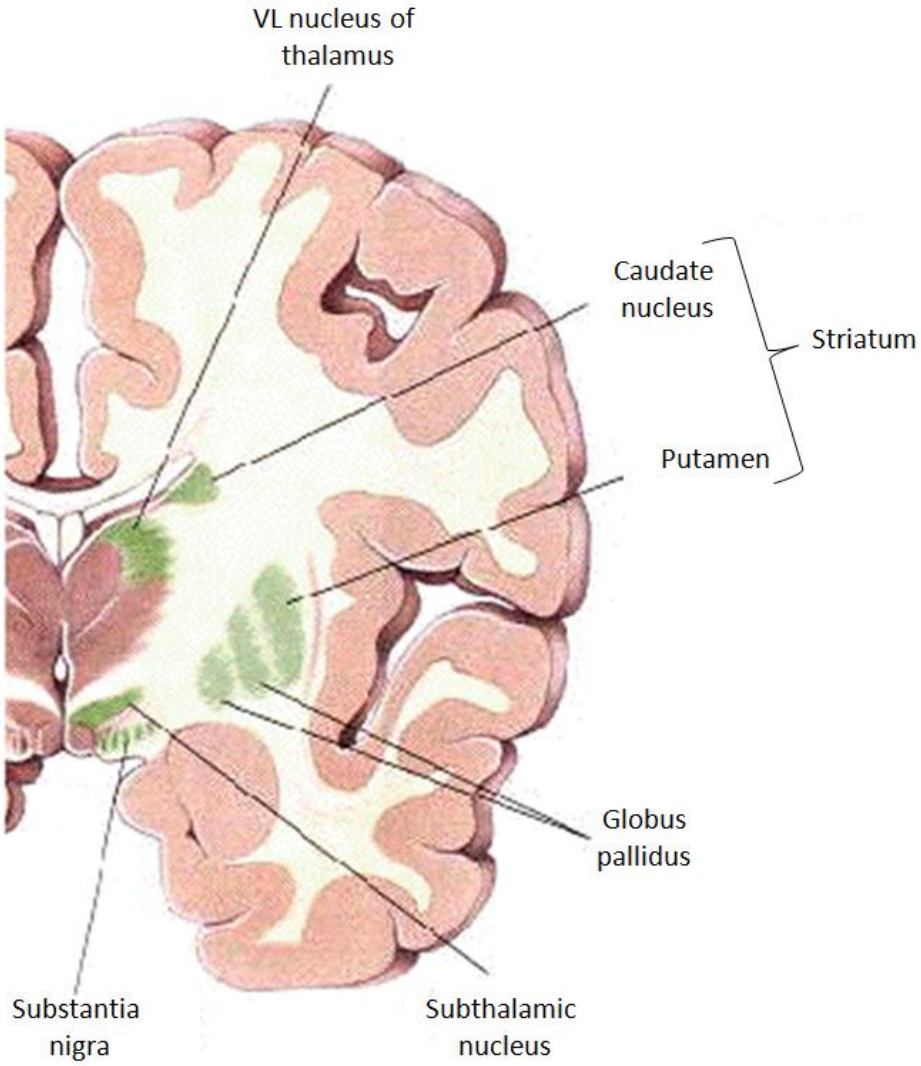

Figure 2. Scheme of a coronal section of human brain, showing the position of the basal ganglia and their different subnuclei. The basal ganglia are composed of four principal nuclei: striatum, the globus pallidus (GP) consisting of external and internal segments (GPi and GPe), the substantia nigra (SN) consisting of pars compacta and reticula (SNc and SNr), and the subthalamic nucleus (STN). Lateral ventricle (VL). (Modified from DERIC'S MINDBLOG).

In the periphery, the two main hallmarks of HD are progressive weight loss and skeletal muscle wasting (Farrer and Meaney, 1985; Saberg et al., 1981). A damaged tolerance to glucose and insulin secretion capacity have been observed in patients, as well as reduced levels of testosterone and reduced numbers of germ cells in men (Bacos et al., 2008; Lalic et al., 2008; Markianos et al., 2005; Van raamsdonk et al., 2007). The main cause of death is respiratory arrest (Lanska et al., 1988).

1.2 HTT protein

The human *HTT* gene (NP_002102) is translated into a 348 kDa protein. The polyQ region, encoded by the CAG stretch, is immediately downstream from amino acid 17 of HTT and upstream of a polyproline (polyP) rich region. The polyP region stabilizes the polyQ tract and maintains its solubility (Steffan et al., 2004). HTT also contains 36 Huntingtin (HTT), Elongation factor 3 (EF3), subunit A of protein phosphatase 2A (PP2A), Target of Rampamicyn 1 (TOR1) (HEAT) repeats which may promote interactions with other proteins and facilitate complex assembly and cellular transport (Takano and Gusella, 2002). HEAT repeats have been found predominantly in proteins involved in intracellular trafficking and chromosomal segregation but their specific function is still unclear. HTT is expressed ubiquitously in humans with the highest levels in brain and testis. In the brain the cerebellar cortex, neocortex, striatum and hippocampus have the highest levels of HTT (Schmitt et al., 1995). In most cells HTT is essentially a cytoplasmic protein associated with various organelles including mitochondria, the endoplasmic reticulum and Golgi complex (Di Figlia et al., 1995; Trottier et al., 1995).

1.3 Function of the HTT protein

The complete function of the HTT protein has also yet to be fully appreciated. HTT is an essential protein involved in early embryonic development (Duyao et al., 1995; Nasir et al., 1995; Zeitlin et al., 1995). The deletion of both *Htt* alleles in mice results in embryonic lethality but mice with one functional copy of *Htt* develop normally. The homozygous Knock-out embryos terminate before E8.5 with signs of abnormal gastrulation prior to organogenesis and somite formation (Duyao et al., 1995; Nasir et al., 1995; Zeitlin et al., 1995). Several studies showed that the loss of *Htt* expression results in embryonic lethality because its absence leads to an impairment of the nutritive functions of the visceral endoderm due to the localization of HTT to the membranes of vesicles associated with microtubules (Dagastis et al., 1998). This lethal phenotype can be rescued by the introduction of embryonic stem cells expressing wild-type *Htt* to support the development and survival of neurons in the mutant embryo (Dragatsis et al., 1998; Reiner et al., 2003). Beyond embryonic development, it has been shown that HTT is involved in the regulation of gene expression, vesicle traffiking and cell survival Zuccato et al., 2003; Gauthier et al., 2004; Dragastis et al., 2000).

1.3.1 HTT regulates brain-derived neurotrophic factor expression

The ability of HTT to regulate gene expression was discovered for the first time through analysing the effect of mutant HTT protein (mHTT) expression on neurotrophin production. HD pathology involves the selective degeneration of striatal neurons, which, in turn, require brain-derived neurotrophic factor (BDNF) for survival and differentiation (Mizuno et al., 1994; Ventimiglia et al., 1995; Ivkovic and Ehrlich, 1999). The major regions of BDNF synthesis are the hippocampus and cortex; the

striatum has no BDNF mRNA and depends, mostly, upon the cortex for the delivery of this trophic factor (Altar et al., 1997; Conner et al., 1997). In neuronal cell lines, and the brains of transgenic HD mice and HD patients, in addition to a dramatic reduction of BDNF mRNA and protein levels, BDNF cortico-striatal anterograde transport has also been shown to be altered (Zuccato et al., 2001; Spires et al., 2004a; Pang et al., 2006). Reduced transcription of BDNF is attributed to a loss of wild-type HTT function. To achieve BDNF transcription, HTT indirectly interacts with the repressor element-1 transcription factor/neuron restrictive silencer factor complex (REST/NEST) and prevents it from entering in the nucleus and binding to the BDNF promoter thereby repressing transcription (Zuccato et al., 2003). mHTT is not able to restrict the REST/NEST complex to its perinuclear localization and thus, transcription of BDNF is repressed (Zuccato et al., 2001). Reduced BDNF cortico-striatal anterograde transport has been attributed to the modulation of HTT-HAP1 (huntingtin-associated protein 1) binding by the polyQ expansion in mHTT, which reduces the efficiency of Kinesin-1 dependent transport of BDNF containing-vesicles (Gauthier et al., 2004). HTT selectively regulates BDNF expression, indeed, expression of other neurotrophins such as nerve growth factor (NGF) and neurotrophin-3 (NT-3) is unaltered in HD. The negative effects of mHTT on BDNF transcription are also restricted to neurons since mHTT protein does not affect BDNF production in non-neuronal cells such as fibroblasts.

It is unlikely that reduced BDNF levels are the only contributing factor to the degeneration that occurs in HD brain and peripheral tissues. Other factors such as a wide-spread transcriptional dysregulation, disrupted protein homeostasis and defects in metabolism are all also likely to contribute to the pathogenesis.

1.3.2 HTT is involved in vesicular trafficking

Several studies suggest a role of HTT in vesicular trafficking. HTT facilitates the dynein/dynactin-mediated transport of vesicles along microtubules and controls cytoskeletal integrity (Diprospero et al., 2004; Gauthier et al., 2004; Caviston et al., 2007; Johnson et al., 2007a; Smith et al., 2007). There is evidence to suggest that HTT promotes the post-Golgi trafficking of various proteins to the plasma membrane through an association with acidic phospholipids (Kegel et al., 2005; Strehlow et al., 2007). The HTT protein has been demonstrated to specifically enhance the transport of BDNF-containing vesicles along microtubules via its interaction with HAP-1 and the p150(Glued) subunit of dynactin which is an essential component of molecular motors (Gauthier et al., 2004). The dynamic protein-protein interaction acts as a molecular switch for antero- as well as reterograde transport in neurons (Colin et al., 2008) and contributes to the anterograde transport of BDNF from the cortex to the striatum.

1.3.3 HTT is involved in anti-apoptotic pathways

HTT promotes cell survival by modulating the signals that trigger programmed cell death (apoptosis). HD patients and mouse models possess impaired mitochondrial function (Panov et al., 2002; Gines et al., 2003). Both wild-type and mutant HTT are associated with the mitochondrial outer membrane (Choo et al., 2004). The calcium threshold required to induce mitochondrial permeability transition pore opening can be reduced in the presence of mHTT fragments; this causes a release of cytochrome c and activation of apoptotic pathways, including the activation of caspases (Choo et al, 2004), calpain (Bizat et al., 2003), and p53 (Bae et al, 2005). Apoptosis is triggered by caspase (cysteine-protease) activity and HTT interacts with caspase-3 (Zhang et al., 2006). Initiation of caspase-3 activity through tumour-necrosis factor receptor (TNFR)

signalling ultimately results in cell death and HTT interacts with activated caspase-3 to inhibit this down-stream pro-apoptotic signal. The presence of wild-type HTT is essential for regulating caspase-3 mediated signalling as HTT depletion leads to overt cell death or increased vulnerability to cell death. Furthermore, the expression of expanded polyQ proteins in PC12 cells and in the fibroblasts of HD patients leads to the production of reactive oxygen species (ROS) and thus to the activation of the DNA damage response (Giuliano, 2003).

1.4 Molecular pathogenesis of HD

A complete picture of the normal activities of HTT has not yet been determined. This is essentially because the protein is a very large, making isolation and analysis difficult. Moreover, HTT is found ubiquitously in different tissues, interacting with hundreds of partners (Harjes and Wanker, 2003; Li and Li, 2004; Borrell-Pages et al., 2006a; Kaltenbach et al., 2007).

As a consequence of HTT interactions with proteins of diverse biological roles, HTT has been implicated in many processes including transcriptional regulation, RNA splicing, signal transduction, intracellular trafficking, cytoskeletal organization as well as protein folding and turnover (Li and Li, 2004). It is, therefore, not surprising that many pathways, cycles, cascades or mechanisms appear to be affected by the presence of mHTT (Fig. 3).

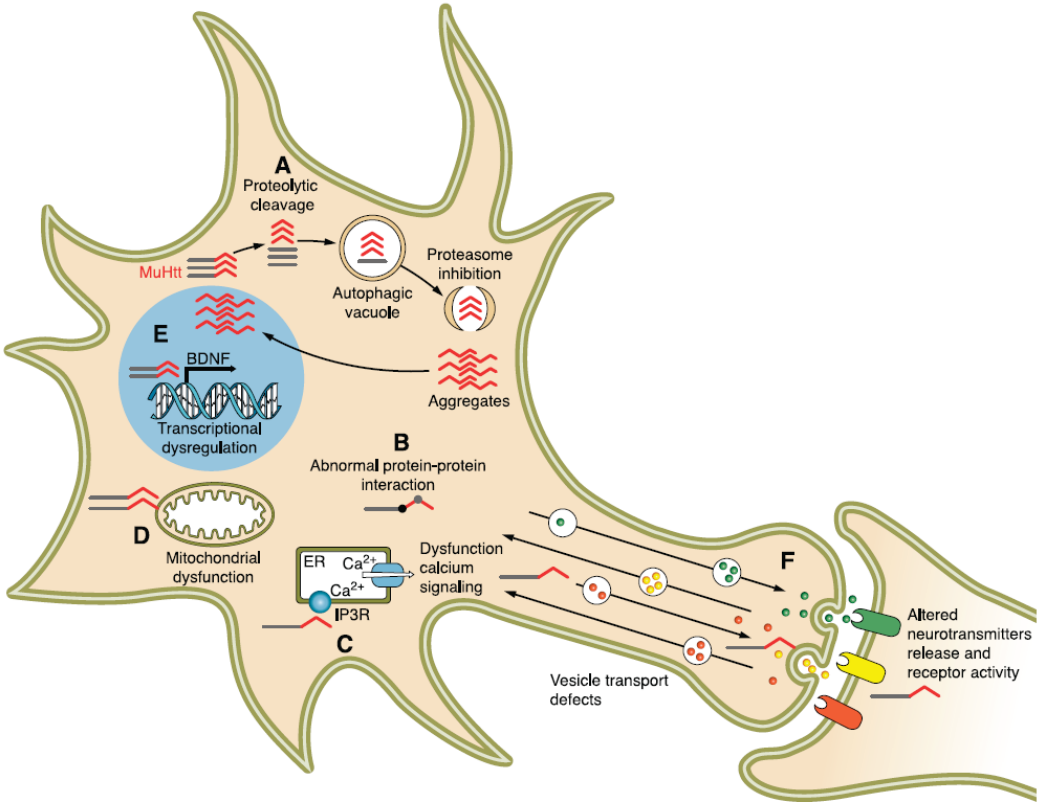

Figure 3. Description of main events contributing to HD pathogenesis.
mHTT is proteolytically cleaved in the cytoplasm (A). Chaperones attempt to re-fold or target mHTT for proteaosomal or autophagic degradation, however, the system is inefficient and mHTT aggregates in the cytoplasm and nucleus. (B) PolyQ expansion leads to mHTT and N-terminal fragments abnormally interacting with proteins and organelle membranes, causing defects in Ca^{2+} signalling (C) and mitochondrial dysfunction (D). (E) N-terminal mHTT fragments translocate to the nucleus where they impair transcription and form intranuclear inclusions. (F) mHTT also causes defects in vesicle transport, recycling and neuronal signalling. Image reproduced from (Zuccato et al., 2010).

1.4.1 Loss of function and gain of function of the HTT protein

The hypothesis that a loss of normal HTT function may play a role in HD pathology followed the finding that HTT is an indispensable protein with antiapoptotic functions (Rigamonti et al., 2000). Indeed, it has been shown that the overexpression of wild-type HTT can have a neuroprotective role in striatal cells exposed to various apoptotic stimuli (Rigamonti et al., 2001). Moreover, the postnatal inactivation of HTT in mouse neurons resulted in a progressive degenerative neuronal phenotype, further supporting the role of HTT in the survival of adult neurons (Dragatsis et al., 2000). Previous studies showed that HTT has an antiapoptotic function through interacting and inhibiting molecules such as Huntingtin Interacting Protein 1 (HIP1) that, once dissociated from HTT activates caspase 8 (Gervais et al., 2002). The protection of wild-type HTT may also occur by activation of BDNF transcription through the interaction with REST and by the stimulation of the vesicular BDNF transport along microtubules (Zuccato et al., 2001; Zuccato et al., 2003; Gauthier et al., 2004).

The events and mechanisms that lead to HD pathological signs have also been attributed to a toxic gain-of-function conferred to mHTT through the expanded polyQ tract, supported by various data. mHTT has been found to rescue the embryonic lethality of knock-out in *Htt* in the mouse, indicating that the HD mutation does not impair normal embryonic HTT functions (Duyao et al., 1995; Nasir et al., 1995). The toxic gain of function scenario is further supported by the fact that similar symptoms and molecular abnormalities are also displayed by patients and models of other polyQ expansion disorders, summarized in Table 1. Although the polyQ expansion occurs in functionally and structurally different proteins, these all share the common strong propensity for aggregation. It has been proposed that elongated polyQ tracts promote

the formation of expanded beta sheet conformations in proteins, these then form parallel alignments of beta-sheet structures which drive proteins aggregation (Perutz et al., 1994).

Disease	MIM number	Gene product	Normal repeat length	Expanded repeat length	Main clinical features
HD	143100	Huntingtin	6–34	36–121	Chorea, dystonia, cognitive deficits, psychiatric problems
SCA1	164400	Ataxin1	6–44	39–82	Ataxia, slurred speech, spasticity, cognitive impairments
SCA2	183090	Ataxin2	15–24	32–200	Ataxia, polyneuropathy, decreased reflexes, infantile variant with retinopathy
SCA3	109150	Ataxin3	13–36	61–84	Ataxia, parkinsonism, spasticity
SCA6	183086	$CACNA1_A$	4–19	10–33	Ataxia, dysarthria, nystagmus, tremors
SCA7	164500	Ataxin7	4–35	37–306	Ataxia, blindness, cardiac failure in infantile form
SCA17	607136	TBP	25–42	47–63	Ataxia, cognitive decline, seizures, and psychiatric problems
SBMA	313200	Androgen receptor	9–36	38–62	Motor weakness, swallowing, gynecomastia, decreased fertility
DRPLA	125370	Atrophin	7-34	49-88	Ataxia, seizures, choreoathetosis, dementia

Table.1: Polyglutamine disorders. HD: Huntington's disease is caused by expansion of a translated CAG repeat located in the N-terminus of HTT; SCAs (1, 2, 3, 6, 7 and 17): Spinocerebellar ataxias are caused by expansion of a translated CAG repeat. Ataxin-1, 2, 3, and 7 are the proteins implicated in SCA1, 2, 3, and 7, respectively, whereas the α1A subunit of the voltage-dependent calcium channel (CACNA1A), the TATA-binding protein (TBP) are implicated in SCA6 and SCA17, respectively; SBMA: Spinal and bulbar muscular atrophy is caused by expansion of a CAG repeat in the first exon of the androgen receptor gene; DRPLA: Dentatorubral-pallidoluysian atrophy is by the expansion of polyQ repeats within the atrophin-1 protein.

1.4.2 Post-translational modifications of HTT

As described previously, HTT is a large protein characterized by several post-translational modification sites which affect its localization, longevity and/or toxicity. For example, there are three lysine (K) residues at the amino(N)-terminus (K6, K9 and K15) that can be either ubiquinated (promoting HTT degradation) or sumoylated (resulting in HTT nuclear localisation) (Steffan et al., 2004). Phosphorylation of HTT occurs at one threonine (T3) and several serine (S13, S16, S421, S434, S536, S1181, S1201, S2076, S2653 and S2657) residues and its outcome can have varying effects depending on the residue in question; this ranges from protection via modulating proteolytic cleavage (S421, S434, S536) (Luo et al., 2005; Schilling et al., 2006; Warby et al., 2009) through to proteosomal targeting (S13 and S16) (Thomson et al., 2009), and modulation of vesicle transport (S421) (Zala et al., 2008).

Acetylation sites have been identified at K9, K178, K236, K345 and K444 (Cong et al., 2011), and it has been demonstrated that the acetylation at K444 promotes the targeting of HTT for degradation by autophagy (Jeong et al., 2009). HTT is also palmitoylated at cysteine 214, which is in line with its proposed role in vesicle trafficking (Yanai at al., 2006).

1.4.3 Proteolytic cleavage and protein aggregation

mHTT is very sensitive to the proteolytic cleavages that generate small toxic N-terminal fragments. It has been proposed that full length HTT is proteolytically processed into smaller toxic N-terminal fragment by caspases, calpains, and matrix metalloproteinases, which can then translocate to the nucleus to exert a toxic effect (Benn et al., 2005; Landles et al., 2010; Miller et al., 2010). The cleavage of HTT into fragments containing the polyQ stretch, and their subsequent translocation to the

nucleus, is likely to be a key step in disease progression (Saudou et al., 1998). Such fragments have a strong propensity to aggregate in the cell, producing different oligomeric species and insoluble aggregates capable of capturing and inactivating proteins essential for normal cell function. Recent data have shown that CAG repeat length–dependent aberrant splicing of exon 1 HTT results in a short polyadenylated mRNA that is translated into an exon 1 HTT protein (Sathasivam et al., 2013).

N-terminal HTT fragments have been identified in neuronal intranuclear inclusions (NIIs) of HD *postmortem* brains (Fig. 4) (DiFiglia et al., 1997). Previous studies suggest that not all the N-terminal fragments resulting from proteolysis are toxic. For example, mice expressing mHTT, resistant to cleavage by caspase 6, but not caspase 3, are characterized by a normal neuronal function and do not develop striatal neurodegeneration (Graham et al., 2006). Indeed, while mHTT cleavage and the formation of inclusions occur both in transgenic animals and in HD patients (Sieradzan et al., 1999), their contribution to HD pathology is still debated.

An association between mHTT aggregates and neuronal dysfunction has been demonstrated. Indeed, the accumulation of large aggregates has been proven to sequester vital cellular proteins, including transcription factors and protein quality control components, supporting for their toxic role in HD pathogenesis (Hay et al., 2004; Jiang et al., 2003; Morton and Edwardson, 2001; Steffan et al., 2000). Interestingly, however, studies have demonstrated that when motor symptoms were ameliorated in R6/2 mice, a concomitant reduction of aggregate load was observed (Mielcarek et al., 2014; Labbadia et al., 2011; 2012). In addition, it has been shown, when proteolysis is prevented by inhibition of caspase or calpain activity or by

modifying the consensus cleavage site in HTT, mHTT toxicity is reduced and disease progression is slowed (Gafni et al., 2004; Luo et al., 2005; Graham et al., 2006).

Neuronal Intranuclear Inclusions (NIIs) are a pathological hallmark of both HD and various other polyQ disorders. It is well known that these structures are dynamic and that the pathway from soluble HTT to inclusion bodies formation is a multi-step process whereby many different species are formed before the mature inclusion. In contrast, some studies have suggested that inclusion formation alone is not sufficient to cause cortical or striatal pathology in mice (Gu et al., 2005; 2007). Work in cell culture models has shown that the formation of large nuclear inclusions correlated with survival and that cell death was best predicted by the presence of smaller oligomeric species (Arrasate at al., 2004; Miller et al., 2011). These results have led some to suggest that the detergent-soluble oligomeric species could be more reactive and toxic than large, insoluble inclusions. In this scenario, cells could be promoting the assembly of small toxic oligomers into large, inert inclusions thereby minimising their deleterious effects.

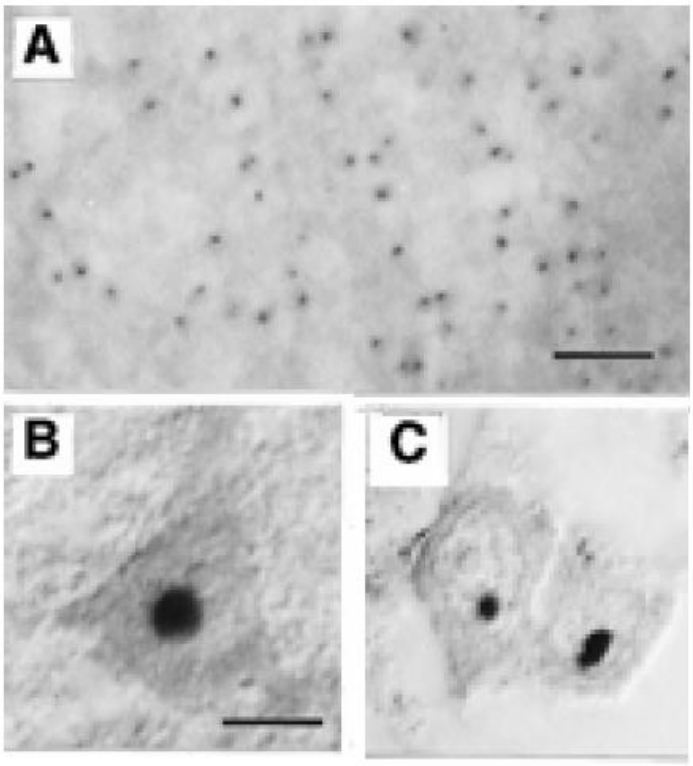

Figure 4. Huntingtin immunoreactivity in HD post-mortem brain. (A) Cortex of a juvenile patient shows numerous inclusions prominently stained. (B) Cortical neurons containing one inclusion. (C) Striatal neurons with inclusions. Reproduced from (Di Figlia et al., 1997)

1.4.4 Protein quality control: HSR, UPS, Autophagy and ER stress in HD

It has been showed that a polyQ expansion induces mHTT to undergo a conformational change that causes it to misfold. Recent data have shown that the Heat shock response (HSR) is inefficient in its ability to degrade the misfolded mHTT. Indeed, a study conducted in our laboratory demonstrated that the HSR is impaired in R6/2 and *Hdh*Q150 mice (Labbadia et al., 2011). Interestingly, the same study showed that pharmacological stimulation of the HSR only transiently improved behavioural phenotype, due to an impairment of the HSR with disease progression.

If mHTT cannot be properly refolded it should be eliminated by the ubiquitin-proteasome system (UPS). Indeed, ubiquitin has been found to be associated with mHTT (Davies et al., 1999), suggesting that the UPS attempts to target mHTT for degradation but fails to execute the final steps (Gutekunst et al., 1999).Whether the impairment of the UPS is, in part, responsible for the HD pathology, remains contentious but HD post mortem brain samples show decreased proteasome activity and this has been confirmed with patient fibroblast and other cell culture models (Bence et al., 2001; Bennett et al., 2005; Seo et al., 2004).

A number of studies have shown that autophagy plays a central role in degradation of unfolded proteins (Ravikumar et al., 2002; Rubinsztein et al., 2006; Settembre et al., 2008). Autophagy is a degradation process aimed at the clearance of long-lived proteins, protein complexes and organelles. There is evidence to suggest that the autophagy process is abnormal in HD brain as well as in cellular and animal models (Larsen et al., 2002; Kegel et al., 2000; Petersen et al., 2001). Furthermore, inhibition of the autophagy process causes a neurodegenerative phenotype in mice, and induction

of autophagy, by treatment with the mTOR inhibitor (rapamycin), reduced aggregation and attenuated toxicity in cells and mouse models of HD (Ravikumar et al., 2004).

Evidence is beginning to emerge to indicate that the clearance pathways responsible for eliminating aggregates are closely regulated by the ER through the UPR (Unfolded Protein Response) stress sensors, such as IRE1α and PERK/eIF2α (Kouroku et al., 2007). Studies aimed at understanding the function of wild-type HTT demonstrated that inhibition of its expression significantly alters the ER morphogenesis (Hilditch-Maguire et al., 2000; Omi et al., 2005). In addition, mHTT perturbs ER calcium homeostasis (Rockabrand et al., 2007). Thus, increasing evidence suggests that mHTT may exert its neurotoxic effect through directly inducing ER stress. Indeed, the accumulation of mHTT inclusions has been shown to trigger activation of the UPR *in vitro* (Kouroku et al., 2007; Reijonen et al., 2008) and subsequently the autophagic clearance of such aggregates (Kouroku et al., 2007; Hoyer-Hansen et al., 2007, Hoyer-Hansen et al., 2007b). Cytoplasmic aggregates stimulate the ER stress signal and induce ER-stress-mediated cell death with caspase-12 activation in mouse cells, presumably by the accumulation of unfolded protein in the ER given the inhibition of retrotranslocation and ER-associated ubiquitin/proteasome degradation (ERAD) (Kouroku et al., 2002). Despite this evidence, the actual involvement of ER-stress in the disease remains elusive.

1.4.5 Transcriptional dysregulation

Transcriptional dysregulation has emerged as a pathogenic mechanism in HD. The majority of transcription factors, interacting with HTT, associate with the N-terminal region of the protein and these interactions are in some cases altered by the polyQ expansion (Steffan et al., 2000; Dunah et al., 2002). So far, the transcription factors found to interact with HTT include Specificity protein 1 (Sp1), CREB-binding protein (CBP), p53, mSin3A, nuclear receptor corepressor (NCoR), C-terminal binding protein (CtBP), CA150, p300/CBP associated factors (P/CAF), TATA-binding protein (TBP)-associated factor (TAFII130), NF-Y and REST/NRSF.

The CRE pathway controls the expression of neuronal genes and neuronal survival. Deletion of CREB causes selective neurodegeneration in the hippocampus and striatum inducing HD-like neurological phenotypes (Mantamadiotis et al., 2002). Soluble mHTT interacts with both the glutamine-rich activation domain and the acetyltransferase domain of the co-activator CBP altering its function (Steffan et al., 2001). The Sp1/TAFII130 pathway is also altered by soluble mHTT in a polyQ-dependent manner, leading to transcriptional downregulation of the nerve growth factor and dopamine D2 receptors (Dunah et al., 2002; Li et al., 2002). mHTT binds p53 and induces its stabilization and transcriptional activity toward proapoptotic genes such as Bax and Puma (Bae et al., 2005). Moreover, the abnormal interaction between mHTT and repressors or activators within the nucleus, (such as N-CoR (Boutell et al., 1999), CtBP (Kegel et al., 2002), the activator CA150 (Holbert et al., 2001)), causes the dysregulation of transcription. Furthermore, within the nucleus, mHTT fragments form aggregates which sequester transcription factors, as in the case of CBP and NF-Y (Nucifora et al., 2001; Yamanaka et al., 2008).

Transcriptional dysregulation also derives from the atypical behaviour of mHTT in the cytoplasm of the cells, as occurs for the REST/NRSF complex which shows reduced binding to mHTT as compared to the wild type. Wild-type HTT, but not the mutant form, promotes BDNF transcription by sequestering REST/NRSF in the cytoplasm thereby preventing it from forming the nuclear co-repressor complex on the neuron restrictive silencer element (NRSE) nuclear site and allowing gene transcription (Zuccato et al., 2003).

Consistent with transcriptional repression playing a role in the pathogenesis of HD, decreased acetylation and increased methylation of histones have been found in both experimental HD models and patients (Steffan et al., 2001; Ferrante et al., 2003; Ryu et al., 2006). The HD protein binds the acetyl transferase domain of different transcription factors such as CBP and p300/CBP Associated Factor (P/CAF), affecting the acetylation of histones (Steffan et al., 2001). An increase in the levels of histone methyl transferases, such as ESET, have been reported to affect chromatin structure and, ultimately, gene transcription in HD patients and mouse models (Ryu et al., 2006).

1.4.6 Excitotoxicity and Synaptic dysfunction

Excitotoxicity was the first identified pathogenic mechanism to be proposed for HD that results in the dysfunction of neuronal interactions and circuitries at the corticostriatal synapse. It has been hypothesized that the excessive activation of glutamate receptors may be due to increased glutamate release from cortical afferents and a reduced uptake of glutamate by glia. Moreover, the hypersensitivity of postsynaptic glutamate receptors on striatal projection neurons, likely in combination with pathological signalling downstream of the glutamate receptor, may also contribute to pathogenesis (Fig. 5).

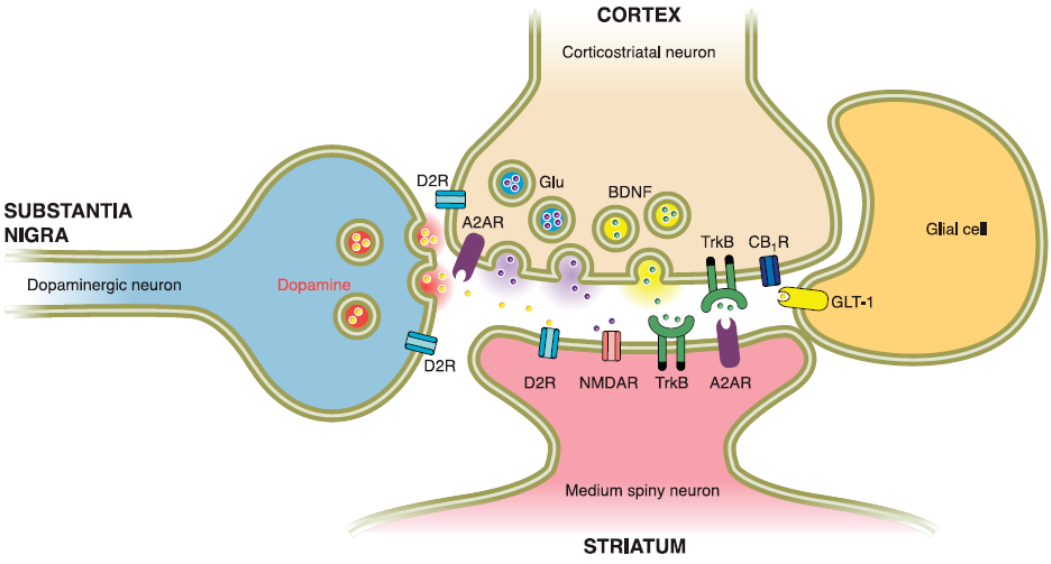

Figure 5. Neurotransmitter systems and growth factors that are dysfunctional at the corticostriatal pathway. Neuronal death may depend on excitotoxicity resulting from increased glutamate (Glu) release from cortical neurons and increased activity of the glutamate receptor (NMDAR). In addition to glutamate, other neurotransmitter systems that control the activity of the corticostriatal synapse can contribute to render striatal neurons more sensitive to excitotoxic stimuli. Reproduced from (Zuccato et al., 2010).

The first mechanism proposed to explain the selective vulnerability of MSNs in HD was excitotoxic cell death. This hypothesis is supported by a study in which MSN's express high levels of NMDARs, and the subsequent over-activation caused an abnormal Ca^{2+} influx, led to apoptosis (Nicholls et al., 2009). Studies have also demonstrated that the sensitivity of NMDAR is enhanced in HD models (Cepeda et al., 2001; Zeron et al., 2002). This could be due to an abnormal interaction of mHTT with the post-synaptic density protein 95 (PSD95). PSD95 is responsible for the clustering NMDARs in lipid rafts at the post-synaptic membrane and changing the NMDAR subunit composition such that the more sensitive NR2B variant is favoured over NR2A (Fig. 6) (Milnerwood et al., 2010; Sun et al., 2001).

In addition to excitotoxicity, it's possible to find many other process that can affect neurons in HD. It has been showed that mHTT can alter the availability of molecules involved in synaptic vesicle exocytosis (synaptobrevin-2, rabphilin 3A, complexin II) and recycling (PACSIN/syndapin) (Modregger et al., 2002; Morton and Edwardson, 2001). Moreover, the level of neurotransmitters such us dopamine, GABA, cannabinoid (CB1), glutamate and others are disturbed in HD mice and patients (Augood et al., 1996; Bibb et al., 2000; Cha et al., 1998-1999; Sun et al., 2005). Microarray studies have shown abnormal expression levels of genes involved in the mantainance of membrane potential, intracellular signalling and neuronal differentiation (Luthi-Carter et al., 2000). Finally, it has been shown that microtubule based transport is impaired in HD due the abnormal interaction of mHTT with HAP1, preventing it from associating with p150(Glued) an important component of dynein/dynactin motor complex (Gauthier et al., 2004; Gunawardena et al., 2003).

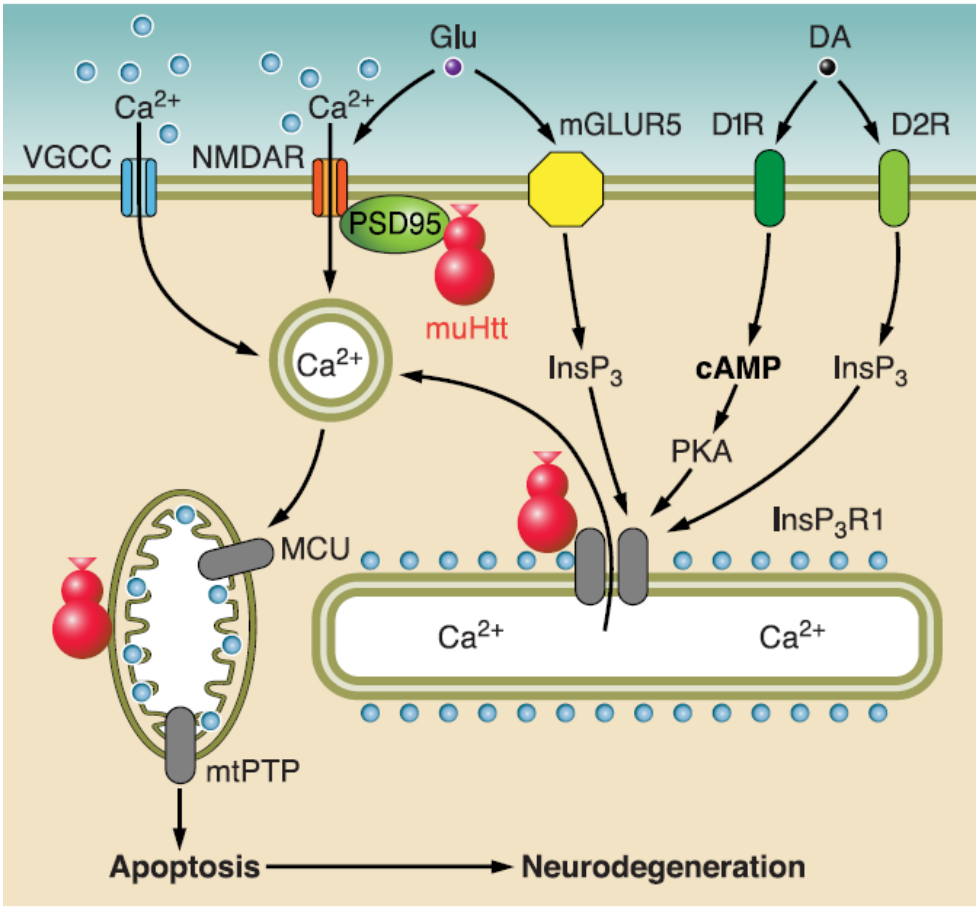

Figure 6. Dysfunction of Ca^{2+} signalling in HD. mHTT causes cytosolic and mitochondrial Ca^{2+} overload and apoptosis of MSNs in HD. mHTT perturbs Ca^{2+} signalling by enhancing NMDAR function, possibly through decreased interaction with the PSD95-NR1A/NR2B complex. Moreover, mHTT binds strongly to $InsP_3$ R1, causing Ca^{2+} release through the $InsP_3$ R1. Dopamine (DA) released from midbrain dopaminergic neurons stimulates D1 and D2 receptors (D1R, D2R). D1R are coupled to activation of adenyl cyclase, increase in cAMP levels, and activation of PKA. PKA potentiates glutamate-induced Ca^{2+} signals by facilitating the activity of NMDAR and $InsP_3$ R1. D2R are coupled directly to $InsP_3$ production and activation of $InsP_3$ R1. Reproduced from Zuccato et al., 2010.

1.4.7 Cholesterol metabolism dysregulation

The cholesterol synthesis pathway is another important metabolic process that is disrupted in HD. Cholesterol is critical to proper neuronal function. For example, cholesterol determines the localisation and functioning of ion channels and membrane receptors by acting as a modulator of membrane fluidity and an organiser of lipid rafts (Allen et al., 2007). Moreover, cholesterol is essential for myelination, proper neurite outgrowth, synaptogenesis, and the synthesis of steroid hormones (Valenza and Cattaneo, 2011). It is thus conceivable that a disruption of cholesterol levels could contribute to HD pathogenesis.

Several studies have already shown a decrease in expression of cholesterol synthesis enzymes in HD and it has been suggested that this is the result of mHTT disrupting the transcriptional activity of a master regulator of cholesterol synthesis SREBP-2 (sterol response element binding protein 2). Decrease activity of HMGCoA, (4-hydroxy-4-methyl-glutaryl Coenzyme A reductase) involved in cholesterol synthesis, and a reduced brain cholesterol content, have also been observed in R6/2, YAC128, *Hdh*Q111 mouse models as well as transgenic rat HD models (Valenza et al., 2005; 2007; 2010).

1.5 HD models

Since the identification of the HD causing mutation, several animal models have been generated to study the disease. Worm, fly and cell culture models are helpful to study the basic mechanism of HD pathogenesis, but the translation of these findings to the human HD is limited. Placing the mutation in the context of a mammalian organism is essential for the proper investigation of disease mechanisms *in vivo*, and the validation of therapeutic strategies. Indeed, the most common HD mammalian models are mice, but rats, pigs, sheep and monkeys have also been generated.

1.5.1 Mouse models of HD

Various mouse models, that develop motor and cognitive deficits, as well as neuropathology relevant to HD, have been developed.

These genetic models can be divided into three categories, according to how they were engineered. **N-terminal transgenic** animals carry the 5' portion of the human *HTT* gene, which contains the mutation; whereas **full-length transgenic** models carry the full-length *HTT* genomic region and express the full-length HTT protein containing expanded polyQ repeats. The third category are **knock-in** models in which have been introduced CAG repeats of varying length into the mouse huntingtin (*Htt*) genomic locus. Models within each of these three broad categories differ in their CAG repeat numbers, the size and species of origin (mouse or human) of the huntingtin gene, the promoters that drive expression of the huntingtin gene, and, indeed, their background strain. Each model exhibits a somewhat different characteristic phenotype, a consequence of the method of their generation, and their intended purpose (Table.2).

Model	Genetic basis	Promoter	Repeat length
R6/2	Human *HTT* exon 1	Human *HTT*	200*
N171	Human *HTT* exon 1,2 and part of 3 (first 171 aa)	Prion promoter	82
BACHD	Human *HTT*	Human *HTT*	97
YAC72	Human *HTT*	Human *HTT*	72
YAC128	Human *HTT*	Human *HTT*	128
***Hdh*Q111**	Mouse *Htt* homologue (*Hdh*); chimeric human/mouse exon 1	Mouse *Htt* homologue (*Hdh*)	111
CAG140	Mouse *Htt* homologue (*Hdh*); chimeric human/mouse exon 1	Mouse *Htt* homologue (*Hdh*)	140
***Hdh*Q150**	Mouse *Htt* homologue (*Hdh*)	Mouse *Htt* homologue (*Hdh*)	150

*Average repeat length of R6/2 mice at the King's College London colony

Table 2. Summary of most commonly used HD mouse models

1.5.2 N-terminal transgenic fragment models

The R6/1 (115 CAG repeats) and R6/2 (155 CAG repeats), which express mutant human exon 1 *HTT*, were the first HD transgenic lines to be produced (Mangiarini et al., 1996) and the R6/2 mouse has been the most extensively studied and utilized mouse model of HD to date. The N-terminal transgenic lines carry a small portion of the 5' end of the human *HTT* gene, including exon 1, containing the CAG repeat region. Because these N-terminal containing transgenic mice were engineered via pronuclear injection, each transgene is integrated randomly at a unique site in the mouse genome. R6/2 mice express a single copy of the first exon of *HTT* under the control of the human HTT promoter that generates an exon 1 HTT transprotein with 150-200 polyQ repeats. These lines ha an accelerated phenotype relative to other genetically engineered lines (Menalled et al., 2009a) and develop behavioural abnormalities such as rotarod and grip strength impairments, hypo-activity and deficits in learning and memory by 8 weeks of age (Carter et al., 1999; Lione et al.,1999). A concomitant loss of body and brain weight, as well as atrophy of the skeletal muscle and testis is also evident (Mangiarini et al., 1996). R6/2 mice also develop cytoplasmic aggregates and nuclear inclusions in the brain and peripheral tissues before symptom onset (Davies et al., 1997; Li et al., 1999; Sathasivam et al., 1999). Disease progression is rapid and consequently R6/2 mice do not typically survive for longer than 15 weeks (at King's College London colony). The N-terminal transgenic lines demonstrate that an N-terminal mHTT fragment was sufficient to elicit HD-like neurological phenotypes in the mouse.

The N171-82Q are also an N-terminal transgenic line (Schilling et al., 1999) expressing a 171 amino acid mHTT cDNA fragment with 82Q under the regulation of

the mouse prion promoter, which directs expression primarily in the brain. These mice develop similar behavioural and physiological abnormalities to R6/2, although onset and disease progression is less aggressive than in R6/2 mice. Weight loss begins around 2-3 months of age, rotarod impairment is evident from 4 months and end-stage disease typically occurs at 6 months of age (Schilling et al., 1999). Cytoplasmic and nuclear inclusions are also formed in N171 mice, however, their distribution across brain regions differs from that observed in both HD patients and R6/2 mice (Schilling et al., 1999). This may be due to the fact that HTT transgene expression in N171 mice is under the control of the prion promoter.

1.5.3 Full-length transgenic models

The two most common HD models in which the full-length *HTT* transgene is carried in either a yeast or bacterial artificial chromosome are YAC (Yeast Artificial Chromosome) and BAC (Bacterial Artificial chromosome), respectively. Both YAC and BAC models express full length human *HTT* under the control of the endogenous human promoter. YAC HD mice are available with a polyQ length of 18, 46, 72 and 128 (Hodgson et al., 1999; Slow et al., 2003), and BACHD mice carry 97Q (Gray et al., 2008).

The well-studied YAC128 transgenic mouse, for example, expresses full-length human HTT with 128 glutamine repeats, encoded by a tract that is composed primarily of CAG codons but also contains 9 interspersed CAA codons (that also encode glutamine) (Pouladi et al., 2012). In contrast, the BAC HD mouse model expresses full-length human HTT containing 97 codons of a mixed CAG/CAA repeat tract (Gray et al., 2008). With regards to germ line and somatic instability in the YAC128 and BAC HD mouse models, some important considerations should be noted. First, in the YAC transgenics the polyglutamine stretch in exon 1 is encoded by a CAG tract that is interspersed with

9 CAA codons (Pouladi et al., 2012). These interspersed CAA codons appear to be enough to stabilize the tract to be resistant to germ line instability as the YAC128 mouse CAG-CAA tract length does not drift over generations. Similarly, in BAC HD mice, the polyglutamine tract is encoded by an ordered sequence comprised of both CAG and CAA codons. Mixing CAG and CAA codons has been shown to confer resistance of the tract to expansions and contractions (Gray et al., 2008). Germ line and somatic instability is not seen over generational time in BAC HD mice.

In contrast to fragment models, transgenic full-length HD mice display a slower disease progression. They typically show a normal life span and also an increase of body weight is observed (Gray et al., 2008; Van Raansdonk et al., 2005). Both models develop motor impairment, activity abnormalities and cognitive deficiencies (Gray et al., 2008; Van Raansdonk et al., 2005). Equally, both models show a decrease in brain weight, and cortical and striatal degeneration evident at 12 months of age (Gray et al., 2008; Van Raansdonk et al., 2005). Like YAC128 mice, BAC HD mice do not exibit reduced cortical and striatal volume until the onset of motor irregularities which are pronounced by 6 months of age suggesting that this is a secondary feature of disease (Gray et al., 2008; Slow et al., 2003).

In YAC128 mice, by 15 months of age, intra-nuclear inclusions are visible in most brain regions including nucleus accumbens, ventral striatum, lateral striatum, motor cortex, sensory cortex and cerebellum (Bayram-Weston et al., 2012). Although disease progression is slower in full-length mouse models of HD, they are a useful resource to investigate the aspects of mHTT toxicity in the context of the full length protein.

1.5.4 "Knock in" HD models

Unlike the N-terminal and full-length HD transgenic models, knock-in HD models are generated by homologous recombination in mouse embryonic stem cells and a specified number of CAGs are introduced directly into the mouse *Htt*. One obvious advantage to these models is the fidelity of the expression that results from the CAG repeat being carried in the context of the mouse *Htt*. Therefore the variability in tissue distribution and expression levels observed in microinjection-based HD transgenic models (due to transgene copy number variation and position affects resulting from random transgene integration) is absent. Like most HD patients, these HD knock-in mice can be heterozygous for one wild-type *Htt* allele and one CAG-expanded allele. Numerous HD knock-in mouse models have been described.

The first group generated an allelic series of knock-in mice as described by Wheeler and MacDonald at Massachusetts General Hospital (MGH) (Wheeler et al., 1999). These knock-in mice have a human exon 1 sequence engineered with repeats of 18, 48, 78, 90 and 109 CAGs targeting one allele of mouse *Htt*. The most well described mouse in this knock-in series is the *Hdh*Q111 mouse (111 glutamines encoded by a $(CAG)_{109}$CAACAG sequence) (Wheeler et al., 2000).

The second group is an allelic series of knock-in mice generated and created by Lin and Detloff at the University of Alabama, Birmingham (UAB) (Lin *et al*., 2001). These knock-in mice have expanded CAG tract with 50, 100, 150, 200, 250, 315 and 365 CAGs in the mouse *Htt* exon 1 sequence (Heng *et al*., 2010b; Lin *et al*., 2001; Sathasivam *et al*., 2013). The 150 CAG-repeat line, denoted *Hdh*Q150, is the most well studied of this series. Unlike the MGH series, these mice contain no human sequence; 100% of the mHTT expressed in these mice is derived from the mouse *Htt* gene.

The third group developed by Zeitlin are knock-in mouse models of HD with a chimeric mouse/human exon 1 containing 140 CAG repeats inserted in the murine *Htt*. They are heterozygous for an *HTT* allele with an expanded CAG repeat size of 71, 94 and 140 in the human *HTT* exon 1 sequence (Levine et al., 1999; Menalled et al., 2003). Consequently, both the MGH and Zeitlin knock-in mice encode the human exon 1 sequence in the context of a full length mouse *Htt* locus while the Detloff knock-in mice are entirely mouse *Htt* sequence.

As for the transgenic full length HTT mice, the knock-in mice exhibit a slow disease progression. However, changes in certain behaviours such as activity and rearing can be detected as early as 1 month of age in the CAG140 mice, though these mice do not display any overt pathological signs such as weight loss, tremor or clasping at 1 year of age (Menalled et al., 2003). *Hdh*Q150 mice do not display physiological abnormality until 12 months of age with rotarod impairment only becoming pronounced by 18 months of age (Woodman et al., 2007). Nevertheless, these mice form cytoplasmic and nuclear aggregates by 6 months of age and by 21-22 months their pattern of aggregation, both the CNS and peripheral tissues, is as widespread as that of R6/2 mice at 12 weeks of age (Woodman et al., 2007; Moffitt et al., 2009). Aggregation is also a feature of disease in *Hdh*Q111 and CAG140 mice, where diffuse nuclear staining can be observed by 1-2 months of age, and nuclear inclusions appear by 6 (CAG140) and 10 months of age (*Hdh*Q111) (Menalled et al., 2003; Wheeler et al., 2000).

1.5.5 HD mouse models: conflicts and similarities

Mouse models of HD share many features but at the same time they show many discrepancies. For example, while R6/2 and *Hdh*Q150 mice develop mHTT inclusions in the brain prior to behavioural abnormalities, this is not the case in YAC and BAC mice where smaller aggregates are more commonly found throughout neuronal nuclei and the neuropil (Woodman et al., 2007; Moffitt et al., 2009; Gray et al., 2008; Slow et al., 2003). The main difference between HD mouse models is the rate of the disease progression. N-terminal HTT fragments mouse models generally develop symptoms earlier than mice expressing full length HTT (Crook and Housman, 2001) (Fig.7).

The rapid disease progression of R6/2 mice allows for efficient preclinical compound screening, but the full-length or knock-in models, with longer pre-manifest stage could be more useful for elucidation of subtle molecular changes that occur before symptom onset in an adult organism. Also, some molecular events and their role in HD pathology, such as proteolytic cleavage, cannot be examined without the context of the full length mutant protein. If, indeed, toxicity is caused by N-terminal fragments, fragment models could be used to study the sequence of pathological events and applicability of therapeutic strategy downstream of HTT cleavage.

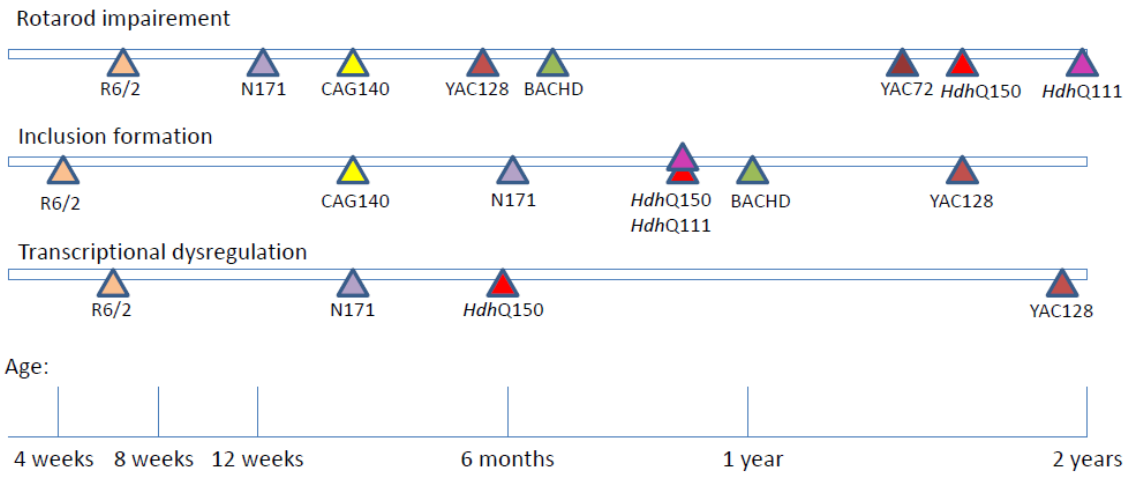

Figure 7. Timeline of Behavioral and Neuropathological Symptoms in HD mouse models. Transgenic fragment (R6/2 and N171) models develop motor dysfunction and molecular pathologies earlier than transgenic full length (BACHD, YAC72 and 128) and knock-in (*Hdh*Q111, CAG140 and *Hdh*Q150) mice. (Modified from Crook and Housman, 2011)

1.6 Histone deacetylases classification and mechanism of reaction

The HDACs can be divided into four classes depending on their sequence homology to yeast enzymes. Class I includes HDAC1, HDAC2, HDAC3 and HDAC8, which are homologous to the yeast enzyme Rpd3 (De Ruijter et al., 2003). Class IIa includes HDAC4, HDAC5, HDAC7 and HDAC9, whereas class IIb contains HDAC6 and HDAC10 (Fig.8) (De Ruijter et al., 2003). All members of class II share most homology with the yeast enzyme Hda1.

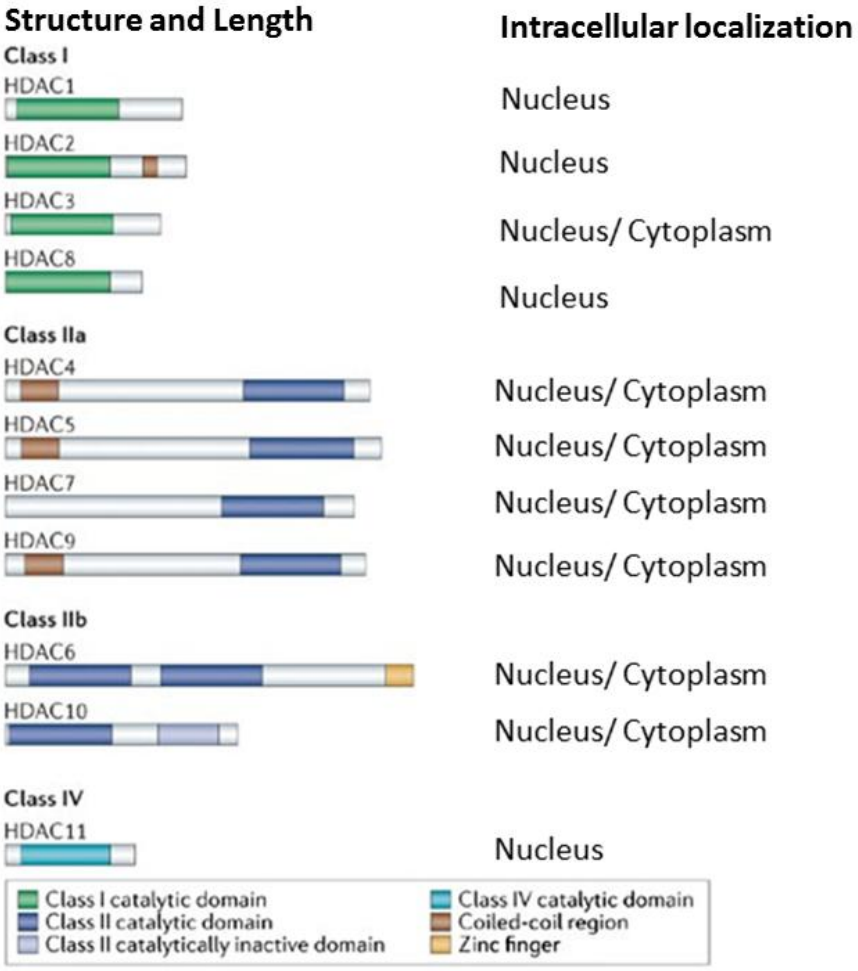

Figure 8. Classification of classes I, II, and IV HDACs by structure and intracellular localization. (Modified from Bolden et al., 2006)

Sirtuins form the class III deacetylases which contain 7 enzymes that are all similar to the yeast Sir2, thus named SIRT1 through SIRT7 (Fig.9) (Finkel et al., 2009).

Class IV's only member is HDAC11, which, due to insufficient sequence homology, cannot be included in any other class (Gao et al., 2002).

The class I, II and IV HDACs have different mechanism of action as compared to the class III deacetylases. HDACs 1 through 11 are all zinc-dependent enzymes and share the same reaction mechanism. The reaction needs Zn^{2+} ion coordinated by histidine and aspartate residues in a highly conserved catalytic core. Deacetylation occurs by the activation of a water molecule by the zinc cation, coupled to the histidine-aspartate charge relay system, within the active site (Finnin et al., 1999). The sirtuin reaction mechanism is NAD^{+} (nicotinamide adenine dinucleotide) dependent and proceeds through the formation of an oxocarbenium-like transition species and release of nicotinamide (NAM). Upon completion, apart from the deacetylated substrate, 2'-O-acetyl ADP ribose is released (Liang et al., 2010).

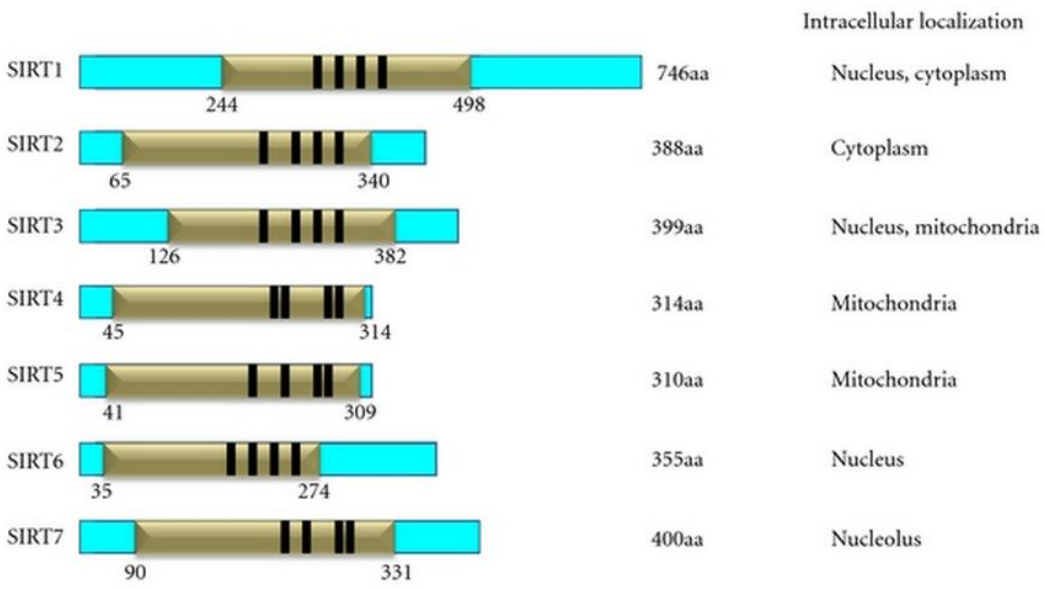

Figure 9. Schematic representation of human sirtuins family members 1–7. NAD-dependent catalytic domain (gold) (NAD-binding pocket), zinc-binding domain (black), and their intracellular localization. Reproduced from Rajendran et al., 2011.

1.6.1 Expression and functions of HDAC enzymes

Class I HDACs are expressed in a variety of tissues suggesting that they have a general regulatory function in transcriptional control (Johnstone et al., 2002). HDAC1 and HDAC2 possess high sequence homology (De Ruijter et al., 2003). Located exclusively in the nucleus, they generally form part of multi-protein transcription modulating complexes such as Sin3, NuRD (nuclear remodelling deacetylase) or Co-REST (co-repressor of rest) (Ahringer et al., 2000; Humphrey et al., 2001). HDAC3 is the only class I member that, in addition to a nuclear localisation signal (NLS), also possesses a nuclear export signal (NES) (Yang et al., 2002). Consistent with this, HDAC3 has been detected in both the nucleus and the cytoplasm where it is believed to localise to the plasma membrane (Emiliani et al., 1998).

HDAC4, HDAC5, HDAC7 and HDAC9 have their catalytic domain at the C-terminus and an NLS at the N-terminus (Yang and Seto, 2008). However, the N-terminus also has conserved domains for binding the C-terminal binding protein (CtBP), myogenic enhancer factor (MEF2) and 14-3-3 proteins (Yang and Gregoire, 2005). MEF2 is essential for muscular differentiation and is inhibited through binding class IIa HDACs (Verdin et al., 2003). This association is disrupted by CaMK phosphorylation and the export of HDACs to the cytoplasm via association with 14-3-3 proteins (McKinsey et al., 2000). HDAC4, HDAC5 and HDAC7 have also been shown to interact with HDAC3 with the N-CoR/SMRT (nuclear co-repressor/silencing mediator for retinoic acid and thyroid hormone receptors) repressive complex (Fischle et al., 2002). In fact, data suggest that HDAC4, HDAC5 or HDAC7 may not possess histone deacetylase activity and therefore associate with HDAC3 to achieve transcriptional repression (Fischle et al., 2002).

HDAC6 and HDAC10 are unique in that they have a duplication of the catalytic domain, although the duplicated domain appears to be functional in HDAC6 only (Yang and Seto, 2008). It has been shown that HDAC6 is involved in α-tubulin acetylation throughout the brain (Bobrowska et al., 2011). HDAC10, as well as the class IV HDAC11, have only recently been identified and little is known of these two enzymes. HDAC10 has so far been implicated in DNA homologous recombination and 3' pre-mRNA processing and appears to be vertebrate specific, whereas HDAC11 is conserved through invertebrates and plants but more investigation is needed to pinpoint its cellular functions (Gao et al., 2002; Kotian et al., 2011; Shimazu et al., 2007; Yang and Seto., 2008).

The sirtuins can be found in the nucleus (SIRT1, SIRT6 and SIRT7), the mitochondrion (SIRT3-5) and in the cytoplasm (SIRT2) (Finkel et al., 2009). So far, SIRT1 has been most extensively studied, due to its highest homology with the yeast Sir2 enzyme and it has been implicated in mediating lifespan extension (Kaeberlein et al., 1999; Tissenbaum and Guarente, 2001). It has also been implicated in the DNA damage response, oxidative stress and heat shock response, cellular differentiation and metabolism (Wang et al., 2008c; Westerheide et al., 2009; Yuan et al., 2007). SIRT2 is the only predominantly cytosolic sirtuin. Like HDAC6, SIRT2 has been proposed to be an α-tubulin deacetylase. While knocking-out HDAC6 in mice led to an increase in α-tubulin acetylation, this was not the case when SIRT2 was knocked-out (Bobrowska et al., 2011). Mitochondrial sirtuins have been shown to function as regulators of energy production through the concerted action of deacetylation and ADP-ribosylation. SIRT3 can deacetylate acetyl-CoA synthetase 2, resulting in an increased production of acetyl-CoA, an intermediate in the Krebs cycle, fatty acid metabolism, and cholesterol

synthesis (Hallows et al., 2006). SIRT4 does not seem to possess deacetylase activity, but instead uses NAD^+ to ADP-ribosylate glutamate dehydrogenase, inactivating it in liver and pancreatic β-cells, and regulating gluconeogenesis and insulin secretion in response to glutamine (Haigis et al., 2006). Little is known about SIRT5, although it has been recently shown to deacetylate carbamoyl phosphate synthetase 1, thereby activating it and inducing increased urea production in the liver (Nakagawa et al., 2009). As SIRT5 mRNA levels are upregulated during fasting, its action on the urea cycle could be protective by increasing the conversion of increased ammonia generated in the process to non-toxic urea (Ogura et al., 2010). SIRT6 is another sirtuin without deacetylase but with ADP-ribosylase activity. The substrates are still unknown, but studies from SIRT6-deficient mice indicate a role for this protein in base-excision repair (Mostoslavsky et al., 2006). SIRT7 is a nucleolar enzyme expressed mainly in proliferative tissues such as liver, spleen and testes, with low expression in heart, brain or muscle (Ford et al., 2006). SIRT7 can associate with Pol I and its over-expression increased transcription of rRNA, suggesting that SIRT7 could promote growth by driving ribosome biosynthesis in proliferating cells (Ford et al., 2006).

1.7 SIRT1 as therapeutic target in HD

Several studies have shown that SIRT1 can delay aging and promote longevity through regulating the activity of proteins such as p53, FOXO and Ku70, which are involved in apoptotic processes or cellular repair mechanisms (Pasinetti et al., 2010). Moreover, there is evidence to demonstrate that caloric restriction can improve motor impairments and extend survival in HD mouse models (Duan et al., 2003), indicating that pathways related to energy metabolism can modify disease. Caloric restriction increases mitochondrial biogenesis and the production of NO (Nitric Oxide) that can activate the *Sirt1* gene (Nisoli et al., 2005; Guarente et al ., 2006). Moreover, SIRT1 has been suggested to mediate some beneficial effects of caloric restriction (Canto and Auwerx et al, 2009; Wakeling et al., 2009; Shimokawa and Trindade et al, 2010; Chalkiadaki and Guarente et al, 2012). The first report demonstrating a link between SIRT1 and HD came from studies by Parker (2005), where overexpression of Sir2.1 (homolog of SIRT1 in *C. elegans*) rescued neuronal dysfunction induced by mutant polyglutamine in *Caenorhabditis elegans*. In contrast to the neuroprotective effect of Sir2.1 in *C. elegans*, Pallos (2008) reported that 50% reduction of Sir2 extended survival and preserved photoreceptor-containing neurons in flies expressing mHTT. Interestingly, in the fly model system, overexpression of Sir2 does not reduce the lethality or the level of neuronal degeneration caused by mHTT. Studies in both *C. elegans* and *Drosophila* suggest that complete loss of Sir2 is deleterious in the worm (Parker et al., 2005) and is deleterious compared with heterozygous loss in mHTT-challenged flies (Pallos et al., 2008). Although heterozygous loss of Sir2 is protective in flies, heterozygous loss of Sir2 in worms was not examined.

Due to these contradictory results, further investigations into the role of SIRT1 in mammalian systems were needed. Indeed, two independent studies from Duan's (Jiang et al., 2011) and Krainc's groups (Jeong et al.,2011) demonstrated that modulating the levels of SIRT1 had some therapeutic benefit in three different HD mouse models. This supports the notion that SIRT1 has beneficial effects in HD mouse models. It is possible to explain the contradictory results on the effects of SIRT1 in models of HD as SIRT1 has numerous targets (Fig. 54), and different models of HD display different phenotypes by activating various targets and mechanisms. Therefore, it is not surprising to observe contradictory data, especially in different models and species.

1.7.1 SIRT1 protein and its proposed function

The SIRT1 gene spans about 34 kb including nine exons. Human SIRT1 encodes a 747 amino acid protein with a nuclear localization signal (NLS) at the N-terminus (aa 41-46) and a sirtuin homology domain at the centre (aa 261-447); this domain is a conserved catalytic domain for deacetylation. SIRT1 is predominately in the nucleus. In addition to possessing two nuclear localization signals, it also contains two nuclear export signals. This can explain the cytosolic and nuclear localization of SIRT1 (Fig.10).

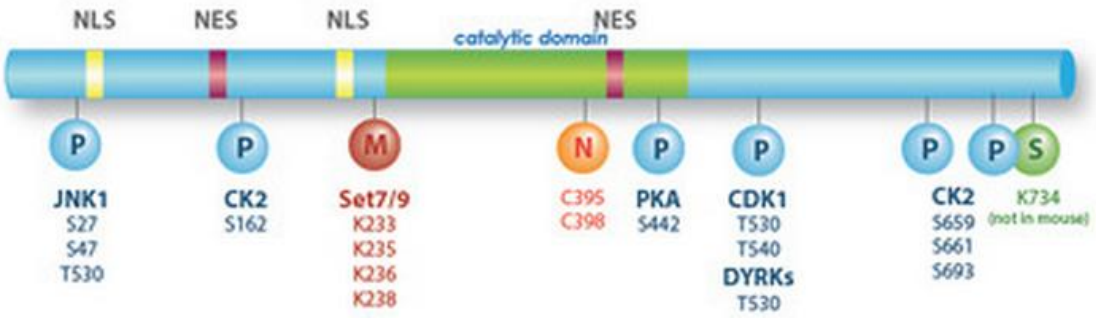

Figure 10. SIRT1 functional domains. Human SIRT1 has two consensus nuclear localization signals (NLS) and two nuclear export signals (NES), one of which is nested in the catalytic domain. SIRT1 can be phosphorylated (P) by JNK1, CK2, PKA, CDK1, and DRYKs. (Modified from Thomas G. Brock, Cayman chemical).

As one of the most conserved mammalian sirtuins, SIRT1 plays essential roles in many biological processes. Nature has evolved a variety of strategies to modulate tightly the activity of SIRT1 in response to different stimuli. In particular, as an enzyme, substrate availability, PTMs, interacting protein partners, or small molecule activators or repressors can directly regulate the activity of SIRT1.

Like all enzymes, the catalytic activity of SIRT1 is dependent on its substrates: acetylated proteins and NAD^+. The SIRT1 enzymatic reaction catalyzes the deacetylation of protein targets by hydrolyzing NAD^+ and transferring the lysine-bound acetyl group to the 2' -OH position of ADP-ribose, thereby generating a protein with a deacetylated lysine residue, 2'-O-acetyl-ADP-ribose, and nicotinamide. The discovery that SIRT1 exclusively utilizes NAD+ as a co-substrate raises the possibility that its activity is also intrinsically linked to the energy status of the cell. In this scenario, a low-energy status would increase SIRT1 activity by increasing the levels of NAD^+, whereas a high-energy status would decrease SIRT1 activity by decreasing the levels of NAD^+.

It has been shown that SIRT1 function is also regulated by post-translational modifications and the main PTM to control its function is the phosphorylation. For example, the MAP kinase JNK1, activated by cellular stresses, phosphorylates SIRT1 on three residues promoting nuclear accumulation of SIRT1 and increasing its deacetylation activity. In mice, persistent JNK1 activation and phosphorylation of SIRT1 at S46 is followed by ubiquitination and proteasomal degradation of SIRT1 (Nasrin et al., 2009). Casein kinase 2 (CK2) can, like JNK1, be activated by stress. Ionizing radiation induces CK2-mediated phosphorylation of SIRT1 on multiple sites. This phosphorylation of SIRT1 increases deacetylation of P53 and protects against apoptosis following DNA damage (Mahlknecht et al, 2009). Phosphorylation of SIRT1

by PKA increases the rate of deacetylation of PGC-1α and augments fatty acid oxidation (Gerhart-Hines et al., 2011). Phosphorylation of SIRT1 by cyclin B/CDK1 appears to be required for normal cell cycle progression (Sasaki et al., 2008). Tyrosine phosphorylation-regulated kinases DYRK1A and DYRK3 target SIRT1, which increases deacetylation of P53 and protects against DNA damage-induced cell death (Guo et al., 2009).

SIRT1 performs several functions, it is involved in obesity-associated-metabolic diseases, cancer, adipose tissue, aging, cellular senescence, cardiac aging and stress, neurodegeneration, inflammatory signalling in response to environmental stress, development and placental cell survival (Luo et al., 2001; Stunkel et al., 2007; Chen et al 2008). One of the most important functions of SIRT1 is to protect the cell against stress. Indeed, SIRT1 up-regulates stress-protective pathways by the deacetylation of FOXO transcription factors, leading to increased transcription of GADD45 (DNA repair) and MnSOD (reactive oxygen detoxification). SIRT1 concomitantly down-regulates FOXO transcription of the proapoptotic factors FAS (Fatty acid synthase) and Bcl-2 interacting mediator of cell death (BIM). Interestingly, under stress conditions SIRT1 also interacts with P53 and deacetylates its C-terminal regulatory domain (Vaziri et al., 2001). This activity downregulates P53 transcriptional effects, which is consistent with the evidence indicating that the deacetylation of the C-terminal domain of P53 weakens DNA binding activity (Vaziri et al., 2001). Importantly, *Sirt1*KO animals have hyperacetylated P53, which suggests that SIRT1 typically regulates P53 acetylation levels in wild-type animals (Cheng H. et al.,2003). Several other SIRT1 protein substrates involved in cell stress response signalling have been identified, including

ku70, a proapoptotic factor which is down-regulated by SIRT1 deacetylation, and the transcriptional coactivator PGC1- α (Rodgers JT et al., 2005).

1.7.2 DBC1 (Deleted in breast cancer-1) is a negative regulator of SIRT1

Several transient protein–protein interactions also play key roles in the regulation of SIRT1 activity. DBC1 (Deleted in breast cancer-1), originally identified as a gene (8p21) homozygously deleted in breast cancer and some other tumors, has been shown to regulate SIRT1 activity. DBC1 is a large protein, found both in the nucleus and cytoplasm, with multiple functions in the cell. It can promote p53-mediated apoptosis by binding to, and inhibiting, the deacetylase activity of SIRT1, resulting in increased p53 acetylation levels and activity (Zhao et al., 2008). DBC1 may be an important regulator of heterochromatin formation as it binds SUV39H1 and inhibits its histone methyltransferase activity (Li et al., 2009). Caspase-dependent processing activates the pro-apoptotic activity of DBC1 during tumor necrosis factor-α (TNF-α)- mediated cell death signalling (Sundararajan et al., 2005).

DBC1 is composed of different domains including a nuclear localization signal, an N-terminal leucine zipper, an EF hand and a C-terminal coiled-coil region (Fig. 11).

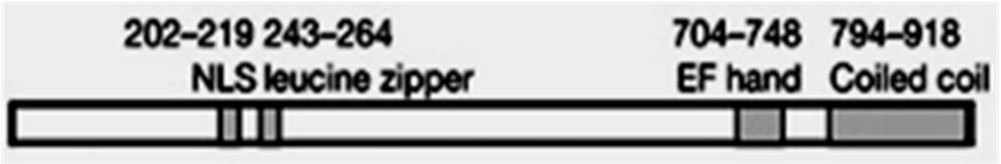

Figure 11. DBC1 functional domains. Reproduced from Kim JE et al., 2008

Ja-Eun Kim and colleagues have shown that the DBC1 leucine zipper domain (243-264) is required for the interaction with the catalytic domain of SIRT1. As consequence, DBC1 forms a stable complex with SIRT1, thus inhibiting SIRT1 activity *in vitro* and *in vivo* (Kim et al., 2008). They also showed that the downregulation of DBC1 expression potentiates SIRT1-dependent inhibition of the apoptosis induced by genotoxic stress (Kim et al.,2008).

It has been shown that SIRT1 adopts a hook conformation. When SIRT1 needs to be activated, its c-terminal region, named ESA, bends like a hook interacting with the catalytic domain. This interaction keeps SIRT1 activated and increases the affinity for its substrates. Moreover the binding site for ESA in the catalytic domain is also the interaction site of DBC1 (Kim et al., 2008). Two CK2 phosphorylation sites seem to be important in controlling the catalytic activity as they are located in the ESA SIRT1 region. It is, therefore, possible that these phosphorylation sites modulate the interaction of the C-terminal region with the catalytic domain. This might affect the catalytic region and substrate binding through an allosteric mechanism. Additionally it might affect the binding of DCB1, which is a SIRT1 inhibitor (Fig. 12).

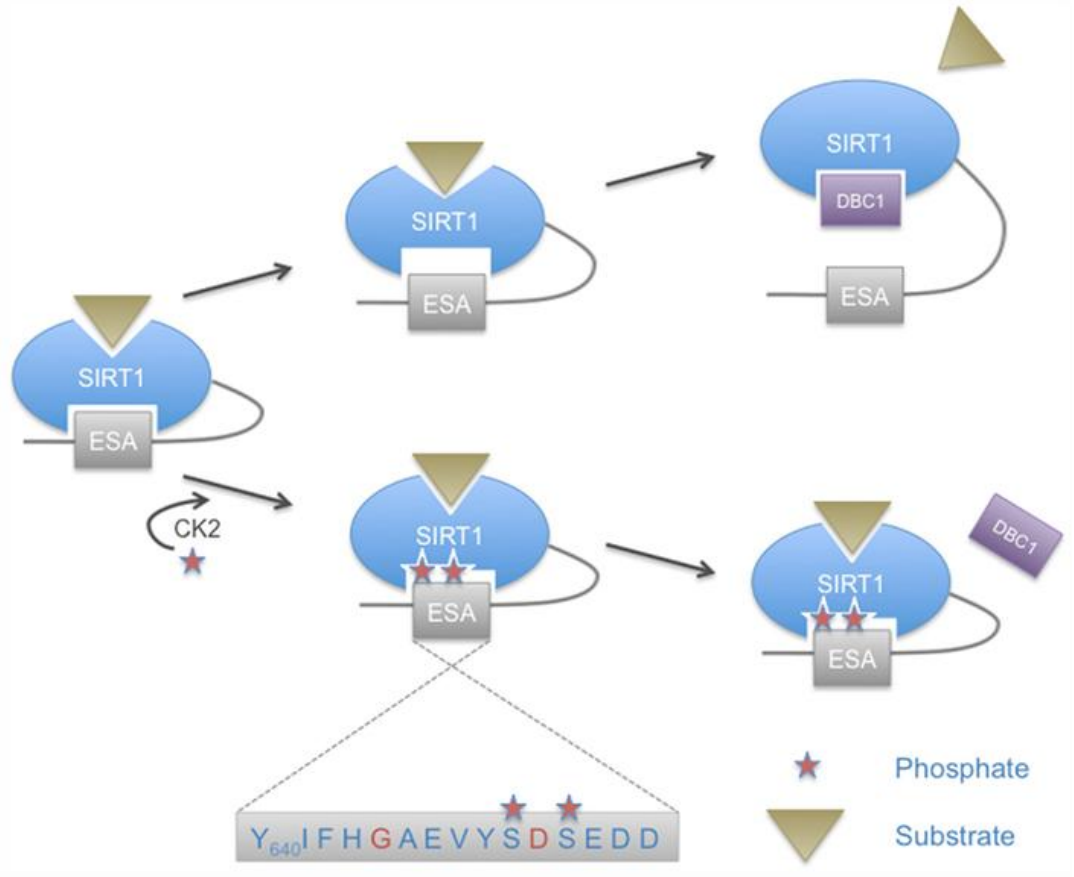

Figure 12. The ESA motif competes with DBC1 binding, a negative regulator of SIRT1. Enhanced interaction of ESA with the core domain of SIRT1 in response to CK2 phosphorylation would prevent binding of DBC1 and thus abrogate its inhibitory effect. Reproduced from Franziska Flick and Bernhard Lüscher, 2012.

It has been observed that PKA activation leads to a rapid, and transient activation of SIRT1 that is DBC1-dependent (Carlos Escande et al., 2012). In fact, an increase in cAMP/PKA activity results in the dissociation of SIRT1 and DBC1 in an AMPK-dependent manner. Pharmacological AMPK activation leads to SIRT1 activation by a DBC1-dependent mechanism. Indeed, Escande and Colleagues found that AMPK activators promote SIRT1-DBC1 dissociation in cells, resulting in an increase in SIRT1 activity (Fig 13).

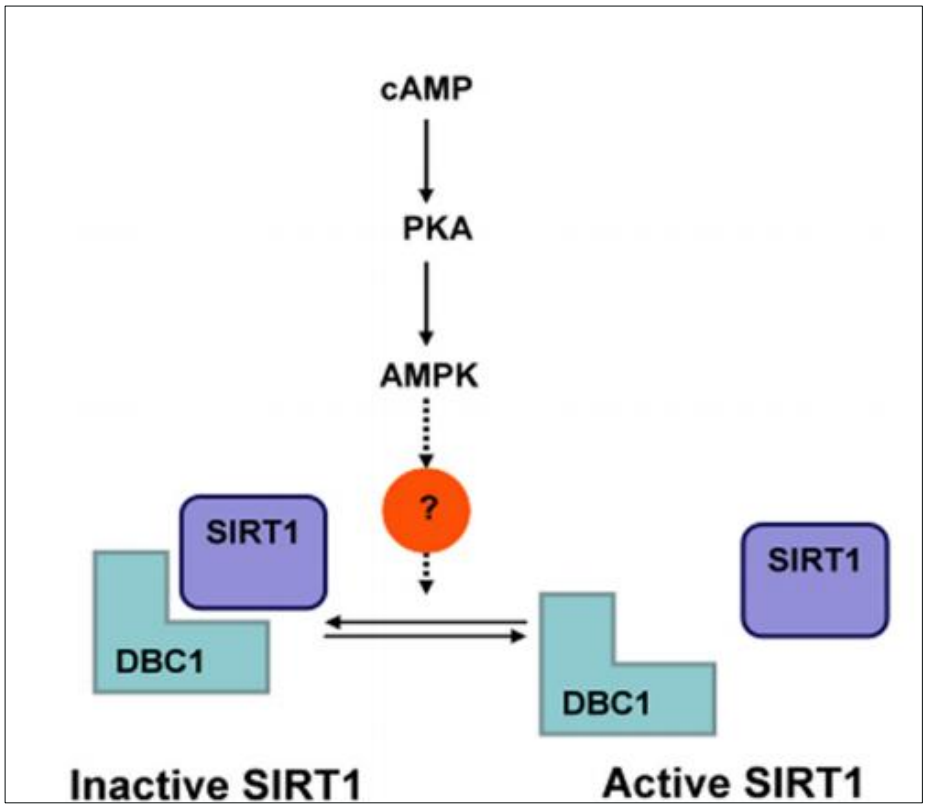

Figure 13. SIRT1 regulation by PKA and AMPK. SIRT1–DBC1 interaction is modulated by input from the cAMP–PKA (protein kinase A) and AMPK signalling pathways. Both these pathways activate SIRT1 by modulating the SIRT1–DBC1 interaction. Reproduced from Escande et al., 2012.

1.7.3 SIRT1 is an anti-apoptotic protein

SIRT1 plays a vital role in the regulation of metabolism, stress responses, genome stability, and ultimately aging. Moreover, much attention has focused on its anti-apoptotic function. In particular, SIRT1 is able to exert the anti-apoptotic function through the deacetylation and inactivation of P53 (Yi et al., 2010). Pathological conditions such as cancer, neurodegeneration, ischemia, cholestasis, and atherosclerosis are all strongly associated with deregulated levels of apoptosis in which P53 dysfunction has a prominent role.

A wide variety of cellular stress signalling pathways engage the P53 network, resulting in the activation of the P53 protein. The DNA damage, the aberrant proliferative signalling, hypoxia are all involved in the activation of P53. As consequence, several proteins can be involved in the activation of this apoptotic factor.

One of the most dramatic effects of P53 activation is the induction of apoptosis. In the mitochondrial pathway, death stimuli target mitochondria either directly or through transduction by proapoptotic members of the Bcl-2 family, such as Bax and Bak. The mitochondria then release apoptogenic proteins, ultimately leading to caspases activation and apoptosis (Vousden et al., 2009). Cells committed to die via P53-dependent apoptosis typically follow the mitochondrial pathway. Furthermore, most evidence suggests that the key contribution of P53 to apoptosis is primarily dependent on transcriptional activity. P53 has the ability to activate transcription of various proapoptotic genes, including those encoding members of the Bcl-2 family, such as the BH-3 only proteins Bax, Noxa, and Puma (Jeffers et al., 2003) (Fig. 14).

In addition to mitochondrial-targeted P53 actions, an alternative cytosolic P53 death pathway has been reported. It directly activates cytosolic Bax. After stress, nuclear P53

induces transcription of PUMA, which in turn, liberates P53 from an inactive pre-existing soluble p53-Bcl-X_L complex, via binding to Bcl-X_L. The cytosolic P53 then induces homo-oligomerization of Bax, followed by Bax mitochondrial translocation (Fig. 14) (Chipuk et al., 2005).

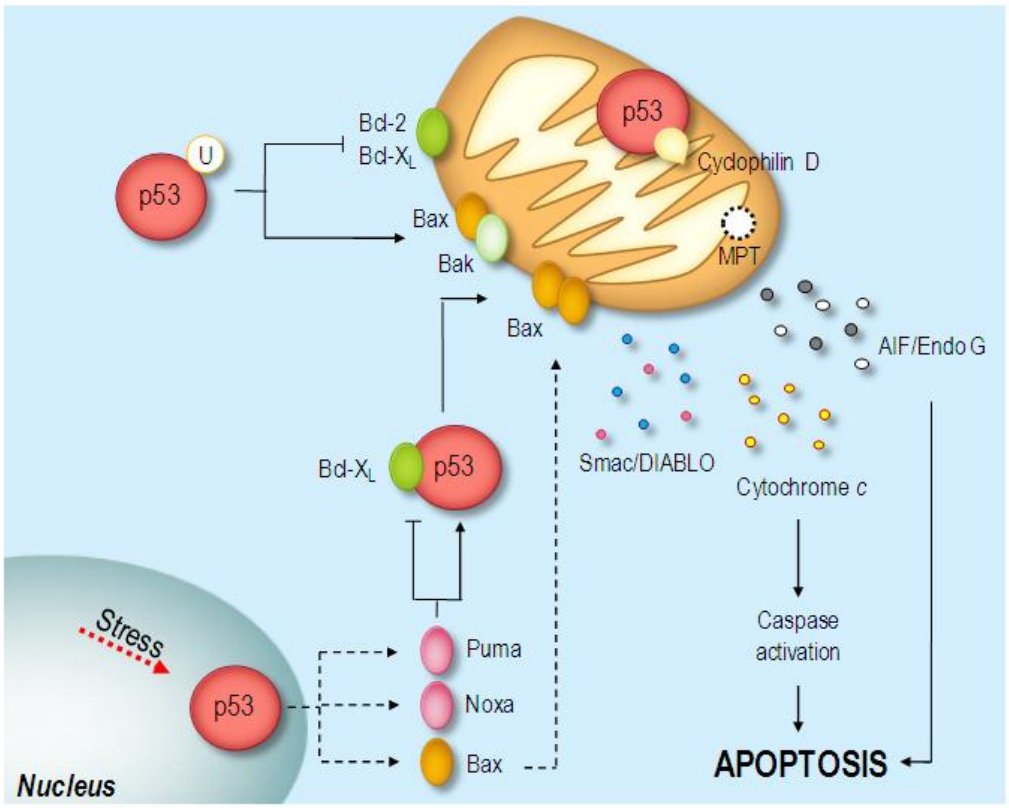

Figure 14. Cytosolic and mitochondrial P53 apoptotic pathways. (Reproduced by Amaral et al., 2010)

1.7.4 Aim of this work

The therapeutic potential of SIRT1 for neurodegenerative disease has been tested in several models of HD. Recent evidence suggests that this enzyme participates in neuronal protection and prevents neurodegenerative diseases in mouse models by modulating deacetylation activities through a variety of substrates including P53 (Kim et al.,2007) and HSF1 (Donmez et al., 2010). However, the exact nature of normal SIRT1 function in the mammalian brain has not been ascertained.

The role of SIRT1 in HD has been previously studied in mouse models. Increased expression of *Sirt1* was found to attenuate neurodegeneration and improve motor function in N171-82Q and BACHD mice (Jiang et al., 2011). Although a second study reported that overexpression of *Sirt1* attenuates brain atrophy and reduces aggregation of mHTT in R6/2 mice (Jeong et al., 2011). Based on these findings, a mis-regulation of SIRT1 function could have important implications in the development and progression of HD.

In this work, we explore the impact of HD pathology on SIRT1 function in the brain. We provide evidence for a considerable down-regulation of SIRT1 activity in the brain of R6/2 and *Hdh*Q150 mice.

Moreover, we tried to understand more about the mechanism that regulates SIRT1 activity in the brain. We show a striatum-specific age-dependent regulatory mechanism of SIRT1 activity in WT mice and we assumed the existence of a link between SIRT1 activity and SIRT1 phosphorylation status in physiological conditions.

Since a specific activator of SIRT1 is not available yet, to rescue the deficit of SIRT1 activity in HD mouse models we used a genetic approach to reduce *Dbc1* expression in R6/2 mice to restore SIRT1 activity and subsequently improve the disease phenotype.

We have therefore crossed R6/2 transgenic mice with mice in which DBC1 has been reduced, or ablated, to evaluate whether the increase of in SIRT1 activity had a beneficial impact on disease progression.

Chapter 2 MATERIALS AND METHODS

2.1 Materials

2.1.1 Commercial Kits

Amersham ECL™ Plus Wester Blotting detection Kit (GE Healthcare)

Bicinchocinic acid (BCA) Assay (Thermo Scientific)

DNase I set (Qiagen)

QIAzol Lysis reagent (Qiagen)

RNeasy Mini Kit (Qiagen)

SIRT1 Fluor-de-lys activity assay (Enzo Life Sciences)

2.1.2 Equipment

7650 accelerating rotarod (Ugo BAsile)

96-well transparent polypropylene PCR plates for genotyping (Bio-Rad)

96-well white polypropylene PCR plates (Bio-Rad)

AM1053 activity cages (Linton Instruments)

Analytical balance (Fisher)

Capex 8C, Charles Austen Vacuum and pressure Laboratory Pump X37-950

CFX96 Real-time system thermocycler (Bio-Rad)

Chromo-4 thermo cycler (Bio-Rad)

Confocal microscope (Leica TCS SP2)

DNA Engine Dyad thermocycler (Bio-Rad)

Fast-Prep Ribolyser (MP Biomedicals)

GD40/50 vacuum gel drier (Life technologies)

Gel-Doc EQ UV-transilluminator (Bio-Rad)

Grip Strength meter (San Diego Instruments)

GS-800 Calibrated Densitometer (Bio-Rad)

Heraeus Fresco 17 Centrifuge (Thermo Scientific)

Heraeus Pico 17 Centrifuge (Thermo Scientific)

L8-80M ultracentrifuge (Beckman Coulter)

Lysing matrix-D tubes (MP Biomedicals)

Nanodrop spectrophotometer (Thermo Scientific)

Omega plate reader (BMG Labtech)

OTC cryostat (Bright Instruments)

Polypropylene tubes (1.5 ml) (Eppendorf)

Protean Minigel Western Blotting system (Bio-Rad)

PT 1200 homogenizer (Polytron)

Semi-transparent shoebox mouse cage (Techniplast Limited)

Shaker IKA KS 260 basic

Sorvall Legend RT Refrigerated Benchtop Centrifuge

Transilluminator TL-33 (UVP)

Transparent activity box (367x207x140 cm) (Techniplast Limited)

UBD2 heating block (Grant instrument)

Ultrasonic bath XB3 (Grant instrument)

Vibra-Cell sonicator (Sonics and Materials incorporated)

X-ray film developer (Xenograps)

2.1.3 Reagents

2'-deoxynucleotide triphosphates (dNTPs) (Invitogen)

2-mercaptoethanol (Sigma)

4-(2-Hydroxyethyl)piperazine-1-ethanesulfonic acid sodium salt (HEPES) (Sigma)

Ammonium persulfate ($(NH_4)_2S_2O_8$)) (Sigma)

Bovine serum albumin (BSA) (Sigma)

Bromophenol blue (Sigma)

Chloroform (Sigma)

Complete protease inhibitor tablet (Roche)

Dimethyl sulphoxide (DMSO) (Sigma)

Dithiothreitol (DTT) (Sigma)

Ethanol (VWR)

Ethidium bromide (Sigma)

Ethylene di-amine tetra-acetic acid (EDTA) (Sigma)

Formaldehyde (Sigma)

Glycerol (Sigma)

Glycine (Sigma)

GoTaq-Flexi DNA Polymerase (Promega)

Hyperfilm ECL (Amersham)

Igepal-CA630 (NP-40) (Sigma)

Lambda Hind III / phiX Hae III Marker (New England Biolabs)

Magnesium chloride ($MgCl_2$) (Sigma)

Methanol (VWR)

MMLV-RT 1st standard buffer (5x) (Invitrogen)

Moloney murine leukemia virus reverse transcriptase (MMLV-RT) (Invitrogen)

Nicotinamide (NAM) (Sigma)

Non-fat dry milk powder (Marvel)

Phenyl methyl sulphonyl fluoride (PMSF) (Fluka)

Phosphate buffer saline (PBS) tablets (Sigma)

Precision mastermix (2x) (Primer Design)

Proteinase K (Fermentas)

Protogel (GeneFlow)

Protogel resolving buffer (GeneFlow)

Protogel stacking buffer (GeneFlow)

Protran nitrocellulose membrane (0.2 µm pore) (Bio-Rad)

RNasin (Promega)

Rodent breeding chow (Special Diet Services)

SDS-PAGE running buffer (10x) (GeneFlow)

Sodium bicarbonate ($NaHCO_3$)

Sodium carbonate ($NaCO_3$)

Sodium chloride (NaCl) (VWR)

Sodium deoxycholate (Sigma)

Sodium dodecyl sulphate (SDS) (Sigma)

Spectra pre-stained protein marker (Fermentas)

Sucrose (VWR)

Taq DNA Polymerase from *Thermus aquaticus* (Sigma)

Tetra methyl ethylene diamine (TEMED) (Sigma)

Trichostatin A (TSA) (Sigma)

Tris base (Sigma)

Triton-X100 (Sigma)

Tween-20 (Sigma)

Ultra-pure agarose (Invitrogen)

Ultra-pure water (Sigma)

2.1.4 Antibodies

Antibody	Catalogue #	Source	Dilution
DBC1	A300-432A	Bethyl lab.	1:1000 (WB) 1:100 (IHC)
SIRT1	ab12193	Abcam	1:1000 (WB) 1:100 (IHC)
P53	sc-6243	Santa cruz	1:100 (IHC)
AcP53	ab122899	Abcam	1:50 (IHC)
MpM2	05-368	Millipore	1:1000 (WB)
HTT	MAB5374(EM48)	Millipore	1:100 (IHC)
HTT	MAB2166	Millipore	1:2500 (WB)
AMPKα1	A300-507A	Bethyl lab.	1:500 (WB)
AMPKα1	ab32047	Abcam	1:10 (IP)
β-actin	sc-47778	Santa-Cruz	1: 10000 (WB)
ATP5B	ab14730	Abcam	1:15000 (WB)
α-tubulin	T9026	Sigma	1:30000 (WB)
Histone H3	ab1791	Abcam	1:30000 (WB)

Table 3. Summary of the application and dilution of all antibodies. WB: western blotting; IP: Immunoprecipitation; IHC Immunohistochemistry.

2.1.5 Genotyping, sequencing and real time quantitative PCR primers and probes.

Name	Application	5'-3' sequence
Dbc1 forward	RT-qPCR	GTACCAGAAGGCAGCTGGAG
Dbc1 reverse	RT-qPCR	TGAAGAGGCTGAGCACAGAA
Dbc1 probe	RT-qPCR	AGGCTACCCCTGCTGTGGCTCCCA
HTT exon 1 forward	RT-qPCR	GAGTCCCTCAAGTCCTTCCAGCA
HTT exon 1 reverse	RT-qPCR	GCCCAAACTCACGGTCGGT
HTT exon 1 probe	RT-qPCR	CAGCTCCCTGTCCCGGCGG
Hdac1 forward	RT-qPCR	TCTGAATACAGCAAGCAGATGCA
Hdac1 reverse	RT-qPCR	ACAGAACTCAAACAAGCCATCAAAC
Hdac1 probe	RT-qPCR	CGGTCCACACCCGCCACCAG
Hdac2 forward	RT-qPCR	AGAAGATTGTCCGGTGTTTGATG
Hdac2 reverse	RT-qPCR	CACAGCCCCAGCAACTGAA
Hdac2 probe	RT-qPCR	TTGAGTTTTGTCAGCTCTCCACGGGTG
Hdac3 forward	RT-qPCR	TCAGCCCCACCAATATGCA
Hdac3 reverse	RT-qPCR	GAACTCGAAAAGTCCTGGAAACA
Hdac3 probe	RT-qPCR	AGACCTAATGGAACAAAAGTGGCTGTGCTG
Hdac4 forward	RT-qPCR	CTGGCATCCCTGTGTCATTTG
Hdac4 reverse	RT-qPCR	ACACAAGACCTGTGGTGAACCTT
Hdac4 probe	RT-qPCR	CTGCCACCTTCCCCATGTCAGTCC
Hdac5 forward	RT-qPCR	CCAGAGCCGGCATAACT
Hdac5 reverse	RT-qPCR	GCAGGATTTCCAAGATGGTT
Hdac5 probe	RT-qPCR	TTCCACCAGGTGAGAAGAGTGATGACCAT
Hdac6 forward	RT-qPCR	GGAGACAACCCAGTA CATGAATGAA
Hdac6 reverse	RT-qPCR	CGGAGGACAGAGCCTGTAG
Hdac6 probe	RT-qPCR	TATCTGCATCCGAACCTCATATTCCTGTGCCTG
Hdac7 forward	RT-qPCR	CCCACCTGTCAGACCCAAGT
Hdac7 reverse	RT-qPCR	AGTCATAGACCAGCCCTGTAGCA
Hdac7 probe	RT-qPCR	CTCAACAGCTCAGAGACA
Hdac8 forward	RT-qPCR	GGCCCATCCATCCCTGTAG
Hdac8 reverse	RT-qPCR	TTTAGATCGCCGGAGACAGTTT
Hdac8 probe	RT-qPCR	TGGACGAGGGACCAGG
Hdac9 forward	RT-qPCR	TGGCAGAATCCTCGGTCAGT
Hdac9 reverse	RT-qPCR	CCCAGCAGGGCCATTGT
Hdac9 probe	RT-qPCR	TCTCCAGGGTCAGGTCCCAGTTCACC
Hdac10 forward	RT-qPCR	CCGCTATGAGCATGGAAGCT
Hdac10 reverse	RT-qPCR	CAACTGCATCTGCATCAGACTCT
Hdac10 probe	RT-qPCR	CTGGCCGTTTCTC
Hdac11 forward	RT-qPCR	TGGGCATGAGCGAGACTTC
Hdac11 reverse	RT-qPCR	GCGGTTGTAAACATCCATGATG
Hdac11 probe	RT-qPCR	TGGGTGACAAGCGAG
Sirt1 forward	RT-qPCR	TGTTGGTTGACTTCATCTTCCTT
Sirt1 reverse	RT-qPCR	TCCAATGGCTTTTGAAAACTTTA
Sirt1 probe	RT-qPCR	TTCATTTGTATGATACATTCGTATGTATG
Sirt2 forward	RT-qPCR	TCCTGCAGAAAAGAATACACGAT
Sirt2 reverse	RT-qPCR	CGATATCAGGCTTTACCACACTC

Sirt2 probe	RT-qPCR	AGAGAAGATCTTCTCAGAAGCAACTCC
Sirt3 forward	RT-qPCR	ACAAGAACTGCTGGATCTTATGC
Sirt3 reverse	RT-qPCR	TCTTGCTGGACATAGGATGATCT
Sirt3 probe	RT-qPCR	ACGTGGCAAGCTG GATGGACAGGA
Sirt4	RT-qPCR	Assay was purchased from Primer Design
Sirt5 forward	RT-qPCR	CAGAGGCGCTGGAGGTTACTGGAG
Sirt5 reverse	RT-qPCR	CCGGGCTTCACACTGGGCAATGGC
Sirt5 probe	RT-qPCR	AGGCTCAGGACCTGGCAACCCCTCAG
Sirt6	RT-qPCR	Assay was purchased from Primer Design
Sirt7 forward	RT-qPCR	GCCTCCCTCTTTCTACTCCTTATC
Sirt7 reverse	RT-qPCR	TGCTCAGACTGGAGGCTTAGTTA
Sirt7 probe	RT-qPCR	TACAAGTGTTCACTTTATAGAAGCCT
Hmgcr	RT-qPCR	Assay was purchased from Primer Design
Hmgcs1	RT-qPCR	Assay was purchased from Primer Design
Fdft1	RT-qPCR	Assay was purchased from Primer Design
Fdps	RT-qPCR	Assay was purchased from Primer Design
Sqle	RT-qPCR	Assay was purchased from Primer Design
Idi1	RT-qPCR	Assay was purchased from Primer Design
Dhcr7	RT-qPCR	Assay was purchased from Primer Design
Cyp51	RT-qPCR	Assay was purchased from Primer Design
Ampk-α1	RT-qPCR	Assay was purchased from ABI

Table 4. Summary of in house designed primer and probe sequences for qPCR. Primers and probe mixes for *Sirt4*, *Sirt6* and cholesterol pathway genes were purchased from Primer Design. All RT-qPCR probes were labelled 5' with FAM and 3' with TAMRA. RT-qPCR real time-quantitative PCR; *HTT* exon 1 (R6/2 transgene).

Housekeeping genes	Tissue examined
Atp5b-Canx-Rpl13a-Ubc	Cortex
Atp5b-Ywhaz-Ubc	Striatum
Atp5b-Rpl13a-Eif4α2	Cerebellum
Atp5b-Ubc-Gapdh	Hippocampus
Atp5b-Ubc-Gapdh	Brain Stem

Table 5. Housekeeping genes used for specific brain regions. Primer and probe mixes for *Atp5b, Canx, Rpl13a, Ubc, Ywhaz* were purchased from Primer Design. All RT-qPCR probes were labelled 5' with FAM and 3' with TAMRA

Name	Application	5'-3' sequence
Dbc1 forward	Genotyping	GTACCTGGAGGGTTTATGTTACCT
Dbc1 reverse WT	Genotyping	ACAAGGTCTTAAGTAGCTTGGGCTGGC
Dbc1 reverse NEO	Genotyping	CAACCCGTCGGATTCTCCGTG
HTT exon 1 reverse	Genotyping	CCTTCATCAGCTTTTCCAGGGT
HTT exon 1 forward WT	Genotyping	TTTTCTATCGCTGGTGCCAGG
HTT exon 1 forward Tg	Genotyping	CTAGGGCTGTCAATCATGCTGG

Table 6. Primers used for mouse genotyping.

2.1.6 Solutions, buffers and gels

All solutions, buffers and gels were prepared with deionised distilled water (d2H2O).

Inhibitors were added to buffers at the following concentrations:

1 mM PMFS

5 µM TSA

10 mM nicotinamide

Complete protease inhibitor cocktail (1 tablet in 50ml)

Agarose gel for resolution of PCR products (Prepared in 1xTAE)

1.5 % (w/v) Ultra pure agarose

0.1 µg/ml Ethidium bromide

Coomassie staining solution

0.25% (w/v) Brilliant blue R-250

50% (v/v) methanol

10% (v/v) acetic acid

Laemmli loading buffer (2x)

125 mM Tris–HCl pH 6.8

20% glycerol

4% SDS

0.01% (w/v) bromophenol blue

Lysis Buffer for DNA extraction

50 mM Tris-HCl pH 8.0

100 mM EDTA

0.5% (w/v) SDS

0.5 mg/ml proteinase K

NETN buffer

20 mM Tris-HCl pH 8

100 mM NaCl

1 mM EDTA

0.5% NP-40

Complete Inhibitors

Phosphate buffer saline (PBS)

137 mM NaCl

2.7 mM KCl

100 mM Na_2HPO_4

2 mM KH_2PO_4

Adjusted pH to 7.4 with HCl

Phosphate buffer saline (PBS) -Triton

137 mM NaCl

2.7 mM KCl

100 mM Na_2HPO_4

2 mM KH_2PO_4

0.1 % (v/v) Triton X100

Adjusted pH to 7.4 with HCl

Phosphate buffer saline (PBS) -Tween 20

137 mM NaCl

2.7 mM KCl

100 mM Na_2HPO_4

2 mM KH_2PO_4

0.1 % (v/v) Tween 20

Adjusted pH to 7.4 with HCl

Resolving Gel

20-60 % (v/v) (for 6-18% acrylamide gels) Protogel

25 % (v/v) Protogel resolving buffer

1 % (w/v) APS

0.1 % (v/v) TEMED

Stacking gel

13 % (v/v) Protogel

25 % (v/v) Protogel stacking buffer

0.1 % (w/v) APS

0.2 % (v/v) TEMED

TKM buffer

50 mM Tris-HCl pH 7.4

25 mM KCl

5 mM MgCl2

0.25 M Sucrose

Complete Inhibitors

Tris–acetate-EDTA (TAE) buffer (1X)

40mM Tris Base pH 8.0

20mM Acetic Acid

1mM EDTA

Western blot transfer buffer

25 mM Tris-HCl pH 8.3

192 mM glycine

20 % (v/v) methanol

2.1.7 Computer programs and internet pages

AM Logger (Linton Instrument)

BLAST (NCBI)

Excel (Microsoft)

GraphPad (California Corporation)

ImageJ (National Institute of Health)

Omega (BMG Labtech)

Pubmed (NCBI)

Quantity one (Bio-Rad)

SPSS statistics software (IBM)

Vector NTI (Invitrogen)

Methods

2.1.8 Ethics statement

All experimental procedures performed on mice were approved by the King's College London Ethical Review Process Committee and carried out under a Home Office License.

2.1.9 Mouse Strains

Hemizygous R6/2 mice (Mangiarini et al., 1996) were bred by backcrossing R6/2 males to (CBA × C57BL/6) F1 females (B6CBAF1/OlaHsd; Harlan Olac). *Hdh*Q150/Q150 homozygous mice (Woodman et al. 2007) on a (CBA×C57BL/6)F1 background were generated by intercrossing *Hdh*Q150/Q7 heterozygous CBA/Ca and C57BL/6J congenic lines (inbred lines from Harlan Olac). *Dbc1* heterozygous mice were obtained from the Mayo Foundation, Mayo Clinic College of Medicine, Rochester, Minnesota, USA (Escande et al., 2010). *SirT1* floxed homozygous (SirT1 Fl/Fl) mice were obtained from the JAX Laboratory (Mouse Strain: B6;129-SirT1tm1Ygu/J) and were bred with β-actin/cre heterozygous mice to generate complete *Sirt1*KO mice.
Sirt1 heterozygous transgenic mice (CBA×C57BL/6J) were obtained from Washington University MI.

2.1.10 Mouse husbandry

At 4 weeks of age, mice were weaned into cages of 5 - 6 animals (*Dbc1*KO x R6/2 phenotypic assessment study only). Each cage contained at least one representative of each genotype. Animals were housed under 12 h light / 12 h dark cycle, with unlimited access to water and food (Special Diet Service, Witham, UK). Cages were environmentally enriched with a cardboard tube (Hockly et al., 2003). R6/2 mice and

all mice in phenotypic assessment trials were always given mash food consisting of powered chow mixed with water from 14 weeks of age until sacrificed.

2.1.11 Mouse genotyping and repeat sizing

All mice were genotyped by PCR of tail tips or ear punches. Tail tips or ear punches were collected at 10 - 14 days of age. The tissue was digested O/N in 300 µl of lysis buffer at 55^{o}C. DNA was precipitated using 200 µl of isopropanol. The DNA was pelleted by centrifugation at 13,000 x *g* for 15 min. The supernatant was discarded and pellets were washed with 70% ethanol, spun for 10 min at 13,000 x *g* and the supernatant removed. Pellets were air dried until all ethanol had evaporated and then re-suspended in 100 µl of 5 mM Tris HCl, pH 7.5.

*Dbc1*KO mice were genotyped with 1 µl of each primer (3 primers) (Table 6) diluted 1:8 (10 µM). 25 µl multiplex reaction also containing 1 µl 50 ng/µl DNA, 2 µl 10 mM dNTP, 5 µl 5X Green GoTaq Reaction Buffer and 0.125 µl GoTaq polymerase. Cycling condition were as follows: 94^{o}C for 5 min, (94^{o}C for 30 s, 62^{o}C for 25 s and 72^{o}C for 45 s) x35, followed by 6 min at 72^{o}C.

R6/2 mice were genotyped with 1 µl of *HTT* exon1 forward Tg and WT primers diluted 1:10 (10 µM) and 1:5 (20 µM) respectively (Table 6). 25 µl multiplex reaction also containing 1 µl 50 ng/µl DNA, 2 µl 10 mM dNTP, 5 µl 5X Green GoTaq Reaction Buffer and 0.125 µl GoTaq polymerase. Cycling condition were as follows: 94^{o}C for 5 min, (94^{o}C for 30 s, 62^{o}C for 25 s and 72^{o}C for 45 s) x35, followed by 6 min at 72^{o}C.

Amplification of the CAG repeat from R6/2 tail DNA was performed with a FAM labelled forward primer and an unlabelled reverse primer in 10 µl reaction containing 100 ng DNA, 0.2 mM dNTPs, 10% DMSO, 1X AM Buffer and 0.5 U AmpliTaq DNA polymerase, using cycling condition of 90 s at 94^{o}C, 94^{o}C for 30 s, 65^{o}C for 30 s and

72°C for 90 s) x24, followed by 10 min at 72°C. Sequencing reactions (FAM-tagged PCR product (1 µl), internal MegaBACE ET90 size standard (0.04 µl) and HiDi-formamide (9 µl)) were denatured at 94°C for 5 min before analysis of products using an ABI3730 sequencer. Data analysis was performed using GeneMapper v5.2 - 3730xl.

2.1.12 Mouse behavioural analysis

All tests were performed blind to the genotype. Body weight and brain weight were determined, immediately after cervical dislocation, using a digital balance.

Forelimb grip strength was assessed at 4 weeks of age and then bi-weekly from 7 weeks of age using a grip strength meter. To measure grip strength, mice were swung gently by the tail so the central bar was securely gripped by the forelimbs. Mice were pulled backwards until the grip on the metal frame was released. The force exerted was recorded by the meter. Five measurements were performed and the best three scores were used for statistical analysis.

Motor coordination was assessed using an Ugo Basile 7650 rotarod, modified to accelerate from 4 to 44 rpm over 300 s. Bicycle inner tubing (Evans Cycle, London, UK) was used to cover the ridges on the plastic drum to provide a smooth non-slip surface. Mice were placed on the rotarod drum for 20 s for acclimatisation before the rotarod was allowed to accelerate. Mice were measured three times a day for 4 days at 4 weeks of age. At 6-, 8-, 10-, 12- and 14 weeks of age, mice were tested three times a day for three days. Data for the first day were not used for statistical analysis.

Spontaneous exploratory motor activity was measured bi-weekly from 5 - 13 weeks of age by placing mice individually in the AM1053 activity cages for 30 min during the light phase. Each cage measured 367 x 207 x 140 cm, had a thin layer of wood chippings, four food pellets and a water bottle distributed so as not to interfere

with the array of infrared beams that measured the mouse activity and mobility. Mice were tested at the same time of day, with male mice always tested before female mice and cages cleaned thoroughly in between the two sexes. Data collection was started immediately after the mouse was placed in the activity cage, by the AM logger software recording the number or beam breaks occurring in 1 min intervals. Data was then exported to Microsoft Excel and analysed for activity (total number of beam brakes in the lower level), mobility (at least two consecutive beam breaks in the lower level), rearing (beam breaks in the upper level) and centre rearing (beam breaks in upper level away from the cage walls).

2.1.13 Tissue preparation

Dissected half brains, brain regions or peripheral tissues were snap frozen in liquid nitrogen and stored at –80^{o}C.

2.1.14 Protein extraction for SDS-PAGE, Western Blotting and Immunoprecipitation

Frozen mouse brain tissue was homogenized in 1 volume of ice cold NETN buffer using a polytron homogenizing probe. Samples were sonicated on ice with vibracell sonicator (10 x 1 s 20 kHz pulses) and spun at 13,000 x *g* for 10 min at 4^{o}C. The supernatant was retained and protein concentrations were determined for each sample by BCA assay.

2.1.15 SDS-PAGE and Western blotting

Protein lysates were diluted with 2X Leammli Buffer and denatured for 10 min at 95^{o}C. Samples, containing an equal amount of protein were loaded for SDS-PAGE analysis. Proteins were separated by running gels at 130 V in 1X SDS-PAGE running buffer and the migration of proteins was determined using the Spectra pre-stained protein marker. Proteins were transferred onto a nitrocellulose membrane at 120 V for 75 min

by submerged transfer apparatus in transfer buffer. Membranes were then blocked in 5% non-fat dried milk in PBS – 0.2% Tween 20 (PBS-T) or 4% BSA for 2 h at RT. Primary antibodies were added overnight at 4^{o}C in 5% non-fat dried milk in PBS-T (DBC1, SIRT1, EM48, Fl-HTT, AMPKα1) or 4% BSA in PBS-T (MpM2). For loading controls of cytoplasmic and nuclear fractionations, membranes were incubated with either β-actin, ATP5B, α-tubulin and histone Pan-H3 for 20 min at RT in 5% non-fat dried milk in PBS – 0.2% Tween 20 (PBS-T). Blots were washed three times for 10 min in 0.2% PBS-T and incubated with the appropriate secondary antibody. The signal was developed using ECL hyper-film and a Xenograph developer. Densitometry of the western blot was performed using a GS-800 densitometer. Developed films were scanned and each band was quantified using QuantityONE. The average pixel density (OD) was measured and the values obtained from the bands of interest were normalised to the OD of α-tubulin, ATP5B or β-actin.

All antibodies used are summarized in Table 3.

2.1.16 Immuno-precipitation

Protein lysates were prepared for IP as described above. Immunoprecipitation reactions were performed in 1 ml of NETN buffer containing from 400 to 1000 µg protein and 1 µg of antibody. Normal rabbit IgG (#2729; Cell Signalling) was used as a negative control. 15 µl of protein G-magnetic beads were added for the last 45 min. Reactions were left on a rotating wheel at 4^{o}C for 90 min (AMPKα1) or 4 h (SIRT1 and DBC1), following which, protein G-magnetic beads were pelleted by brief centrifugation at 13,000 x *g* for 30 s, put on a magnetic rack, washed 4X with 1 ml of NETN buffer and re-suspended in 15 µl of 2X Leammli buffer. Immuno-precipitated

complexes were eluted from the beads by denaturation at 100^{o}C for 10 min and immediately loaded for SDS-PAGE analysis.

2.1.17 Nuclear/Cytoplasmic fractionation

All steps were performed on ice. Brain tissue was cut into small pieces and homogenized 10X with a Dounce homogenizer in TKM buffer (0.25 M sucrose; 50 mM Tris-HCl, pH 7.4; 25 mM KCl; 5 mM MgCl2 and 1 mM PMSF). The homogenate was filtered through cheesecloth and centrifuged twice at 800 x *g* for 10 min. The supernatant, containing the cytoplasmic fraction, was cleared with a centrifugation at 13,000 x *g* for 10 min. The resuspended pellet was added to the top of tubes that contained an equal volume of a cushion composed (from top to bottom) of 0.5 ml 1.0 M sucrose solution, 0.5 ml 1.5 M sucrose solution, and 1.5 ml 2.1 M sucrose solution, all in TKM buffer. Tubes were centrifuged at 28000 x *g* for 60 min, and the resulting pellet was resuspended in homogenizing medium and sedimented at 800 x *g* for 10 min. The final pellet containing the purified nuclei was resuspended in 4% PFA to perform an immunohistochemical analysis or in NETN buffer and protein concentration was determined for each sample by BCA assay.

2.1.18 Immunohistochemistry

Isolated brain nuclei were extracted as described above. Samples were fixed on the slide for 30 min with 4% paraformaldehyde prepared in PBS, permeabilized with 0.1% Triton X-100 in PBS for 15 min, washed 3X with PBS, and incubated for 1 h at RT in blocking buffer (PBS with 0.1% Triton and 1% BSA). Nuclei were incubated with the primary antibody in blocking buffer (DBC1, SIRT1, P53 and Ac-P53) overnight at 4^{o}C, washed 3X with PBS at RT and then incubated with the secondary antibody and DAPI in

PBS-0.1% Triton for 1 h at RT. Samples were mounted using VECTASHIELD mounting medium. Nuclei were visualized using a Leica confocal microscope.

2.1.19 RNA extraction

RNA extraction was performed using QIAZOL, an RNeasy mini-kit and Rnase-free DNaseI supplied by Qiagen, according to manufacturer's instructions. All steps were performed at RT. Frozen mouse tissues were homogenized in 0.5 ml of QIAZOL using a polytron homogenization probe and snap-frozen on dry ice. After thawing, the homogenates were left for 5 min at RT. Subsequently, 200 µl of chloroform was added and the homogenates were shaken vigorously for 10 s and spun at 11400 x *g* for 15 min at 4^{o}C and the resulting upper aqueous phase was transferred to a new polypropylene tube containing 300 µl of 70% ethanol. After mixing, samples were transferred to an RNeasy Mini spin column in a 2 ml collection tube. Binding of the RNA and all subsequent washing steps were achieved by centrifugation for 15 s at 13,000 x *g*. Columns were washed with 350 µl buffer RW1 (provided with the kit) and 80 µl of Qiagen RNase-free DNaseI (10 µl DNaseI stock in 70 µl RDD buffer) was added to the column and incubated at RT for 30 min. Columns were washed again with 350 µl buffer RW1 and then twice with 500 µl buffer RPE (provided with kit). Columns were spun again at 13,000 x *g* to remove any residual buffer. Columns were placed in 1.5 ml collection tubes and 40 µl of RNase-free water was added directly to column membranes and incubated for 1 min before centrifugation. RNA concentrations were assessed by measuring the absorbance at 230 nm and 260 nm by a nanodrop spectophotometer (Thermo Scientific) for each sample.

2.1.20 cDNA synthesis

Reverse transcription reactions were performed by adding 1 µg of total sample RNA to 9 µl of DEPC water, 2 µl of DTT (0.1 M) and 1 µl of random hexamers (100 ng/µl). Samples were then incubated at 94^{o}C for 2 min. 8 µl of mastermix (0.75 µl DepC H_2O, 4 µl MMLV-RT 1st strand buffer (5X), 2 µl dNTPs (10 mM) and 0.25 µl of RNAsin was added to each sample. Reverse transcription reactions were performed in a Dyad thermocycler using conditions of 23^{o}C for 10 min, 37^{o}C for 40 min and 95^{o}C for 5 min. The resulting cDNA was cooled to 4^{o}C and diluted 1:10 with ultra-pure water.

2.1.21 Real time quantitative PCR (qPCR)

Taqman RT-qPCR reactions were performed in triplicate for each sample using white 96 well PCR plates and the CFX96 Real-Time System (Bio-Rad). For assays purchased from Primer Design, 3 µl of cDNA was incubated with 0.6 µl primer/probe mix, 6 µl precision Master Mix (2X) and 2.4 µl water. For other assays, 3 µl of cDNA was combined with 0.45 µl of each primer (100 µM), 0.3 µl of probe (100 µM), 7.5 µl of precision Master Mix (2X) and 3.3 µl of water. The reactions for houskeeping genes were incubated for 10 min at 95^{o}C, followed by 40 cycles of 95^{o}C for 15 s, 50^{o}C for 30 s and data were collected. The reaction for genes of interest incubated for 10 min at 95^{o}C, followed by 40 cycles of 95^{o}C for 15 s, 60^{o}C for 30 s and data were collected. Gene expression was then calculated relative to levels of houskeeping genes using the ΔCt method.

All Taqman RT-qPCR primers used are summarized in Table 4

2.1.22 Fluor de Lys assay

SIRT1 activity was determined with a SIRT1 Fluorometric Kit (Biomol International) according to the manufacturer's instructions. Protein extraction was performed as described above. Homogenates were then incubated for 10 min at 37^{o}C to allow degradation of any contaminant NAD^{+}. Next, 10 mM DTT was added to the medium, and homogenates were incubated again for 10 min at 37^{o}C. The homogenates (20–30 µg protein/well) were then incubated in SIRT1 assay buffer in the presence of either 100 µM Fluor de Lys–SIRT1 substrate (Enzo Life Sciences) and 5 µM TSA to determine the SIRT1-independent activity, or with 100 µM Fluor de Lys–SIRT1 substrate, 5 µM TSA, and 200 µM NAD^{+} to determine the SIRT1-dependent activity. After 60 min of incubation at 37^{o}C, the reaction was terminated by adding a solution containing Fluor de Lys Developer (Enzo Life Sciences) and 2 mM nicotinamide. Plates were incubated at 37^{o}C for 0-, 20-, 40- and 60 minutes. Values were determined by reading fluorescence on a fluorometric plate reader (Spectramax Gemini XPS; Molecular Devices) with an excitation wavelength of 360 nm and an emission wavelength of 460 nm.

2.1.23 Statistical Analysis

Statistical analysis was performed with SPSS (one-way ANOVA multiple comparisons and repeated measures ANOVA General Linear Model) or Microsoft Excel (Student's *t*-test) software. For mouse phenotypic assessment, weight, rotarod and grip strength were analysed with repeated measures ANOVA and at each time point with one-way ANOVA multiple comparisons. Brain weight was analysed by one-way ANOVA multiple comparisons. Activity was analysed with repeated measures ANOVA at each time point

separately. For western blotting, IP and qPCR, group means were compared by Student's *t* -test or one-way ANOVA multiple comparisons.

Chapter 3

RESULTS: SIRT1 ACTIVITY IS IMPAIRED IN HD MOUSE MODELS

3.1 Measurement of SIRT1 activity in the mouse brain

There is considerable evidence to support a beneficial effect of SIRT1 overexpression in HD mouse models, although the impact of this pathology on SIRT1 functions has not been fully elucidated. As such, we decided to analyse SIRT1 activity and the mechanisms involved in its regulation in two different HD mouse models, R6/2 and *Hdh*Q150 homozygous mice.

To measure SIRT1 activity in the HD brains we needed an assay able to detect specifically SIRT1 activity. Interestingly, studies have demonstrated that SIRT1 binds to and regulates the activity of several transcription factors among which is P53 (Langley et al., 2002). SIRT1 can interact with and deacetylate P53 on Lys382 inhibiting its function (Solomon et al., 2006). Indeed, we tested two different assays able to measure the ability of SIRT1 to deacetylate P53:

1. Fluor de Lys assay (BML-AK555)
2. Immunohistochemistry assay on isolated nuclei

3.2 Measurement of SIRT1 activity with Fluor de Lys assay

To validate a method for measuring SIRT1 activity in mouse tissues we used the commercial kit (BML-AK555). This assay uses a small lysine-acetylated peptide, corresponding to K382 of human P53, as a substrate. The lysine residue is deacetylated by SIRT1, and this process is dependent on the addition of exogenous NAD^+. Deacetylation of the substrate sensitises the substrate so that, in the second

step, treatment with the Fluor de Lys-Developer II produces a fluorophore (Fig. 15). Values were determined by reading fluorescence on a fluorometric plate reader.

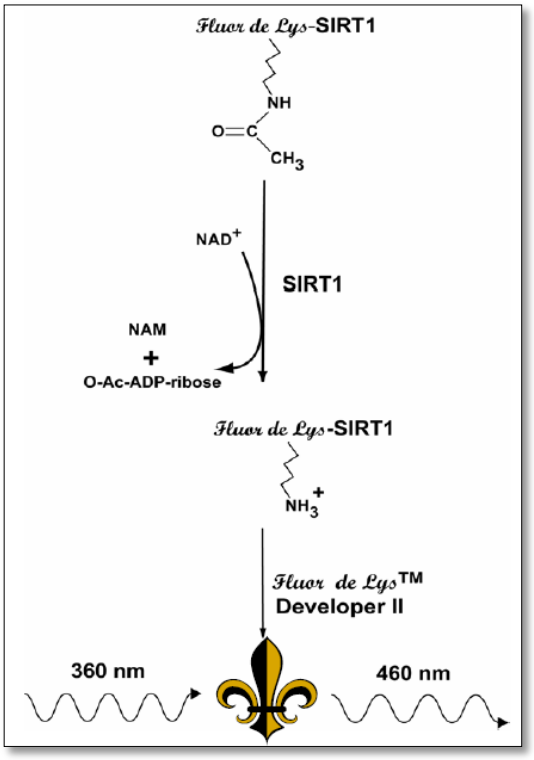

Figure 15. Reaction scheme of the SIRT1 Fluorescent Activity Assay. NAD^+-dependent deacetylation of the substrate by recombinant human SIRT1 sensitizes it to Developer II, which then generates a fluorophore (symbol). The fluorophore is excited with 360 nm light and the emitted light (460 nm) is detected on a fluorometric plate reader. NAD^+ is consumed in the reaction to produce nicotinamide (NAM) and O-acetyl-ADP-ribose.

In order to investigate the specificity of the Fluor de Lys assay for SIRT1 activity, we performed a test including WT samples, SIRT1-recombinant human protein and *Sirt1*$^{-/-}$ knock-out (*Sirt1*KO) samples at three different substrate concentrations (50 µM, 100 µM and 200 µM):

- ✓ WT sample: we added the cortex lysate from WT mice, the substrate and NAD^+
- ✓ SIRT1-recombinant human protein: we added SIRT1 recombinant human protein, the substrate and NAD^+
- ✓ *Sirt1*KO sample**:** we added the cortex lysate from *Sirt1*KO mice, the substrate and NAD^+

Unfortunately, no differences could be detected with the Fluor de Lys assay between WT and *Sirt1*KO tissues (Fig. 16). This result suggests that the Fluor de Lys assay (BML-AK555) is not specific for SIRT1 activity and that it is not an appropriate tool to measure SIRT1 activity in animal tissue lysates.

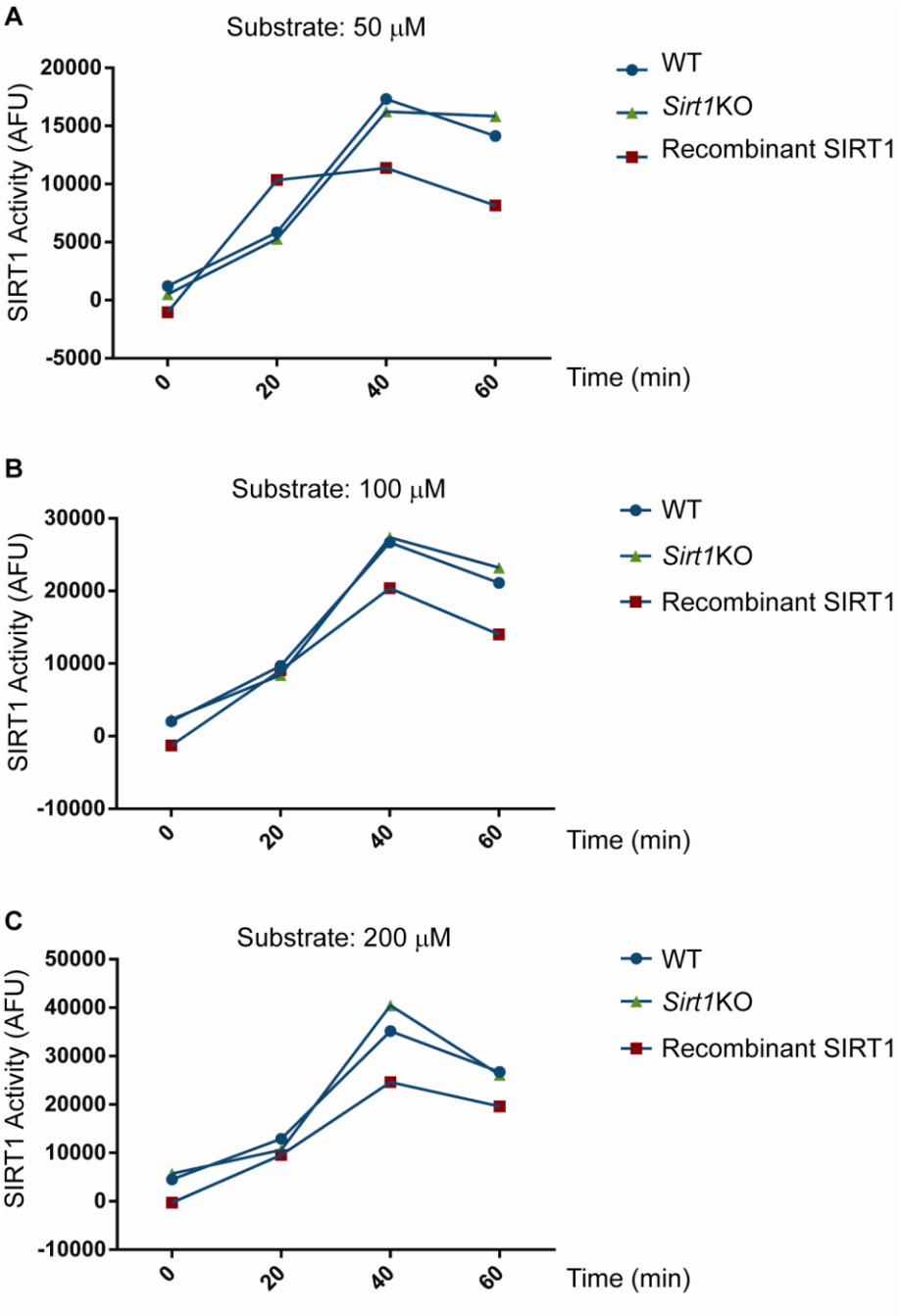

Figure 16. Measurement of SIRT1 activity with Fluor de Lys assay. Fluorescence signal obtained after 0, 20, 40 and 60 minutes of incubation at 37 ^{o}C. 25 μg of protein from cortex lysates of WT or *Sirt1*KO mice and 2U/well of SIRT1-recombinant protein were incubated with 50, 100 or 200 μM of substrate and with 200 μM of NAD^{+}. N=2/genotype.

3.3 Measurement of SIRT1 activity with immunohistochemistry on isolated nuclei.

To monitor SIRT1 activity on P53, we isolated cell nuclei from mouse brains to perform an immunostaining assay. To confirm the specificity of this assay we immunostained nuclei extracted from half brains of *Sirt1*KO and *Sirt*1 transgenic (*Sirt1*Tg) mice at 4 weeks of age. Nuclei were immunostained for SIRT1, P53 and acetylated-P53 (AcP53), and counterstained with DAPI. To measure specifically SIRT1 activity we used an acetylated-P53 antibody able to recognize the acetylation of a Lys- residue that can be deacetylated only by SIRT1. We did not detect any variation in the intensity level of P53 staining between *Sirt1*KO and *Sirt1*Tg mice samples and the corresponding WT (Fig. 17 A and B). Interestingly, we also observed increased levels of AcP53 in the brain of *Sirt1*KO mice and a decrease in the acetylation of endogenous P53 in the *Sirt1*Tg samples, consistent with a decrease in SIRT1 activity in the knock-out line and an increase in SIRT1 activity in the transgenic line respectively (Fig. 17 A and B). The genotypes of the mice used for the experiment were confirmed by western blot (Fig. 18 C). This result suggests that the immunohistochemistry assay is specific for SIRT1 activity and that it is an appropriate tool to measure SIRT1 activity in animal tissues.

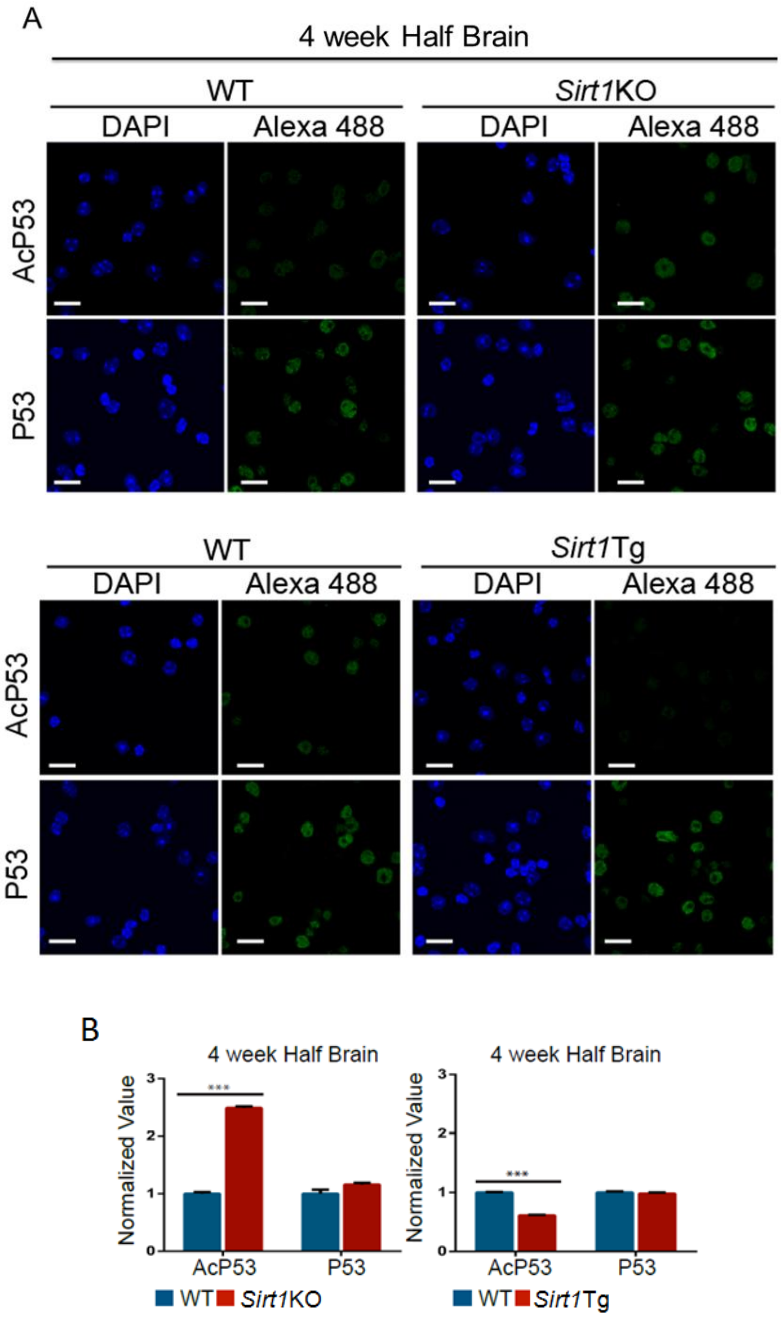

Figure 17. SIRT1 activity is reduced in SIRT1 knock-out and increased in SIRT1 transgenic mice. (A) Representative immunofluorescence image of isolated nuclei extracted from half brains from *Sirt1*KO and *Sirt1*Tg mice brains at 4 weeks of age immunostained for P53 and AcP53 and counterstained with DAPI. To measure specifically SIRT1 activity we used an acetylated-P53 antibody able to recognize the acetylation of a Lys- residue that can be deacetylated only by SIRT1. (B) Relative intensity level of P53 and AcP53 from the immunostained nuclei shown in A. The quantification indicates that the level of acetylated p53 is higher in the *Sirt1*KO mice, consistent with a decrease in SIRT1 activity and lower in *Sirt1*Tg mice, consistent with a increase in SIRT1 activity. Data are the mean ± SEM. *** $p<0.001$. Scale bar, 10 µm; n=4 / genotype.

3.4 *Sirt1KO* mice express the inactivated form of SIRT1

Previously we showed that *Sirt1*KO mice are characterized by a decrease in SIRT1 function. Despite this, they did not show any reduction in the intensity level of SIRT1 as compared to WT littermates (Fig. 18 A and B). The western blot analysis shows clearly that the full-length form of SIRT1 is not produced in the *Sirt1*KO mice and the SIRT1 doublet (first and second band from the top) is shifted down as compared to WT and *Sirt1* transgenic mice (Fig. 18 C). The unchanged intensity level of SIRT1 in the immunohistochemistry and the shift of SIRT1 doublet in *Sirt1*KO mice, shown by western blot, indicate that the mechanism used to induce the ablation of SIRT1 in these mice is not able to knock out the protein but it is efficient to inactivate SIRT1.

The region that encode for the catalytic domain of SIRT1 is located in the exon 4. To generate the *Sirt1*KO mice the exon 4 has been floxed (Fig. 18 D). Since the exon 4 comprises 153 bp when it is removed the reading of the protein is still in frame promoting the translation of the inactivated form of SIRT1. Without the exon 4 the translated protein is less heavy as compared to the full-length and this can explain the shift down of the SIRT1 doublet. The antibody used to detect SIRT1 recognizes a C-terminal amino acid epitope (722-737 aa) of mouse SIRT1, this further confirms the ability of this antibody to detect both full-length SIRT1 and its inactivated form.

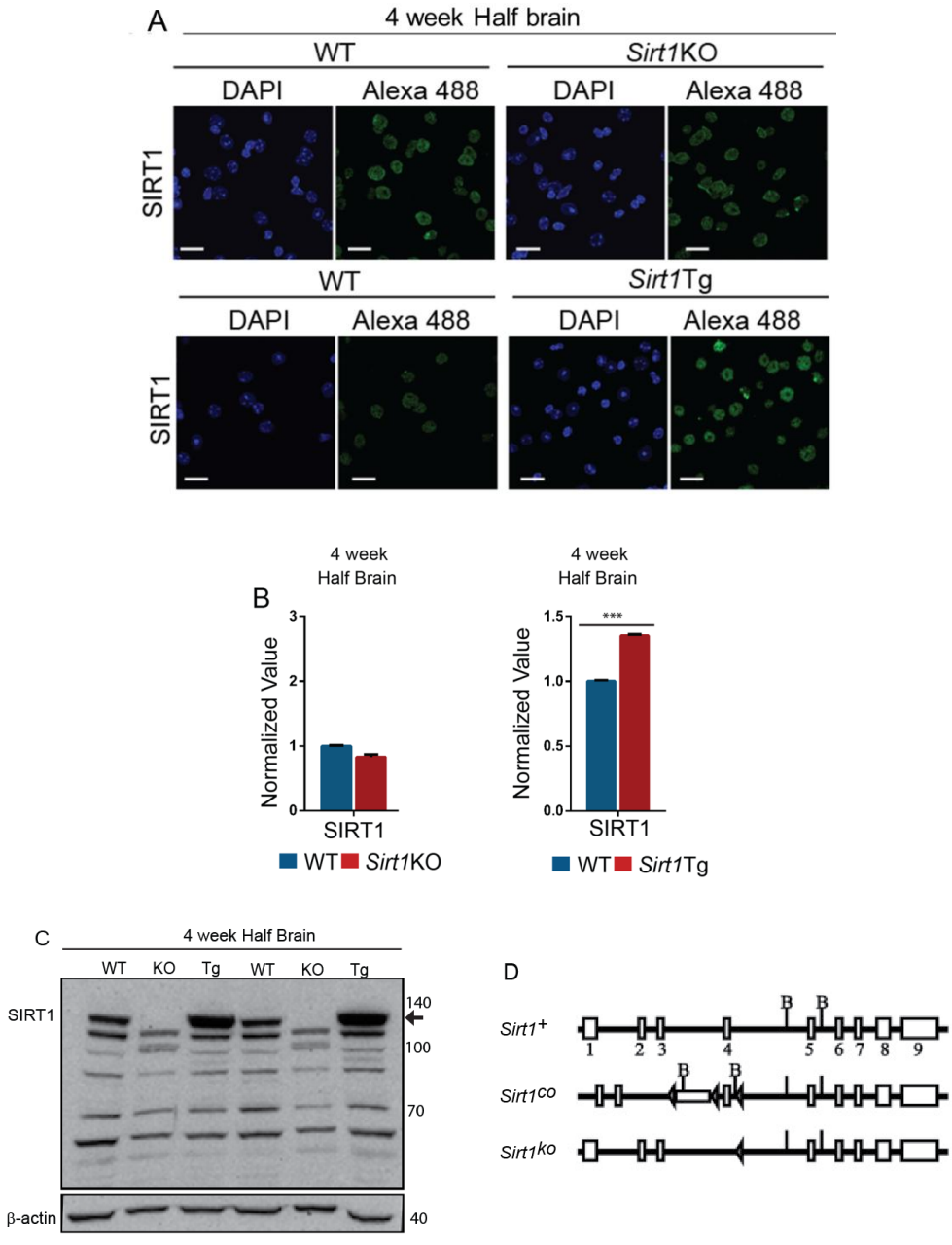

Figure 18. SIRT1 levels in SIRT1 knock-out and SIRT1 transgenic mice. (A) Representative immunofluorescence image of isolated nuclei extracted from half brains from *Sirt1*KO and *Sirt1*Tg mice brains at 4 weeks of age immunostained for SIRT1 and counterstained with DAPI. (B) Relative intensity level of SIRT1 from the immunostained nuclei shown in A. (C) Representative western blot for SIRT1 in half brains from *Sirt1*KO and *Sirt1*Tg mice at 4 weeks of age. (D) Mouse *Sirt1* wild-type allele ($Sirt1^{+}$), conditional targeted allele ($Sirt1^{co}$), and knockout allele ($Sirt1^{ko}$). Data are the mean ± SEM. *** p<0.001. Scale bar, 10 µm; KO: *Sirt1*KO; Tg: *Sirt1*Tg. n=4 / genotype.

3.5 *Sirt1*tg mice overexpress SIRT1

The *Sirt1* transgenic mouse line was generated by the overexpression of the hemagglutinin-tagged (HA tagged) *Sirt1* transgene driven by the mouse prion protein promoter (PrP). The *Sirt1* transgene (HA tagged) was constructed by inserting a 2.3-kb fragment of mouse *Sirt1* cDNA into the vector carrying the mouse PrP promoter. The PrP-*Sirt1*-HA transgene was linearized, purified and microinjected into C57BL/6J × CBA hybrid blastocysts in the Washington University Mouse Genetic Core Facility (Satoh et al., 2010). The *Sirt1*Tg tissues show an increase of the intensity level of SIRT1 staining followed by an increase of SIRT1 activity , as compared to WT littermates (Fig. 17 A and B, Fig. 18 A and B). The genotype is also confirmed by western blot (Fig. 18 C).

3.6 SIRT1 function is progressively compromised in the brains of HD mice

To understand the impact of HD pathology on SIRT1 activity, we isolated cell nuclei from half brains of R6/2 mice at 4, 9 and 14 weeks of age, *Hdh*Q150 homozygous mice at 2 and 22 months of age and aged-matched control WT mice. Nuclei were immunostained for SIRT1, P53 and acetylated-P53 (AcP53), and counterstained with DAPI. Notably, we did not detect any variation in the intensity level of SIRT1 and P53 staining between HD samples and the corresponding WT at each age of analysis (Fig. 19 A and B). Interestingly, we found that the levels of acetylation of endogenous P53 was equivalent in HD as compared to WT brains at an early stage of the disease (i.e. 4 week R6/2 and 2 month *Hdh*Q150 homozygous), whereas the level of AcP53 was significantly higher (≥ 1.5 fold) in the HD samples as the disease progressed, suggesting that SIRT1 activity became impaired in the brains of HD mice (Fig. 19 A and B).

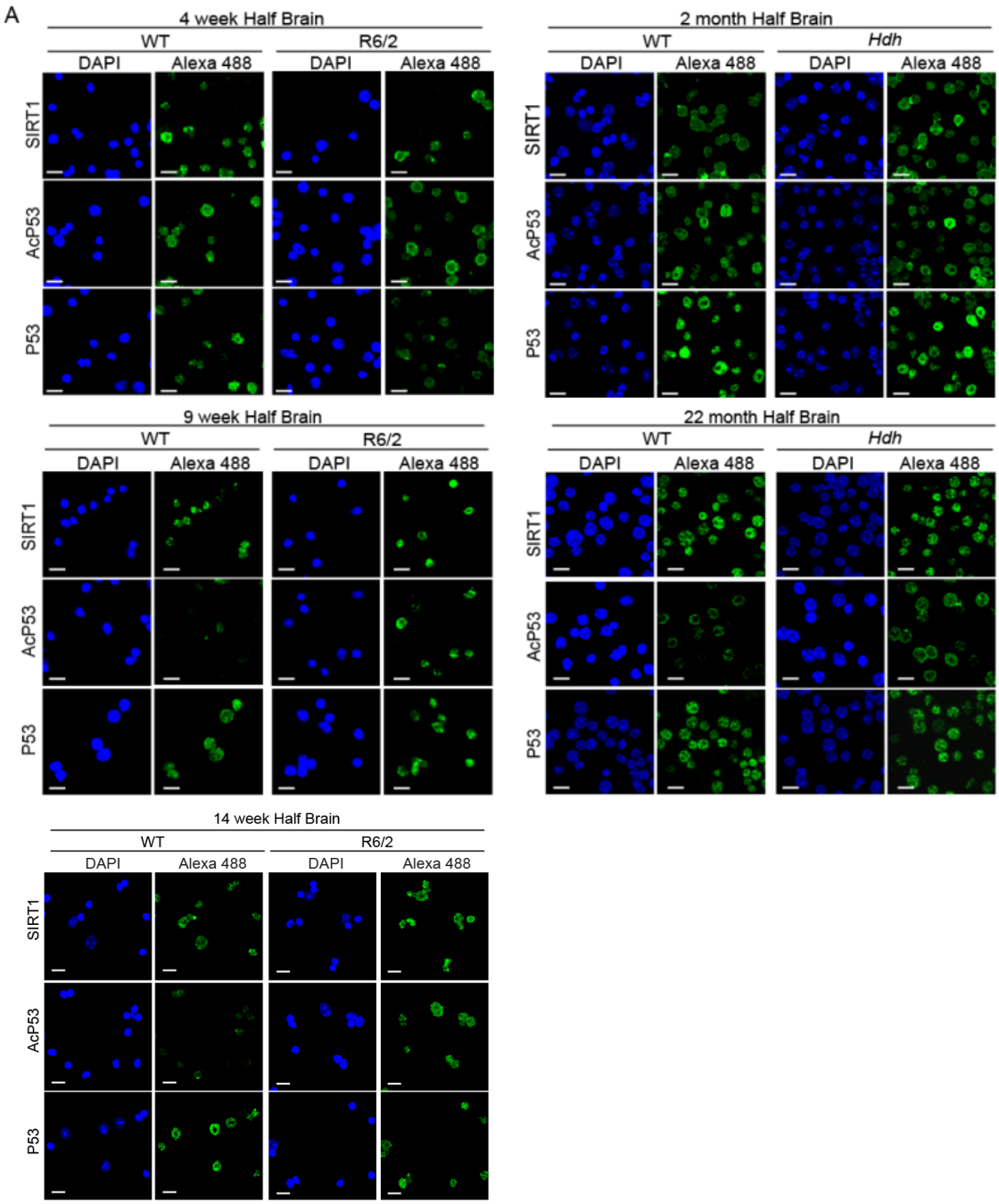

Figure 19 A. SIRT1 activity became reduced with disease progression in HD mouse models. Representative immunofluorescence image of isolated nuclei extracted from half brains from R6/2 mice at 4, 9 and 14 weeks of age and *Hdh*Q150 homozygous at 2 and 22 months immunostained for SIRT1, P53 and AcP53 and counterstained with DAPI. To measure specifically SIRT1 activity we used an acetylated-P53 antibody able to recognize the acetylation of a Lys- residue that can be deacetylated only by SIRT1. *Hdh*, *Hdh*Q150 homozygotes. n=4 / genotype.

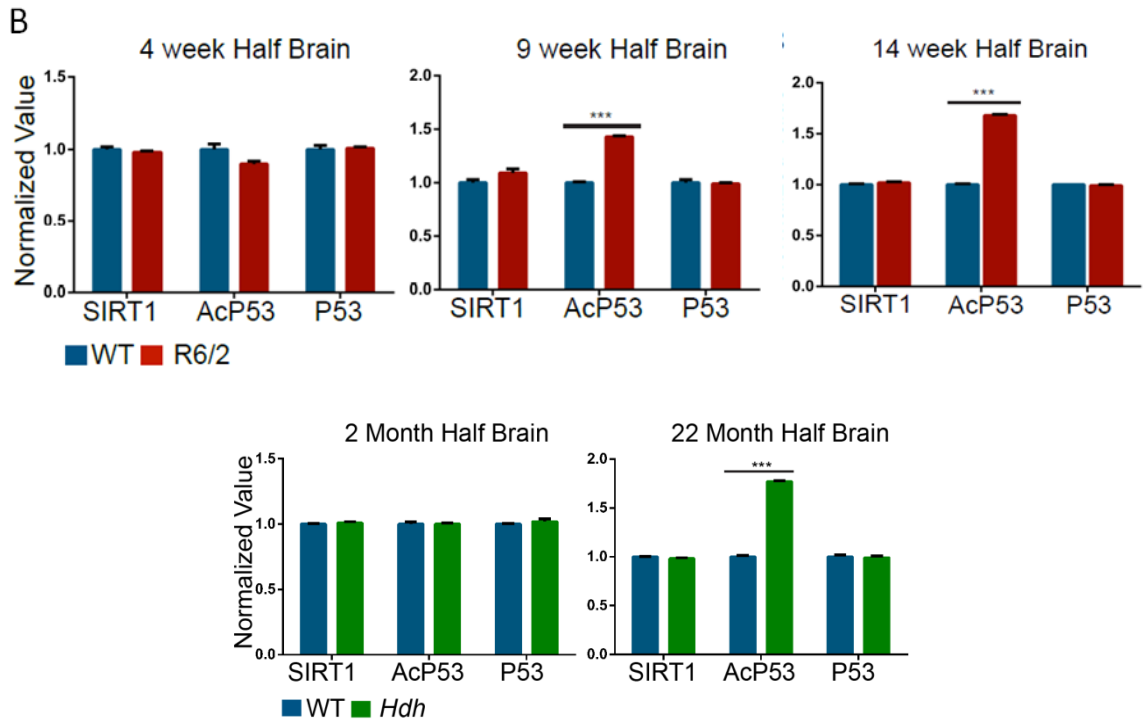

Figure 19 B. SIRT1 activity became reduced with disease progression in HD mouse models. Relative intensity level of SIRT1, P53 and AcP53 from the immunostained nuclei shown in A. The quantification indicates that the level of acetylated P53 is higher in the HD models, consistent with a decrease in SIRT1 activity. Data are the mean ± SEM. ****p*<0.001. Scale bar, 10 µm. *Hdh*, *Hdh*Q150 homozygotes. n=4 / genotype.

3.7 SIRT1 does not co-localize with mutant HTT inclusions and is aberrantly phosphorylated in HD mice

Previous studies showed that SIRT1 interacts with HTT *in vitro* (Jeong et al., 2011). To rule out the sequestration of SIRT1 into mHTT inclusions as the cause of altered SIRT1 activity, we performed a double staining for SIRT1 and HTT (EM48) on nuclei isolated from half brains of 14 week R6/2, 22 month *Hdh*Q150 homozygous and age-matched WT mice. Interestingly, we did not detect a co-localization of SIRT1 with mHTT inclusions (Fig. 20 A). To further support this finding, we did not observe any reduction in SIRT1 protein in HD brains by western blot as compared to WT mice (Fig. 20 B).

The role of post-translational modifications (PTMs) in the regulation of SIRT1 activity has been the subject of several studies and phosphorylation has been described as a major control mechanism (Sasaki et al., 2008) (Fig. 10). Therefore, in the attempt to understand how mHTT can affect SIRT1 activity, we decided to monitor the phosphorylation status of SIRT1 in HD mice. We performed SIRT1 immunoprecipitation from half brains of R6/2 mice at 9 weeks of age and *Hdh*Q150 homozygous mice at 22 months of age and detected the phosphorylation level of SIRT1 by western blot using MpM2 antibody (Westendorf et al., 1994). MpM2 antibody can be used to detect phosphorylation on Serine and Threonine residues followed by Proline (S/T-P sites) present on any protein and it is not specific for any particular phosphorylation sites (full sequence of SIRT1 protein and residues Ser-Pro and Thr-Pro can be found in the Appendix 1). Interestingly, both R6/2 and *Hdh*Q150 homozygous showed a higher level of phosphorylated SIRT1 as compared to the corresponding WT mice (Fig. 20 C). As previously shown *in vitro* (Jeong et al., 2011), we were also able to co-immunoprecipitate endogenous full-length wild-type HTT from R6/2 lysates and both

mutant and wild-type HTT from *Hdh*Q150 homozygous and WT lysates respectively (Fig. 20 C).

These results suggest that the impairment of SIRT1 function in the brain of HD mice may not be related to a sequestration into mHTT inclusions and that the link might be found in an altered phosphorylation profile.

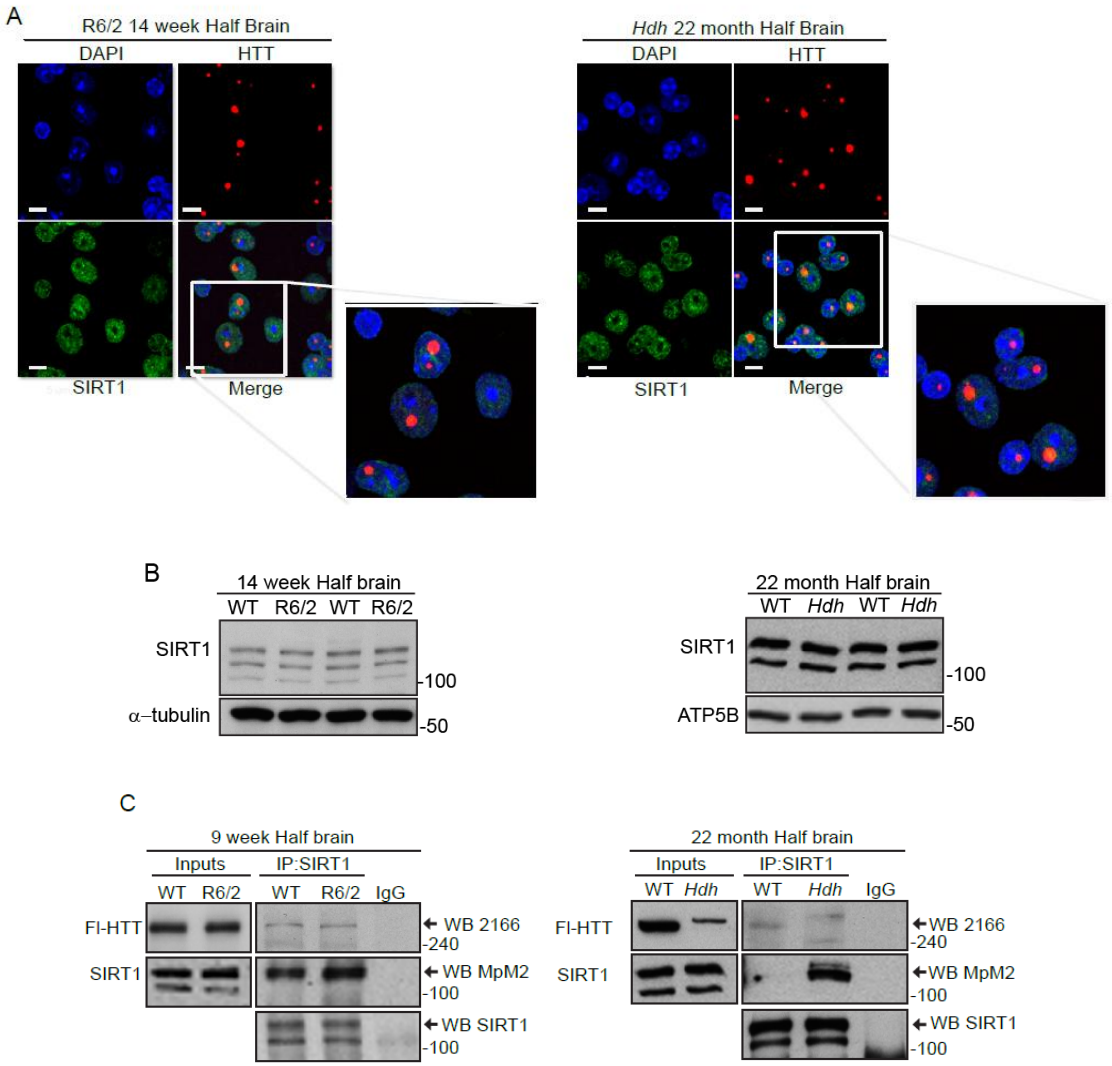

Figure 20. SIRT1 does not co-localize with HTT inclusions and is aberrantly phosphorylated in HD mice. (A) Representative immunofluorescence image of isolated nuclei extracted from half brains from R6/2 mice at 14 weeks of age and *Hdh*Q150 homozygotes at 22 months immunostained for both SIRT1 and mHTT (EM48), and counterstained with DAPI. (B) Representative western blot showing SIRT1 levels in half brains from R6/2 mice at 14 weeks of age and *Hdh*Q150 homozygotes as compared to their WT littermates. Note the shift of Fl-HTT in *Hdh*Q150 homozygous mice as compare to WT littermates. (C) Western blots of SIRT1, phosphorylated SIRT1 (MpM2) and HTT after SIRT1 immunoprecipitation from half brain lysates of R6/2 and *Hdh*Q150 homozygotes as compared to their WT littermates. MpM2 antibody (used to detect the phosphorylation profile of SIRT1) is able to detect the phosphorylation on Serine and Threonine residues followed by Proline (S/T-P sites) present on any protein and it is not specific for any particular phosphorylation sites. IP, immunoprecipitation; WB, western blotting; Hdh, *Hdh*Q150 homozygotes. Scale bar, 10 µm. Data representative of at least three independent experiments.

3.8 Progressive decrease in SIRT1 phosphorylation in the striatum and increase in the cerebellum of HD mice

HD neuropathology hallmarks are more pronounced in the striatum and cortex than other brain regions (Bates, Tabrizi and Jones, 2014). Therefore the analysis of half brains might mask or dilute any regional pathological changes. As such, we decided to extend the analysis of SIRT1 phosphorylation to the striatum, cortex and cerebellum, and to include different ages to highlight any link to the progression of the disease. Interestingly, we did not detect any difference in the phosphorylation status of SIRT1 at presymptomatic stages of the disease (i.e. 4-week-old R6/2 and 2-month-old *Hdh*Q150 homozygous mice) between HD mice and their WT littermates in any brain regions (Fig. 21 A, B, C, D and E). In keeping with our functional data obtained from half brain, which showed an impairment of SIRT1 activity by 9 weeks of age in R6/2 and in 22-month-old *Hdh*Q150 homozygous mice, we observed an altered phosphorylation level of SIRT1 both in the striatum and cerebellum of R6/2 mice by 9 weeks of age (Fig. 21 A and C) and in 22-month *Hdh*Q150 homozygous mice (Fig. 21 B and D). Surprisingly, the level of phosphorylation of SIRT1 remained unchanged in the cortex of R6/2 mice at these later stages (Fig. 21 E). Notably, we detected a reduction in the phosphorylation level of SIRT1 in the striatum of R6/2 and *Hdh*Q150 homozygous mice, whereas phosphorylation was higher in the cerebellum of both HD models as compared to WT littermates (Fig. 21 A, B, C and D). Taken together, these results demonstrate that the presence of mHTT affects the phosphorylation status of SIRT1 as the disease progresses and that the changes go in the opposite direction for the striatum and cerebellum.

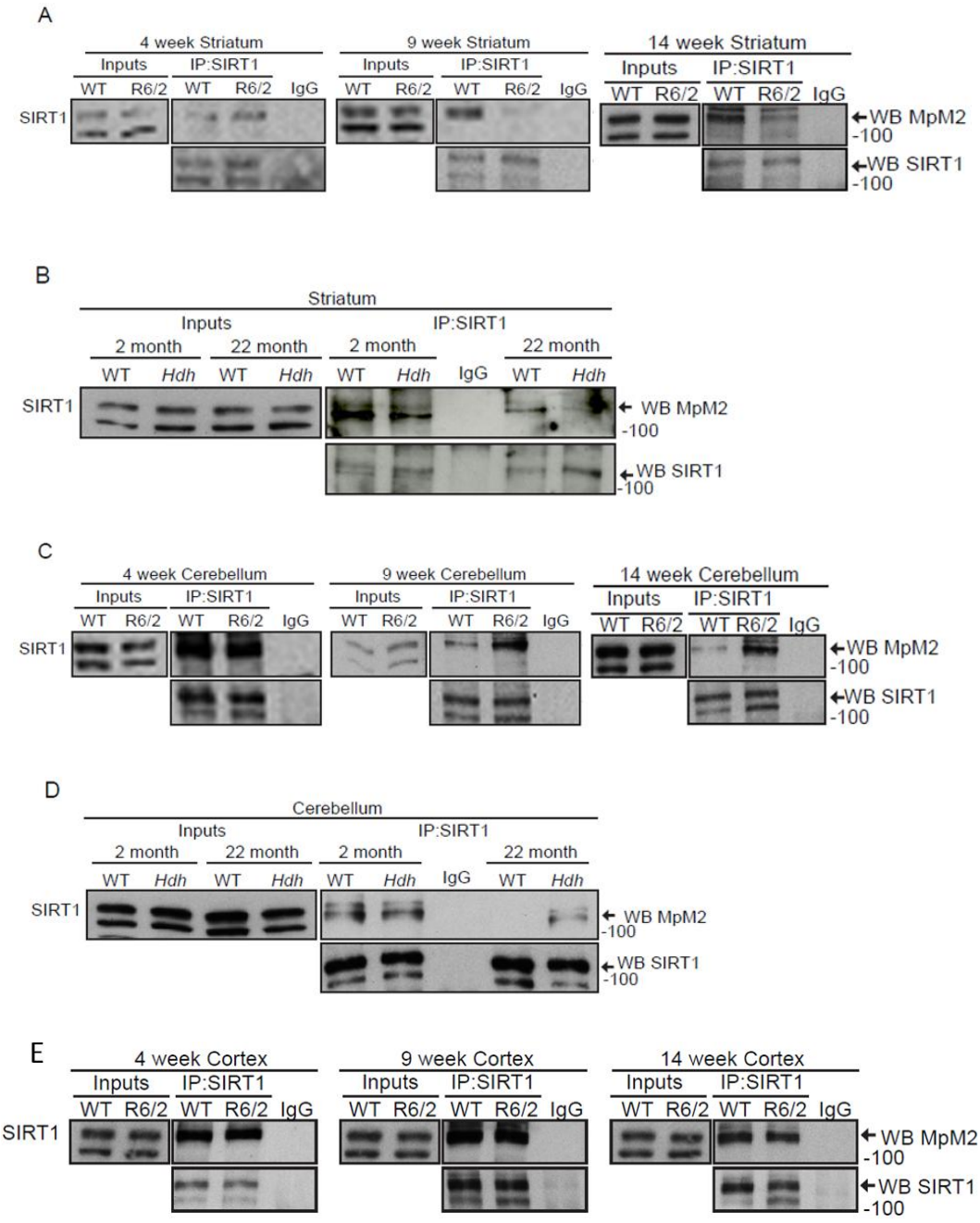

Figure 21. SIRT1 phosphorylation is altered in HD mouse models. (A, B) Western blots of SIRT1 and phosphorylated SIRT1 (MpM2) after SIRT1 immunoprecipitation from the striatum of R6/2 mice at 4, 9 and 14 weeks of age and *Hdh*Q150 homozygotes at 2 and 22 months as compared to their WT littermates. (C, D) Western blots of SIRT1 and phosphorylated SIRT1 after SIRT1 immunoprecipitation from the cerebellum of R6/2 mice at 4, 9 and 14 weeks of age and *Hdh*Q150 homozygotes at 2 and 22 months as compared to their WT littermates. (E) Western blots of SIRT1 and phosphorylated SIRT1 after SIRT1 immunoprecipitation from cortical lysates of R6/2 mice at 4, 9 and 14 weeks of age compared to WT littermates. IP, immunoprecipitation; WB, western blotting; *Hdh*, *Hdh*Q150 homozygotes. Data representative of at least three independent experiments.

3.9 Induction of SIRT1 activity is blocked in the striatum

Phosphorylation plays a central role in controlling protein activity, cellular localization and degradation (Johnson LN, 2009). To determine whether the differentially altered phosphorylation profile of SIRT1 in striatum and cerebellum corresponded to a compromised SIRT1 function in both these brain regions, we immunostained for SIRT1, P53 and AcP53 nuclei isolated from striatum and cerebellum of R6/2 and WT mice at 4, 9 and 14 weeks of age. Consistent with the data obtained from half brain, we did not detect any change in the intensity level of SIRT1 and P53 staining either the striatum or cerebellum between R6/2 and WT mice, at any of the age studied (Fig. 22 A and C, Fig. 23 A and C). Interestingly, we observed a significant reduction in the level of AcP53 in the striatum of WT mice, corresponding to an increase in SIRT1 activity, from 4 to 14 weeks of age, which was absent in the striatum of R6/2 mice (Fig. 22 B). In contrast, when we analysed SIRT1 activity in the cerebellum we detected no change in the level of AcP53 in WT samples at these ages and a significant progressive increase of AcP53 in the cerebellum of R6/2 mice from 4 to 14 weeks of age (Fig. 23 B), corresponding to a progressive impairment in SIRT1 activity. These data highlight for the first time that SIRT1 activity is regulated by different mechanisms in the striatum and cerebellum of WT mice between 4 and 14 weeks of age. SIRT1 activity is induced in the striatum between 4 and 9 weeks of age, whereas it remains constant in the cerebellum. The presence of mHTT can block this induction process in the striatum and causes a reduction of normal SIRT1 function in the cerebellum, resulting in an impairment of SIRT1 activity in both brain regions.

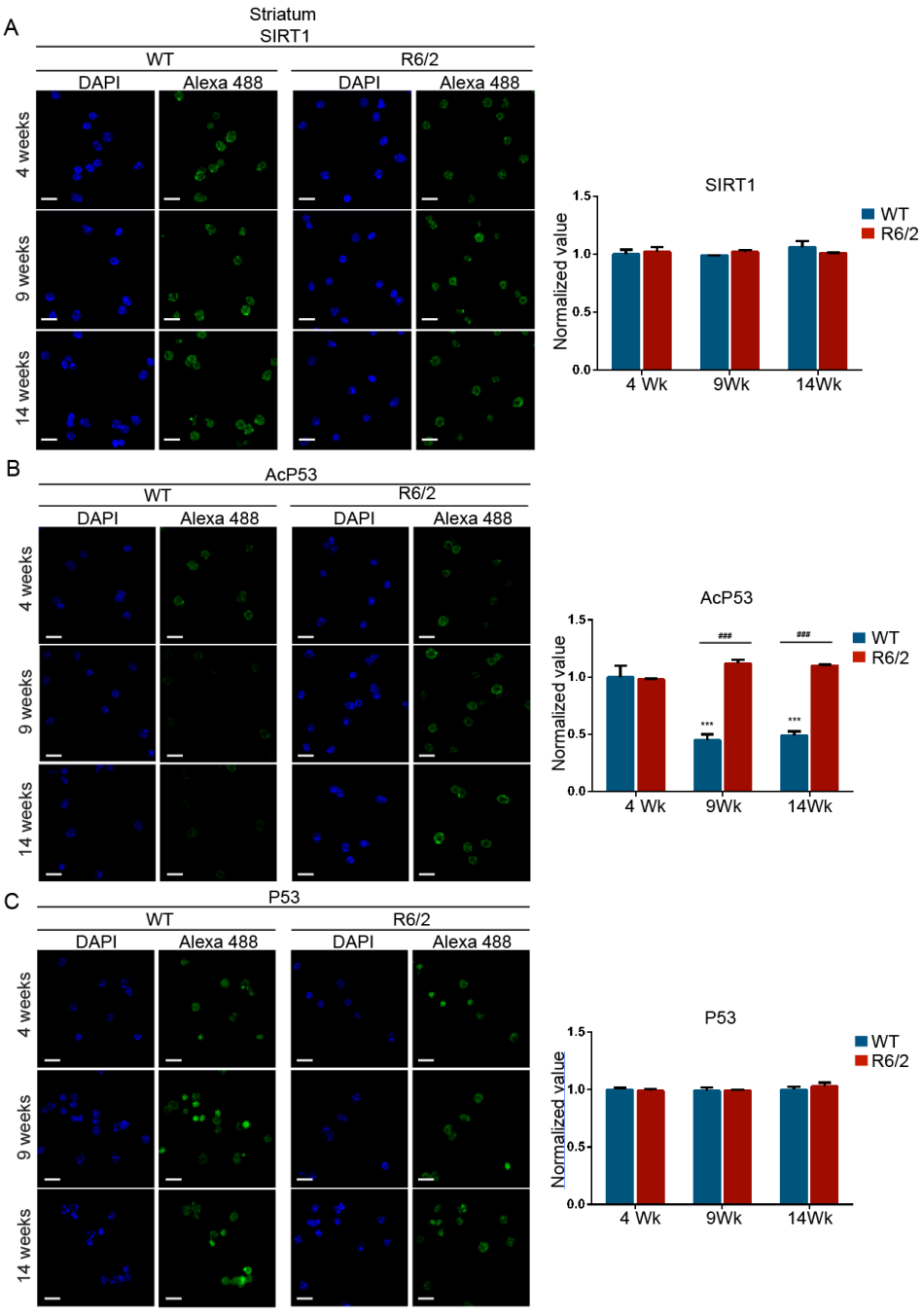

Figure 22. The induction of SIRT1 activity is blocked in the striatum Representative immunofluorescence image of isolated nuclei extracted from the striatum of WT and R6/2 mice at 4, 9 and 14 weeks of age immunostained for (A) SIRT1, (B) AcP53 and (C) P53, and counterstained with DAPI. The relative intensity levels of SIRT1, P53 and AcP53 are depicted alongside. The quantification indicates that the level of acetylated P53 is lower in WT mice, consistent with an increase in SIRT1 activity with age. Scale bar, 10 µm. Data are the mean ± SEM. *** p<0.001: statistically significant difference compared to 4 week WT. ### p<0.001: statistically significant difference between R6/2 and WT. n=4 / genotype.

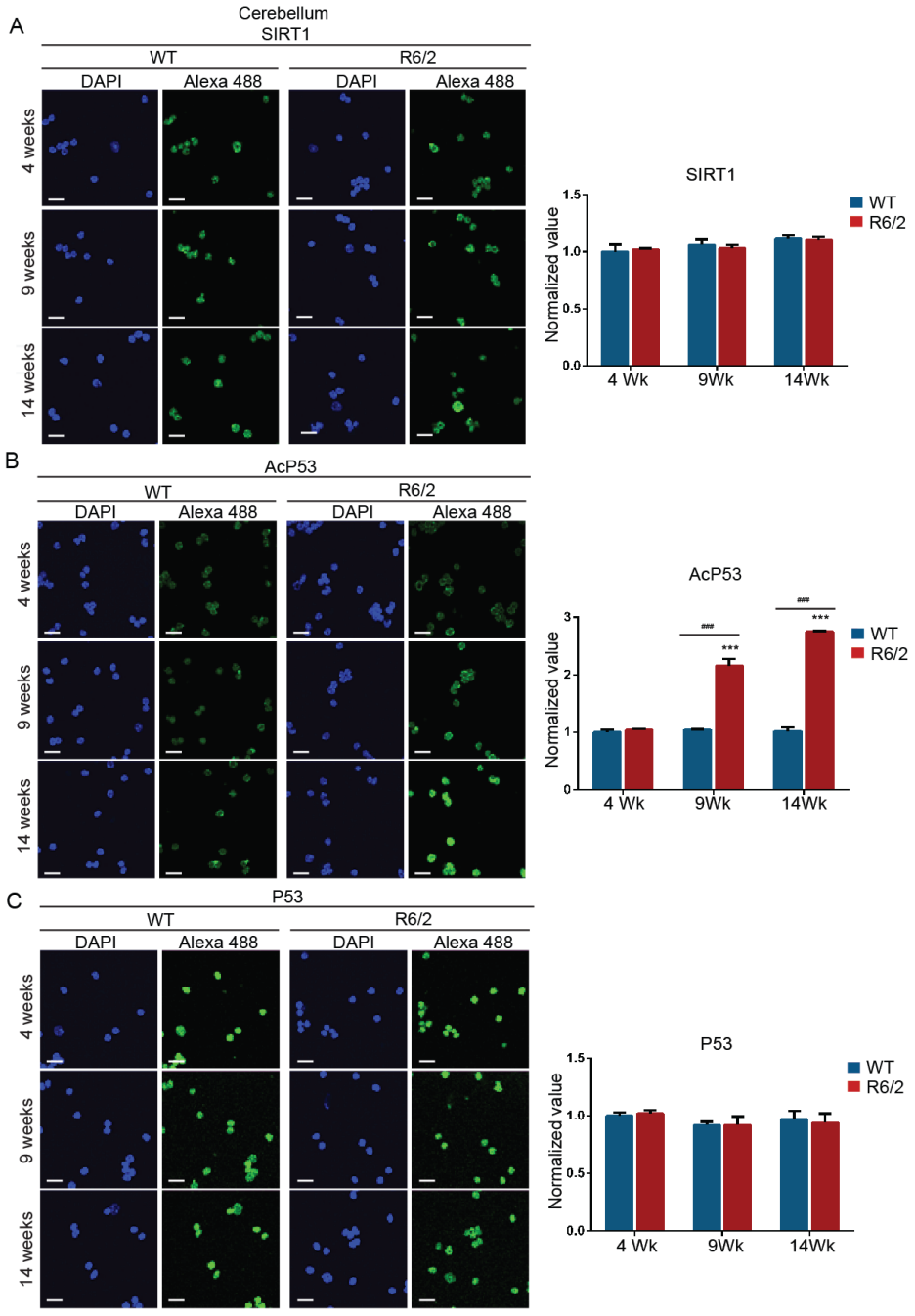

Figure 23. SIRT1 activity is impaired in the cerebellum Representative immunofluorescence image of isolated nuclei extracted from the cerebellum of WT and R6/2 mice at 4, 9 and 14 weeks of age immunostained for (A) SIRT1, (B) AcP53 and (C) P53, and counterstained with DAPI. The relative intensity levels of SIRT1, P53 and AcP53 are depicted alongside. The quantification indicates that the level of acetylated P53 is higher in R6/2 mice, consistent with a decrease in SIRT1 activity with age. Scale bar, 10 µm. Data are the mean ±SEM. *** p<0.001: statistically significant difference compared to 4 week WT. ### p<0.001: statistically significant difference between R6/2 and WT. n=4 / genotype

3.10 Striatum-specific age-dependent phosphorylation controls SIRT1 induction

The comparison of SIRT1 activity in the striatum and cerebellum between R6/2 and WT mice at different ages revealed the existence of different mechanisms to control SIRT1 function between these two brain regions in WT mice. In addition, these findings provide evidence of a striatum-specific mechanism by which SIRT1 is activated with age. This process does not occur in the cerebellum. To monitor the phosphorylation level of SIRT1 in normal physiological conditions in different brain regions, we immunoprecipitated SIRT1 from the striatal and cerebellar lysates of WT mice at 4, 9 and 14 weeks of age and immunoprobed with the MpM2 antibody to detect the phosphorylation status of SIRT1. Notably, we observed a fluctuation in the level of SIRT1 phosphorylation in the striatum (Fig. 24 A), whereas SIRT1 phosphorylation remained constant in the cerebellum (Fig. 24 B), between ages.

Specifically, the level of SIRT1 phosphorylation in the striatum dramatically dropped between 4 and 9 weeks of age, when the functional data revealed an increase in SIRT1 activity (Fig. 22 B), and then went up again at 14 weeks of age (fig. 24 A), stage at which the functional data still highlighted an higher (~50%) degree of activity of SIRT1 as compared to 4 weeks of age (Fig. 22 B). Conversely, SIRT1 activity remains constant during these ages in the cerebellum and this reflect a phosphorylation level that does not change. It is worth mentioning, again, that MpM2 antibody detects phosphorylation on Serine and Threonine residues followed by Proline (S/T-P sites) and it is not specific for any particular SIRT1 phosphorylation sites; therefore, the phosphorylation signals at 4, 9 and 14 weeks might be the results of phosphorylation on different residues of SIRT1. Taken together these data provide a link between the

phosphorylation status of SIRT1 and its activity, suggesting that in the striatum a change in SIRT1 phosphorylation level between ages might be related to an induction of SIRT1 activity.

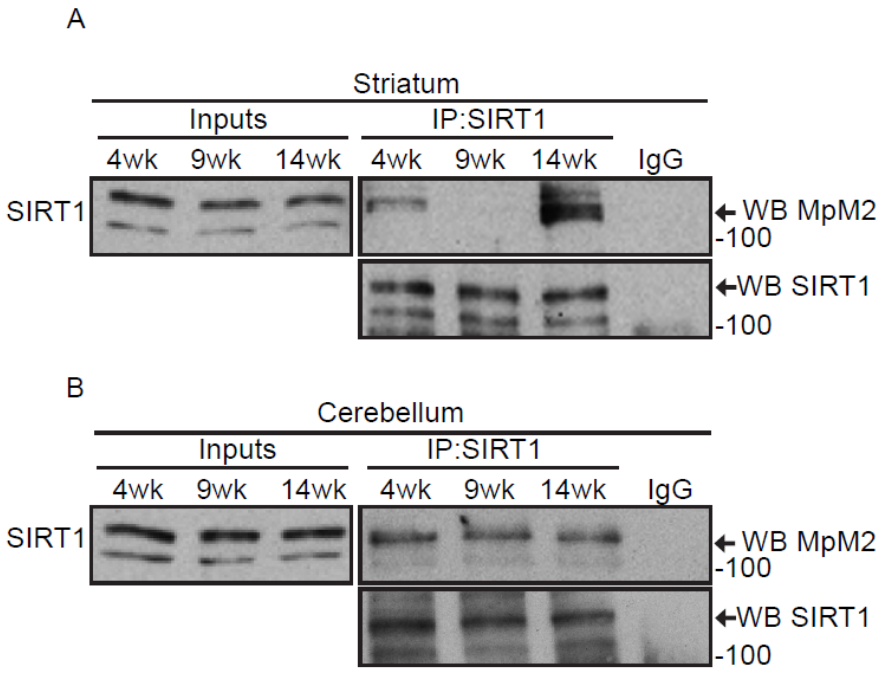

Figure 24. The phosphorylation status of SIRT1 changes in the striatum but not in the cerebellum with age. Western blots of SIRT1 and phosphorylated SIRT1 after SIRT1 immunoprecipitation from (A) the striatum of WT mice at 4, 9 and 14 weeks, and from (B) the cerebellum of WT mice at 4, 9 and 14 weeks; IP: immunoprecipitation; WB: Western blot. Data representative of at least three independent experiments.

3.11 The sub-cellular distribution of SIRT1 is not altered in R6/2 mice

Previous studies suggested that the phosphorylation of human SIRT1 can increase its nuclear localization and enzymatic activity (Nasrin et al., 2009). To assess whether the mis-regulation of SIRT1 phosphorylation could affect its nuclear localization we prepared nuclear and cytoplasmic fractions from the striatum and cerebellum of R6/2 and WT mice at 9 and 14 weeks of age. Notably, we did not detect any difference in the distribution of SIRT1 at any age between R6/2 and WT mice in either the striatum or cerebellum (Fig. 25 A and B). Interestingly, the level of SIRT1 in the nuclear fraction was more pronounced at 14 weeks as compared to 9 weeks of age in the striatum and cerebellum of both R6/2 and WT mice (Fig. 25 B). We went to analyse the phosphorylation level of SIRT1 in these two cellular compartments by immunoprecipitation, using nuclear and cytoplasmic extracts from the cerebellum. Interestingly, a strong phosphorylation signal was detected in the nuclear fraction of both R6/2 and WT samples and, as previously shown on total lysates, the level of phosphorylation was much higher in R6/2 as compared to WT mice (Fig 25 C). We tried to immunoprecipitate SIRT1 from striatal nuclear and cytoplasmic fractions but the amount of protein extracted resulted to be not enough to perform the immunoprecipitation.

These results demonstrate that the sub-cellular distribution of SIRT1 is not affected by the presence of mHTT and suggest, once again, that the phosphorylation levels might be directly linked to the regulation of SIRT1 activity.

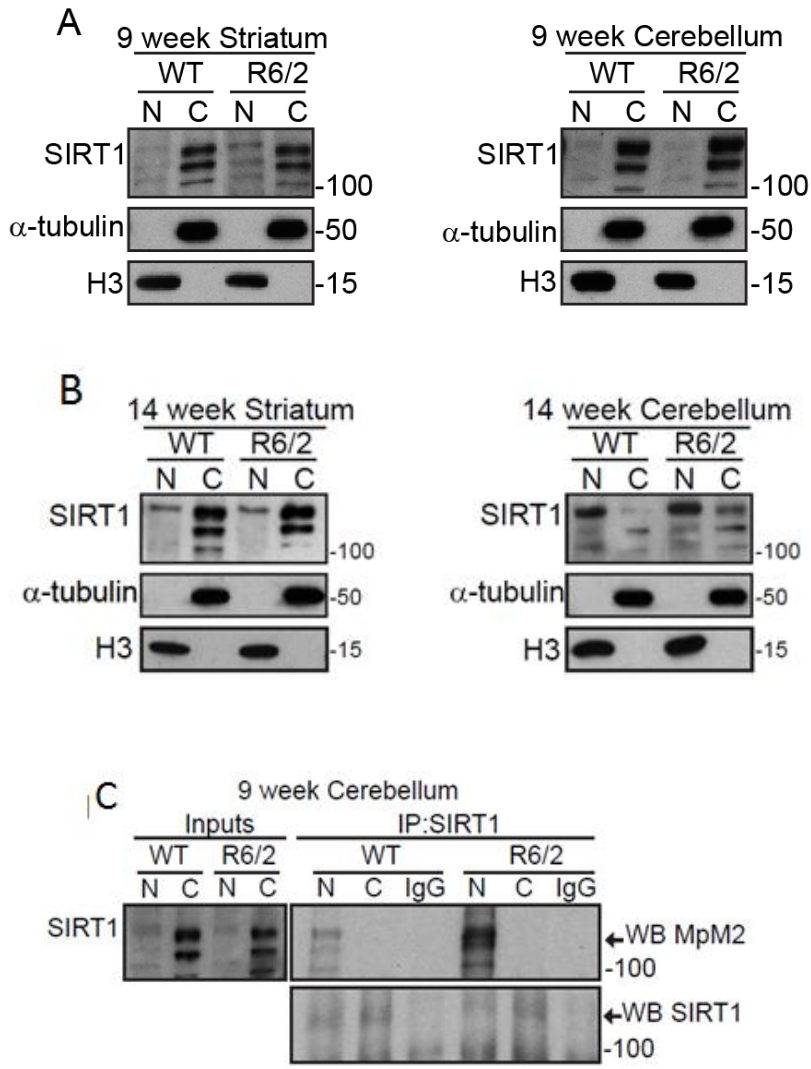

Figure 25. The sub-cellular distribution of SIRT1 is not altered in R6/2 mice. (A) Western blot for SIRT1, -tubulin and histone H3 of nucleo-cytoplasmic extracts from striatum and cerebellum of R6/2 and WT mice at 9 weeks of age. (B) Western blot for SIRT1, - tubulin and histone H3 of nucleo-cytoplasmic extracts from striatum and cerebellum of R6/2 and WT mice at 14 weeks of age. (C) Western blot of SIRT1 after SIRT1 immunoprecipitation from nuclear and cytoplasmic fractions extracted from cerebellum of R6/2 and WT mice at 9 weeks of age. IP: immunoprecipitation; WB: Western blot. Data representative of at least three independent experiments.

3.12 AMPK-α1 as regulator of SIRT1 affected by mHTT

Previous studies showed that DBC1 (deleted in breast cancer 1) directly interacts with the catalytic domain of SIRT1 inhibiting its activity both *in vitro* and *in vivo* (Escande et al., 2010). This dynamic interaction is sensitive to the energetic state of the cell (Escande et al., 2010). Activation of AMP-activated protein kinase-α1 (AMPK-α1), an important cellular energy sensor in circumstances of low cellular energy, was recently shown to induce the activation of SIRT1 through its dissociation from DBC1 (Escande et al., 2012; Lau *et al.*, 2014). To identify the possible role of AMPK-α1 and DBC1 in the molecular phenotypes described so far, we decided to study the interaction between these two opposing modulators of SIRT1 using co-immunoprecipitation.

We immunoprecipitated AMPK-α1 from the striatum and cerebellum, as well as half brain, of 9-week R6/2, 22-month *Hdh*Q150 homozygous and aged-matched WT mice and detected the co-immunoprecipitated DBC1. Interestingly, we observed a stronger interaction between AMPK-α1 and DBC1 in the striatum of HD as compared to WT mice (Fig. 26 A), whereas equal amounts of DBC1 were co-immunoprecipitated with AMPK-α1 from cerebellar extracts of HD and WT samples (Fig 26 B). An increased interaction between AMPK-α1 and DBC1 was also observed in half brain lysates of HD as compare to WT mice (Fig 27). These data suggest two possible scenarios: either the increased interaction of AMPK-α1 with the SIRT1-DBC1 complex might promote SIRT1 activation in the striatum of HD mice through the dissociation from DBC1, or the inability to induce SIRT1 in R6/2 mice might be due to an inhibitory retention of AMPK-α1 via DBC1.

To gain insight into the molecular events characterising this process we examined the cellular distribution of AMPK-α1 and DBC1 in the striatum and

cerebellum of R6/2 and WT mice at 9 and 14 weeks of age by western blot of nucleo-cytoplasmic extracts. Consistent with the phenotypes described so far, the striatum and cerebellum showed a different profile. Interestingly, we were able to detect DBC1 in both cellular compartments and although at 9 weeks of age DBC1 was slightly more abundant in the striatal cytoplasmic fraction, this balance was reverted by 14 weeks of age for both R6/2 and WT mice (Fig. 26 C). In contrast cerebellar DBC1 levels remained constant between the two cellular compartments at 9 and 14 weeks of age for both R6/2 and WT mice (Fig. 26 D). Using immunostaining of nuclei isolated from the striata of R6/2 and WT mice at 4, 9 and 14 weeks of age we then monitored the distribution of AMPK-α1. At 9 weeks of age WT striatum showed signal of AMPK-α1 in the nucleus, whereas this did not occur in the striatum of R6/2 mice until 14 weeks of age (Fig. 26 E). Conversely, cerebellar extracts showed an early nuclear accumulation of AMPK-α1 in R6/2 at 9 weeks of age as compared to WT mice, where AMPK-α1 could only be detected in the nucleus at 14 weeks of age (Fig. 26 F). We confirmed these data by immunostaining for AMPK-α1 nuclei extracted from the cerebellum of R6/2 and WT mice at 4, 9 and 14 weeks of age (Fig. 26 E). The nuclear accumulation of AMPK-α1 at 9 weeks of age in the striatum of WT mice might indeed support a role for this kinase in the activation of SIRT1 a mechanism that appears to be compromised in the R6/2 mice in which AMPK-α1 only reaches the nucleus at 14 weeks of age. Therefore, the increased interaction between AMPK-α1 and DBC1 might retain AMPK-α1 in the cytoplasm, inhibiting the activation of SIRT1, and/or attempt to rescue SIRT1 activity by preventing DBC1 from binding to SIRT1. Conversely, the early nuclear accumulation of AMPK-α1 in the cerebellum of R6/2 at 9 weeks of age as compared to WT mice might be an attempt to increase impaired SIRT1 activity. Taken together, these data

suggest that the inhibition of SIRT1 function in the striatum of R6/2 might arises through an altered functionality of AMPK-α1 and that AMPK-α1 might be involved in rescuing a deficient SIRT1 function both in the striatum and cerebellum, although through different molecular mechanisms.

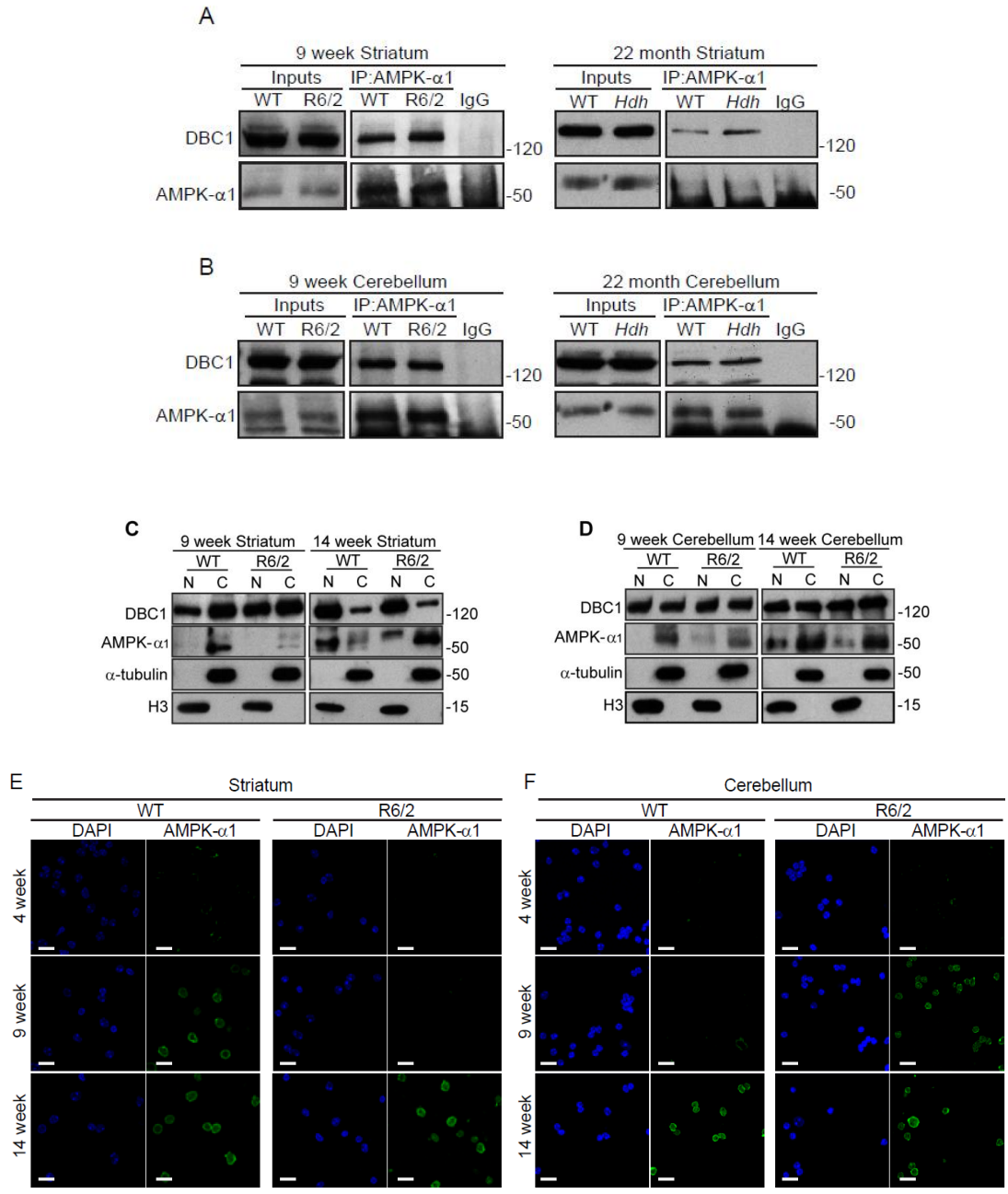

Figure 26. DBC1-AMPK-α1 interaction and their subcellular distribution in HD mice. (A-B) Western blots of DBC1 and AMPK-α1 after AMPK-α1 immunoprecipitation from (A) the striatum of 9-week R6/2 and 22-month *Hdh*Q150 homozygotes, and (B) from the cerebellum of 9-week R6/2 and 22-month *Hdh*Q150 homozygotes. (C-D) Western blot for DBC1, AMPK-α1, α-tubulin and histone H3 of nucleo-cytoplasmic extracts from (C) striatum and (D) cerebellum of WT and R6/2 mice at 9 and 14 weeks of age. (E-F) Representative immunofluorescence image of nuclei extracted from (E) striatum and (F) cerebellum of WT and R6/2 mice at 4, 9 and 14 weeks of age immunostained for AMPK-α1 and counterstained with DAPI. Scale bar, 10 µm. IP, immunoprecipitation.

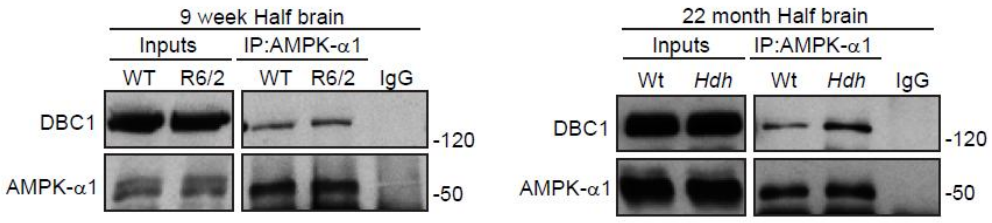

Figure 27. DBC1-AMPK-α1 interaction in mouse half brain. Western blot of DBC1 and AMPK-α1 after AMPK-α1 immunoprecipitation from half brain lysates of 9-week R6/2, 22-month *Hdh*Q150 homozygotes and age-matched WT mice. IP, immunoprecipitation. *Hdh*, *Hdh*Q150 homozygotes. Data representative of at least three independent experiments.

3.13 SIRT1, AMPK-α1 and DBC1 as partners in the same regulatory circuit to control SIRT1 activity in the Striatum

We observed an active role of AMPK-α1 in trying to rescue SIRT1 deficiency both in the striatum and cerebellum of R6/2 mice. To obtain further evidence of a regulatory circuit involving these three proteins we went to compare the expression levels of SIRT1, DBC1 and AMPK-α1 in the striatum and cerebellum of R6/2 at 4, 9 and 14 weeks of age, *Hdh*Q150 homozygous at 2 and 22 months of age and age-matched control WT mice. Strikingly there was a synchronised significant down-regulation of all three genes at the mRNA level from 4 to 9 weeks of age in the striatum of WT mice (Fig. 28 A). Interestingly, we detected the same significant reduction in the striatum of R6/2 mice for *Dbc1* and *Ampk*-α1, but this did not occur for *Sirt1* (Fig. 28 A). Notably, the cerebellum of both WT and R6/2 mice did not show the same regulatory circuit as no coordinated changes in the expression levels of *Sirt1*, *Dbc1* and *Ampk*-α1 were detected, although the expression level of *Sirt1* was significantly higher in WT mice at 9 and 14 weeks as compared to 4 weeks of age (Fig. 28 D). Protein analysis revealed steady-state levels of DBC1, consistent with the nucleo-cytoplasmic data, both in striatum and cerebellum of R6/2 and WT mice at all ages (Fig. 28 B, C, E and F). Interestingly, we observed a significant upregulation of AMPK-α1 in the striatum of WT mice at 9 and 14 weeks as compared to 4 weeks of age, which did not occur in the striatum of R6/2 mice (Fig. 28 B and C). Protein levels of AMPK-α1 were even and stable in the cerebellum of WT and R6/2 mice at all ages under analysis (Fig. 28 E and F). When we analysed SIRT1 protein level we detect no change in striatum with age, (Fig. 28 B and C) and a significant downregulation in the cerebellum of WT and R6/2 at 14 weeks as compared to 4 weeks of age (Fig. 28 E and F). Interestingly, *Hdh*Q150

homozygous mice showed no difference in the protein levels of SIRT1, DBC1 and AMPK-α1 at 2 and 22 months of age as compared to WT mice (Fig. 29 A and B). Taken together these data show the presence of an age-related downregulation of *Sirt1*, *Dbc1* and *Ampk*-α1 taking place between 4 and 9 weeks of age in the striatum of WT mice, which is maintained in the striatum of R6/2 mice only for *Dbc1* and *Ampk*-α1, but not for *Sirt1*. This might suggest that in WT mice a negative feedback mechanism responds to SIRT1 activation and as SIRT1 activity is not induced in the striatum of R6/2 mice such a feedback mechanism is not instigated. Furthermore, the increased levels of AMPK-α1 in WT striatum at 9 and 14 weeks of age may also suggest that this protein has become stabilised and that this does not happen in R6/2 mice, contributing to the mis-regulation of SIRT1 (Fig. 54A).

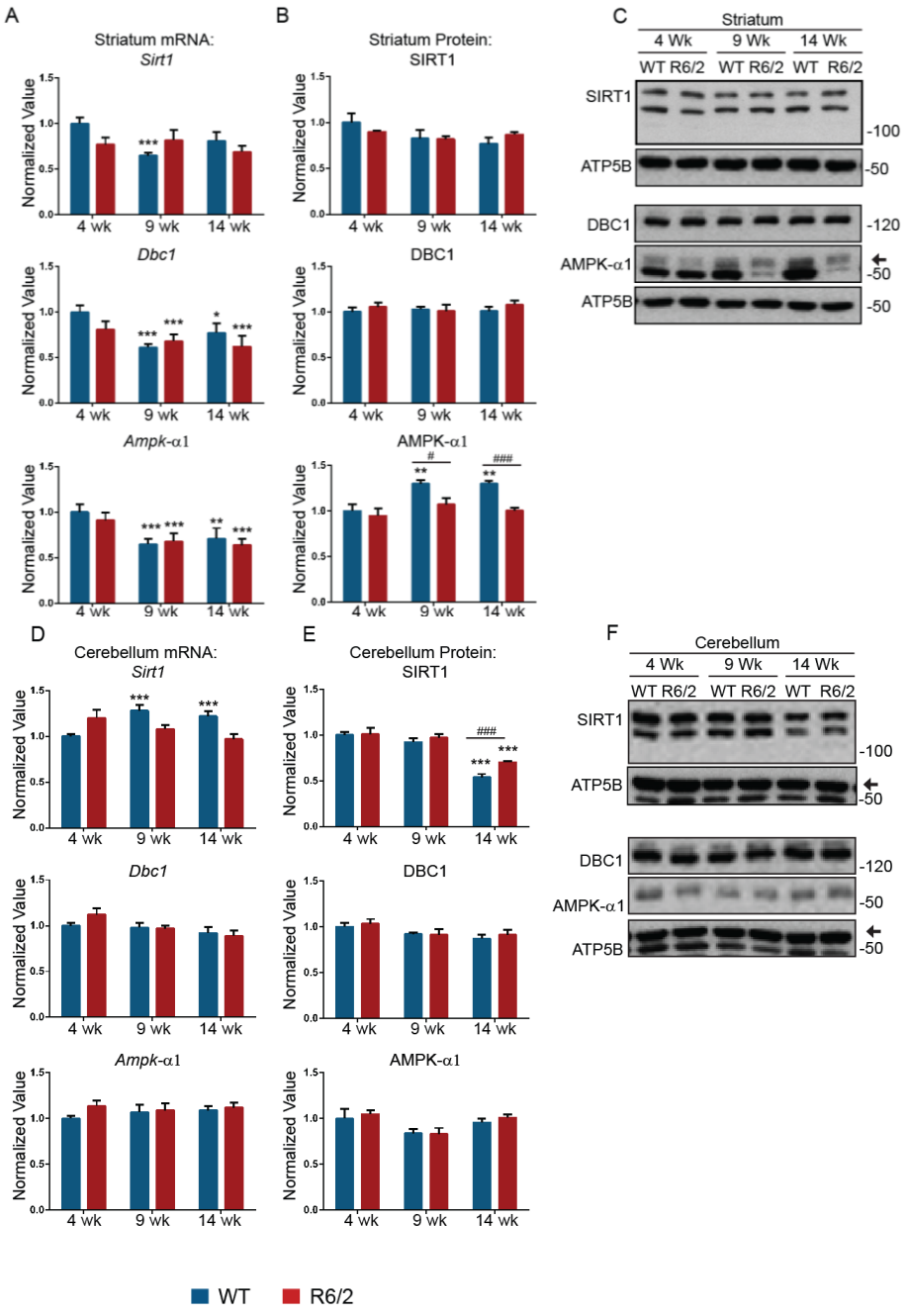

Figure 28. RNA and protein analysis of SIRT1, DBC1 and AMPK-α1 in R6/2 mice. qPCR analysis of the expression level of *Sirt1*, *Dbc1* and *Ampk-α1* in (A) striatum and (D) cerebellum of R6/2 and WT mice at 4, 9 and 14 weeks of age. Values were calculated relative to 4-week WT mice. Relative protein level of SIRT1, DBC1 and AMPK-α1 in (B) striatum and (E) cerebellum of R6/2 and WT mice at 4, 9 and 14 weeks of age. Densitometric values were calculated relative to 4-week WT mice. Representative western blots for SIRT1, AMPK-α1 and DBC1 in (C) striatum and (F) cerebellum of R6/2 and WT mice at 4, 9 and 14 weeks of age. Data are the mean ± SEM. * $p<0.05$; ** $p<0.01$; *** $p<0.001$: statistically significant difference as compared to WT at 4 weeks of age. $^{\#}$ $p<0.05$; $^{\#\#\#}$ $p<0.001$: statistically significant difference between WT and R6/2. For qPCR n=8 / genotype, for WB n=4 / genotype.

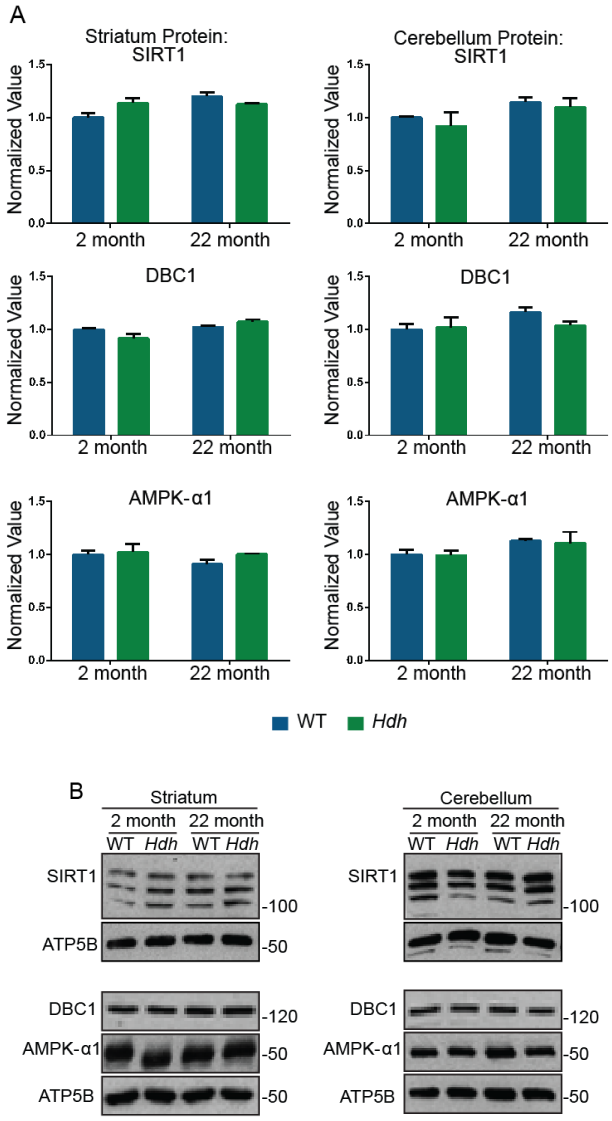

Figure 29. Protein analysis of SIRT1, DBC1 and AMPK-α1 in *Hdh*Q150 homozygous mice. (A) Relative protein levels and (B) representative western blots of SIRT1, DBC1 and AMPK-α1 in striatum and cerebellum of 2 and 22-month *Hdh*Q150 homozygotes and WT mice. Densitometric values were calculated relative to 2-month WT mice. Data are mean ± SEM. *Hdh*, *Hdh*Q150 homozygotes. n=4 / genotype.

3.14 General comments

In this work, we explore the impact of HD pathology on SIRT1 function in the brain. We provide evidence for a considerable down-regulation of SIRT1 activity in the brain of two well-characterized HD mouse models: R6/2 and *Hdh*Q150 mice.

These models are used in various preclinical studies because of their particular strengths in genetic and phenotypic characteristics. The mHTT fragment transgenic models exhibit early-onset and rapidly progressing behavioural and neuropathological phenotypes associated with significant weight loss and premature death. The advantage of the Knock-in is that they may better resemble the pathogenic mechanisms that occur in the patients (Gusella and MacDonald, 2006; Van Raamsdonk et al., 2007). Moreover, since the *Hdh*Q150 mice do not contain human sequence but they express 100% of the mHTT derived from the mouse *Htt* gene, they are the most precise genetic model of HD and hence are valuable to study molecular mechanisms and therapeutic interventions requiring such precise level of mutant *Hdh* expression in the endogenous genomic context.

Mouse models of HD share many features but, at the same time, they show many discrepancies. A critical question is which mouse model or models should be used in a preclinical study of a therapeutic candidate. An ideal HD mouse model should have:

1. a genetic construct that is similar if not identical to the patients;
2. robust behavioural deficits and selective neuropathology mimicking the patients;
3. these phenotypes are early onset, rapidly progressing, easily quantifiable, and have limited variability between mice.

From our description of the preclinical HD mouse models, it is apparent that each of the current models only partially satisfies such requirements. The fragment models (i.e., R6/2) have very rapid onset and progression of disease, as well as low phenotypic variability (10–20 per treatment group in preclinical trials); weight loss and early lethality in these models can be used as surrogate markers of disease. However, there are also some concerns with the use of mHTT fragment models to determine the preclinical efficacy of therapeutic candidates. First, the neuropathology in the fragment models is more widespread and relatively non-selective. Second, because the disease progression in patients is usually very slow, another concern is that a potential efficacious therapeutic mechanism or candidate in human HD may not be effective in the fragment model. Third, the fragment models only express a small portion of mHTT regulatory elements and proteins; thus, the study of HD in the contest of Fl-HTT cannot be performed.

The availability of several Knock-in mouse models provides new opportunities to test HD preclinical candidates in model systems that have genetic, genomic, and protein context more similar to human HD; moreover, they have a slowly progressing disease process that may be more closely related to the process in the human disease; and also they have neuropathology that is selective to the striatum and cortex. However, the main concern in the use of the full-length models in preclinical trials is cost. Because the length of the trial in these mice is very long (i.e., up to 1–2 years in Knock-in mice) and the variability of their outcomes is very high, which may require a larger number of mice for each study, to work with these mice can result very expensive.

It is clear that both the mHTT fragment models and the full-length models have their potential strengths and weaknesses in the preclinical studies. A good idea could be to

perform a screening assay in a fragment mouse model of HD. R6/2 mice may be a preferred model for this purpose because of the model's rapid disease course. Such a therapeutic screen, with primary outcomes focusing on behavioural and neuroprotection, can provide relatively rapid information on the potential therapeutic efficacy of a large number of preclinical candidates at a reasonable cost. After demonstrating therapeutic efficacy in the fragment model, the clinical study should be performed in a full-length model. At this point, if the compound has proven safety in humans and/or is already in clinical use, direct clinical study in HD patients may be warranted.

We should also consider that the R6/2 show a very aggressive phenotype and this could mask a positive effect of a clinical trial. For this reason, a different approach could be to perform a study in both HD mouse models at the same time.

In this work, we performed a parallel study in N-terminal transgenic and Knock-in mouse models.

The data presented so far provide evidence of a progressive impairment in SIRT1 activity in HD mice. P53 has been shown to be located in the nucleus and it is one of the main substrate of SIRT1. We used an immunohistochemistry on isolated nuclei to measure the deacetylation of P53 by SIRT1. The advantage of this technique is to focus only on the nuclear fraction keeping away any cytoplasmic contamination. Moreover, this is the first technique to date to be able to detect specifically SIRT1 activity in mouse tissues. On another hand, this method does not allow to distinguish among all the cellular populations present in the brain. This limit could be overcome performing a double staining with marker that can recognize a specific cell population (but unfortunately we do not have specific marker for all kind of cell populations) or

performing a sorting of all the cell populations of the brain but a cell sorting will never provide an adequate number of cells to perform an immunohistochemistry.

The data presented so far provide evidence of a progressive impairment in SIRT1 activity in HD mice. We showed that the impairment of SIRT1 function is not related to a sequestration of SIRT1 protein into mHTT inclusions. To confirm these data, we performed a western blot from HD and WT brain lysates and did not detect a reduction in SIRT1 protein levels in HD mouse models as compared to WT.

These data suggest that mHTT acts through other mechanisms to control SIRT1 activity. Several studies have shown that SIRT1 activity is mainly regulated by post-translational modification such as phosphorylation (Sasaki et al., 2008). Therefore, to understand the effect of mHTT on SIRT1 function, we monitored the phosphorylation status of SIRT1 in HD mice. The immunoprecipitation of SIRT1 data, representative of at least three independent experiments, from half brains and brain regions of R6/2 and *Hdh*Q150 homozygous mice revealed that the phosphorylation status of SIRT1 is altered in HD mouse models. This indicates that the impairment of SIRT1 function in the brain of HD mice might be related to an altered phosphorylation profile. Interestingly, the levels of phosphorylated SIRT1 remain unchanged in the cortex with age. However, we found an opposing pattern of phosphorylation between the striatum and cerebellum; surprisingly, we detected a reduction of phosphorylated SIRT1 in the striatum both R6/2 (9 weeks) and *Hdh*Q150 homozygous (22 months) mice compared to WT, while phosphorylated SIRT1 was increased in the cerebellum of both HD mouse models. These data further confirm that the status of SIRT1 phosphorylation is altered in presence of mHTT and with disease progression. The Mpm2 antibody provides information about the different phosphorylation profile of SIRT1 between WT and HD

mice but it does not specify which SIRT1 residue is characterized by an alteration of the phosphorylation status in HD mouse model. Other techniques can be used to overcome the limit showed by the MpM2 antibody. For example, a mass spectrometry analysis could detect homologies and differences in the phosphorylation of SIRT1 residues between WT and HD mice and it could be really useful to understand which residues have an altered phosphorylation profile in presence of mHTT.

To investigate whether the altered pattern of SIRT1 phosphorylation in striatum and cerebellum of HD mice was related to an impairment of SIRT1 function, we monitored acetylation status of P53 by immunohistochemistry on isolated nuclei from both these brain regions of R6/2 and WT mice. Interestingly, we detected a robust reduction in the level of AcP53 in the striatum of WT mice from 4 to 14 weeks of age, consistent with an increase in SIRT1 activity. We did not detect the same increase in the striatum of R6/2 mice. We did not find any change in the acetylation status of P53 in the cerebellum in WT mice, but we found a significant increase in AcP53 in R6/2 cerebella from 4 to 14 weeks of age, corresponding to a progressive impairment in SIRT1 activity. This is one of the most important experiments performed so far. Indeed, this experiment confirms that:

1. the impairment in SIRT1 activity happens in conjunction with an alteration in the SIRT1 phosphorylation status.
2. the mechanism that control SIRT1 function in physiological condition is different in different brain regions.
3. the mechanism underlying the impairment in SIRT1 function is different in different brain regions. This can explain why we found a different alteration of SIRT1 phosphorylation in different brain regions. Indeed, in physiological

condition SIRT1 activity is induced in the striatum between 4 and 9 weeks, whereas it remains constant in the cerebellum. The presence of mHTT can block this induction process in the striatum (Fig.53 A) and cause a reduction in normal SIRT1 function in the cerebellum resulting in an impairment of SIRT1 activity in both brain regions.

The induction of SIRT1 activity in the striatum and the unchanged level of SIRT1 function in the cerebellum of WT mice with age led us to monitor the phosphorylation status of SIRT1 in both brain regions from WT mice. The immunoprecipitation of SIRT1 from WT mice at 4, 9 and 14 weeks revealed a change in the phosphorylation status of SIRT1 in the striatum with age, suggesting that in the striatum, a change in the phosphorylation status of SIRT1 can be related to an induction of SIRT1 activity. The cerebellum showed a constant phosphorylation status of SIRT1 in WT mice with age, consistent with a lack of a change in SIRT1 activity.

To check if the miss-regulation of SIRT1 phosphorylation could affect its nuclear localisation, we prepared nuclear-cytoplasmic fractions from the striatum and cerebellum of R6/2 and WT mice at 9 and 14 weeks of age. Interestingly, we did not detect any difference in the distribution of SIRT1 between R6/2 and WT mice in both striatum and cerebellum at any age.

It has been shown that DBC1 can interact, *in vitro* and *in vivo*, with the catalytic domain of SIRT1 (Escande et al., 2010) and inhibit its activity (Zhao et al., 2008). In contrast AMPK-α1 is a positive regulator of SIRT1. Indeed, AMPK-α1 is an important cellular energy sensor that in circumstances of low cellular energy can induce the activation of SIRT1 through the dissociation from DBC1 (Escande et al., 2012; Lau *et al.*, 2014). We analysed the interaction between these two opposing modulators of SIRT1

in the context of HD pathogenesis. AMPK-α1 immunoprecipitation from the striatum and cerebellum of R6/2 (9 weeks) and *Hdh*Q150 homozygous (22 months) mice showed that the interaction between AMPK-α1 and DBC1 in the striatum of HD mice was increased as compared to WT mice, whereas there was no difference in this interaction in the cerebellum. The increased interaction between DBC1 and AMPK-α1 could be interpreted a follow:

1. the increased interaction of AMPK-α1 with the SIRT1-DBC1 complex might promote SIRT1 activation in the striatum of HD mice through the dissociation from DBC1
2. the inability to induce SIRT1 in R6/2 mice might be due to an inhibitory retention of AMPK-α1 via DBC1.

At the same time, we monitored the sub-cellular distribution of DBC1 and AMPK-α1 using nucleo-cytoplasmic preparations from R6/2 striatum and cerebellum at 9 and 14 weeks of age. This was complemented with immunohistochemistry for AMPK-α1 on isolated nuclei extracted from R6/2 and WT mice striatum and cerebellum at 4, 9 and 14 weeks of age. DBC1 was found more concentrated in the cytoplasmic than the nuclear fraction at 9 weeks of age. This balance reverted at 14 weeks of age in both R6/2 and WT mice. In contrast, the level of DBC1 was constant between the two cellular compartments in the cerebellum at 9 and 14 weeks of age in both R6/2 and WT mice. The immunohistochemistry on isolated nuclei extracted from R6/2 and WT mice showed that AMPK-α1 was present in the nuclei of WT striatum at 9 weeks of age, whereas it was not detected in the striatum of R6/2 mice until 14 weeks of age. Conversely, cerebellar extracts showed an early nuclear accumulation of AMPK-α1 in R6/2 at 9 weeks of age as compared to WT mice, where AMPK-α1 could be detected in

the nucleus only at 14 weeks of age. The delayed accumulation of AMPK-α1 in striatal nuclei of R6/2 mice might be caused by its retention by DBC1 in the cytoplasm and this can impede SIRT1 activation (Fig. 53 A), whereas AMPK-α1 nuclear accumulation in the cerebellum of R6/2 mice was anticipated by 9 weeks of age, maybe trying to reduce the SIRT1 inhibition dictated by mHTT. Whether DBC1 was involved in a cytoplasmic retention of AMPK-α1 could be further confirmed performing the same experiments in tissues *Dbc1*$^{-/-}$::R6/2 but unfortunately we didn't have time to do it.

Analysis of mRNA expression showed that *Sirt1*, *Dbc1* and *Ampk-α1* are downregulated in WT striatum from 4 to 14 weeks of age. Interestingly, we detected the same significant reduction in the striatum of R6/2 mice for *Dbc1* and *Ampk*-α1, but this did not occur for *Sirt1*. The levels of these three genes were not downregulated in the cerebellum of WT and R6/2 mice. We observed no change in the protein level of SIRT1 and DBC1 in the striatum of WT and R6/2 mice at 9 and 14 weeks of age as compared to 4 weeks. There was a significant upregulation of AMPK-α1 in the striatum of WT mice at 9 and 14 weeks as compared to 4 weeks of age, which did not occur in the striatum of R6/2 mice. The protein levels of DBC1 and AMPK-α1 were stable in the cerebellum of WT and R6/2 mice at all ages under analysis.

However, there was a significant downregulation of SIRT1 in the cerebellum of WT and R6/2 at 14 weeks as compared to 4 weeks of age. Interestingly, *Hdh*Q150 homozygous mice showed no difference in the protein levels of SIRT1, DBC1 and AMPK-α1 at 2 and 22 months of age as compared to WT mice.

Chapter 4

RESULTS: EFFECT OF *Dbc1* ABLATION ON HD PHENOTYPE

4.1 *Dbc1* knock-out mice characterization

Dbc1 knock-out (*Dbc1*$^{-/-}$) mice were generated by targeted insertion of a neomycin resistance gene between exon 6 and exon 7 of the *Dbc1* gene (geneID 219158) (Escande et al., 2012) (Fig. 30). The insertion introduced a stop codon that results in the nonsense-mediated decay of the *Dbc1* mRNA. The *Dbc1* gene was targeted in an embryonic stem cell line (XN876) and the ES cells were injected into C57BL/6 blastocysts to generate chimeric mice. Chimeras were then backcrossed with C57BL/6 mice to generate *Dbc1* heterozygous (*Dbc1*$^{+/-}$) mice, which were used for subsequent breeding. However, the specific position, length and sequence of the insertion are unknown. To confirm the insertion that disrupted the *Dbc1* gene in *Dbc1*$^{-/-}$ mice, genotyping primers (Table 6) were used to obtain a DNA fragment that contained a part of the *Dbc1* gene and part of the insertion.

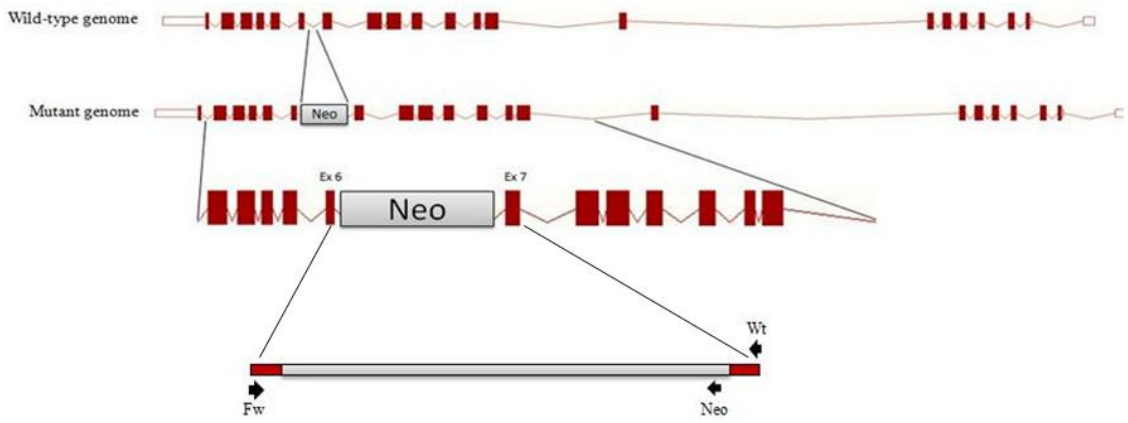

Figure 30. Exon-Inton structure of the *Dbc1* gene in mouse. Insertion of the NEO cassette between the exon 6 and exon 7. Positions of PCR primers are shown.

To investigate how the insertion in the *Dbc1* gene affects *Dbc1* expression, RNA was extracted and cDNA synthesised from cortex of WT, *Dbc1*$^{+/-}$ and *Dbc1*$^{-/-}$ mice at 4 weeks of age. Levels of *Dbc1* mRNA were measured by real-time qPCR. As expected, genetic ablation in *Dbc1* resulted in a significant decrease of *Dbc1* mRNA levels in *Dbc1*$^{+/-}$ and *Dbc1*$^{-/-}$ as compared to WT mice (Fig. 31 A). *Dbc1*$^{+/-}$ and *Dbc1*$^{-/-}$ mice were found to express 70% and 20% of *Dbc1* mRNA as compared to WT levels respectively. Levels of DBC1 protein were measured by western blotting of cortical lysates from WT, *Dbc1*$^{+/-}$ and *Dbc1*$^{-/-}$ mice at 4 weeks of age using DBC1 antibody produced by Bethyl laboratories (DBC1/p30 antibody A300-432A). This antibody is able to recognise the epitope A300-432A that is encoded by a gene sequence between exon 9 and exon 12, which should be absent in *Dbc1*$^{-/-}$ mice. *Dbc1*$^{+/-}$ and *Dbc1*$^{-/-}$ mice were found to express 60% and 15% of DBC1 protein as compared to WT mice respectively (Fig. 31 B and C), indicating that a very low percentage of DBC1 protein is still expressed in *Dbc1*$^{-/-}$ mice.

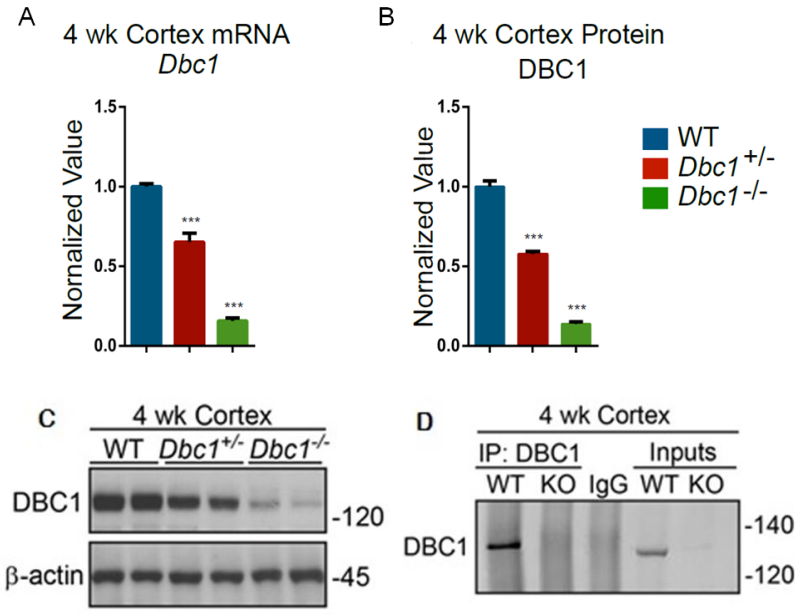

Figure 31. DBC1 mRNA and protein levels in 4 week old cortex from WT, *Dbc1*$^{+/-}$ *(Dbc1 heterozygous)* and *Dbc1*$^{-/-}$ (*Dbc1* knock-out) mice. (A) *Dbc1* mRNA levels in 4 week old cortex from WT, *Dbc1*$^{+/-}$ and Dbc1$^{-/-}$ mice. Expression levels were normalised to the housekeeping genes *Atp5b*, *Canx* and *Rlp13a* (Fig.33) and expressed as fold change of WT levels ± SEM. n=8/ genotype. (B) Relative DBC1 protein levels and (C) representative western blots of WT, *Dbc1*$^{+/-}$ and *Dbc1*$^{-/-}$ lysates 4 week old from cortical mice. Values were normalised to β-actin and expressed as fold change of WT ± SEM. n=4/ genotype. (D) Western blots of DBC1 after DBC1 immunoprecipitation from cortex of WT and *Dbc1*$^{-/-}$ mice (KO) at 4 weeks of age. ***P<0.001 statistically significant as compared to WT. IP: immunoprecipitation.

Unlike the result obtained by western blot, DBC1 immunoprecipitation (Fig. 31 D) and DBC1 immunostaning on isolated nuclei (Fig. 32 A) did not reveal a DBC1 signal in *Dbc1*$^{-/-}$ mice. Taken together, these results may suggest that the DBC1 antibody has a greater affinity for the A300-432A epitope when the DBC1 protein is denatured. Furthermore, the low percentage of the DBC1 protein in *Dbc1*$^{-/-}$ mice indicates that the mechanism used to induce the ablation of DBC1 in these mice is leaking. Since, the NEO cassette is located in an intron it could be possibly removed during splicing, promoting the transcription of the full-length gene and the translation of DBC1 protein.

4.1.1 *Dbc1* knock-out mice show a robust increase of SIRT1 activity in the brain

A previous study has suggested that DBC1 protein is a negative regulator of SIRT1 activity (Kim et al., 2008). To examine the role of DBC1 in the control of SIRT1 activity, we investigated whether DBC1 regulates SIRT1 function *in vivo*. We examined the effect of DBC1 down-regulation on endogenous SIRT1 deacetylase activity by monitoring the levels of endogenous P53 acetylation. To confirm the release of the inhibitory effect of DBC1 on SIRT1 we immunostained nuclei extracted from half brains of WT, *Dbc1*$^{+/-}$ and *Dbc1*$^{-/-}$ mice at 4 weeks of age for DBC1, P53, AcP53 and SIRT1 and counterstained with DAPI. Notably, the absence of DBC1 did not affect the level and nuclear accumulation of SIRT1 and/or P53 (Fig. 32 A and B). As expected, the ablation of DBC1 resulted in an increase of SIRT1 activity as reported by significant reduction in signal intensity for AcP53 in *Dbc1*$^{+/-}$ (≈50%) and *Dbc1*$^{-/-}$ (≈90%) mice as compared to WT mice (Fig. 32 A and B).

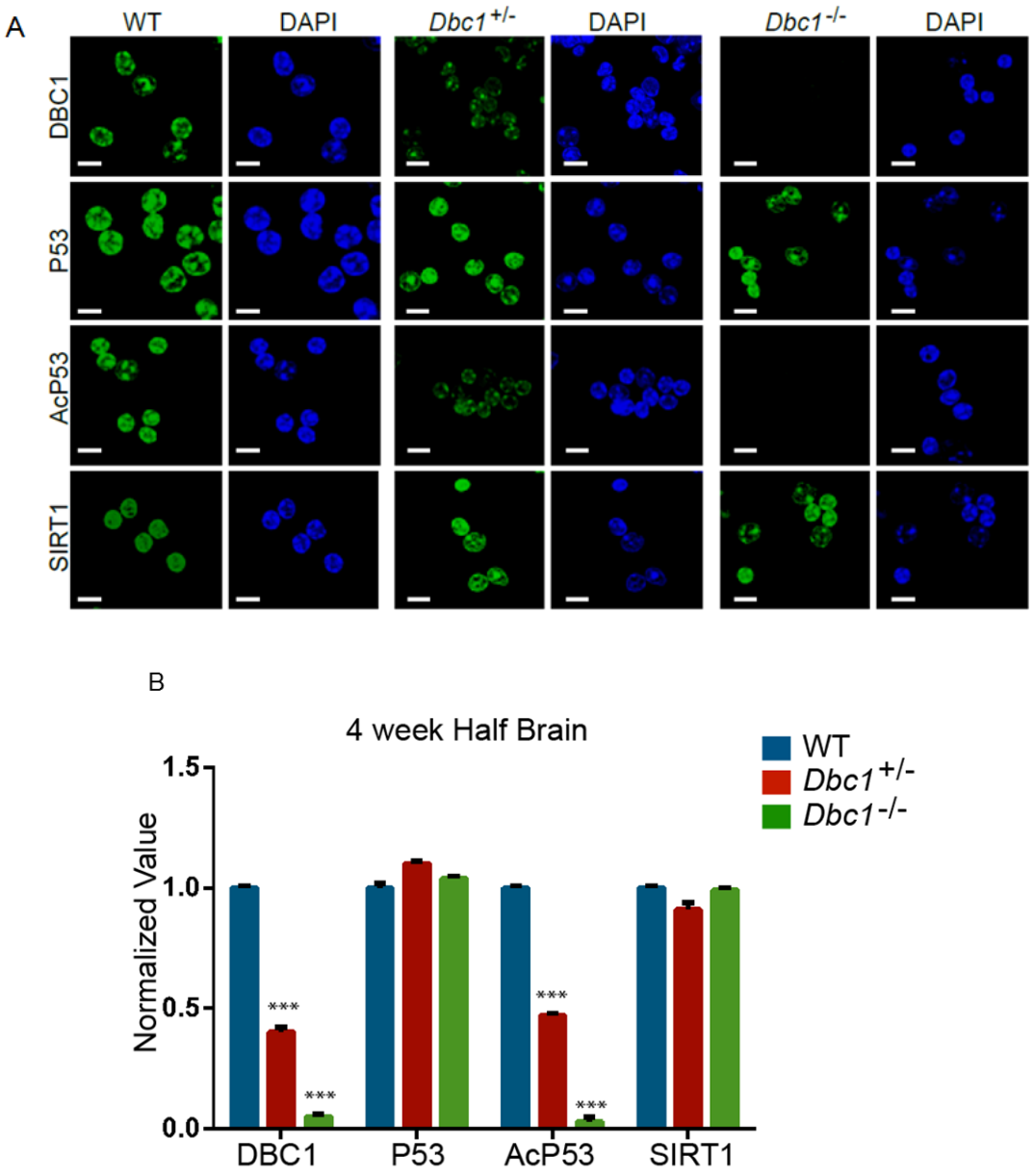

Figure 32. SIRT1 activity levels in 4 week old cortex from WT, *Dbc1*$^{+/-}$ *(Dbc1 heterozygous)* and *Dbc1*$^{-/-}$ (*Dbc1* knock-out) mice. (A) Representative immunofluorescence image of nuclei extracted from half brains of WT, *Dbc1*$^{+/-}$ and *Dbc1*$^{-/-}$ mice at 4 weeks of age immunostained for DBC1, P53, AcP53 and SIRT1, and counterstained with DAPI. (B) Relative intensity level of DBC1, P53, AcP53 and SIRT1 immunostaning in A. The quantification indicates that the level of acetylated p53 is lower in *Dbc1*$^{+/-}$ and *Dbc1*$^{-/-}$ mice, consistent with an increase in SIRT1 activity. Scale bar: 10 µm. Data are mean ±SEM. ***p<0.001 statistically significant as compared to WT. n=4 / genotype.

4.1.2 Effect of *Dbc1* Ablation on Sirtuins and Hdacs gene expression in the brain regions

To demonstrate that the ablation of *Dbc1* increases SIRT1 activity without affecting its expression level, we performed real-time qPCR and western blotting on cortex from WT, *Dbc1*$^{+/-}$ and *Dbc1*$^{-/-}$ mice at 4 week of age. We observed that the genetic reduction of *Dbc1* does not alter mRNA and protein levels of SIRT1 (Fig. 33 A, B and C).

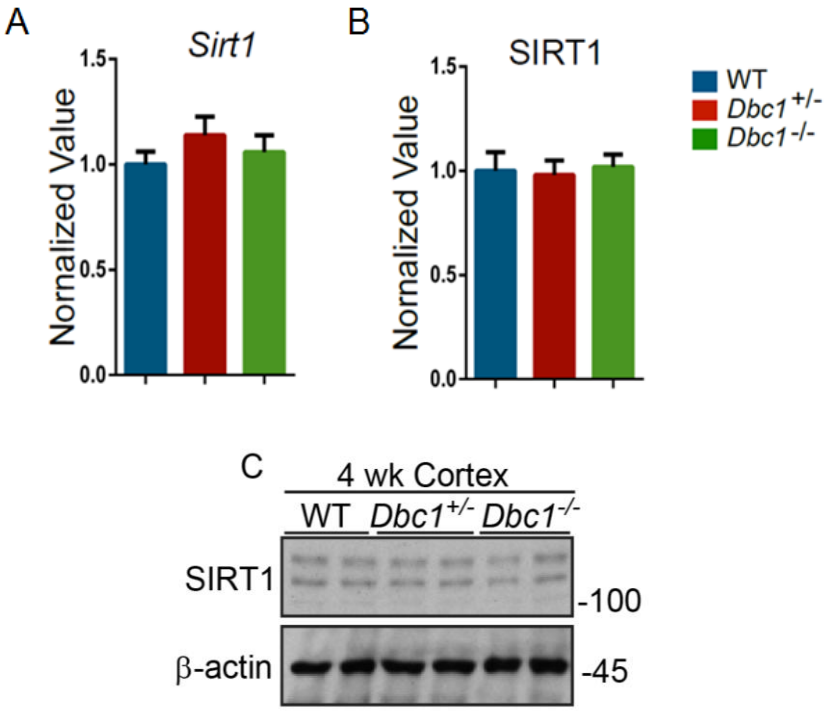

Figure 33. SIRT1 mRNA and protein levels in 4 week old cortex from WT and *Dbc1*$^{-/-}$ (*Dbc1* knock-out) mice. (A) *Sirt1* mRNA levels in 4 week old cortex from WT, *Dbc1*$^{+/-}$ and *Dbc1*$^{-/-}$ mice. Expression levels were normalised to the housekeeping genes *Atp5b*, *Canx* and *Rlp13a* (Fig. 33) and expressed as fold change of WT levels ± SEM. n=8 / genotype. (B) Relative SIRT1 protein levels and (C) representative western blots of WT, *Dbc1*$^{+/-}$ and *Dbc1*$^{-/-}$ cortex lysates 4 week old. Values were normalised to β-actin and expressed as fold change of WT ± SEM. n=4 / genotype.

Subsequently, to ascertain that the reduction or depletion of *Dbc1* does not affect the mRNA expression of the other *Hdacs* or *Sirtuins*, we performed real-time qPCR in five brain regions of WT, *Dbc1*$^{+/-}$ and *Dbc1*$^{-/-}$ mice at 4 week of age. As expected, genetic ablation of *Dbc1* resulted in a significant decrease in *Dbc1* mRNA levels in all five brain regions of *Dbc1*$^{+/-}$ and *Dbc1*$^{-/-}$ as compared to WT mice. Notably, we did not detect any significant changes in the gene expression levels of all *Sirtuins* and *Hdacs* among the three different genotypes (Fig. 34, 35, 36, 37 and 38).

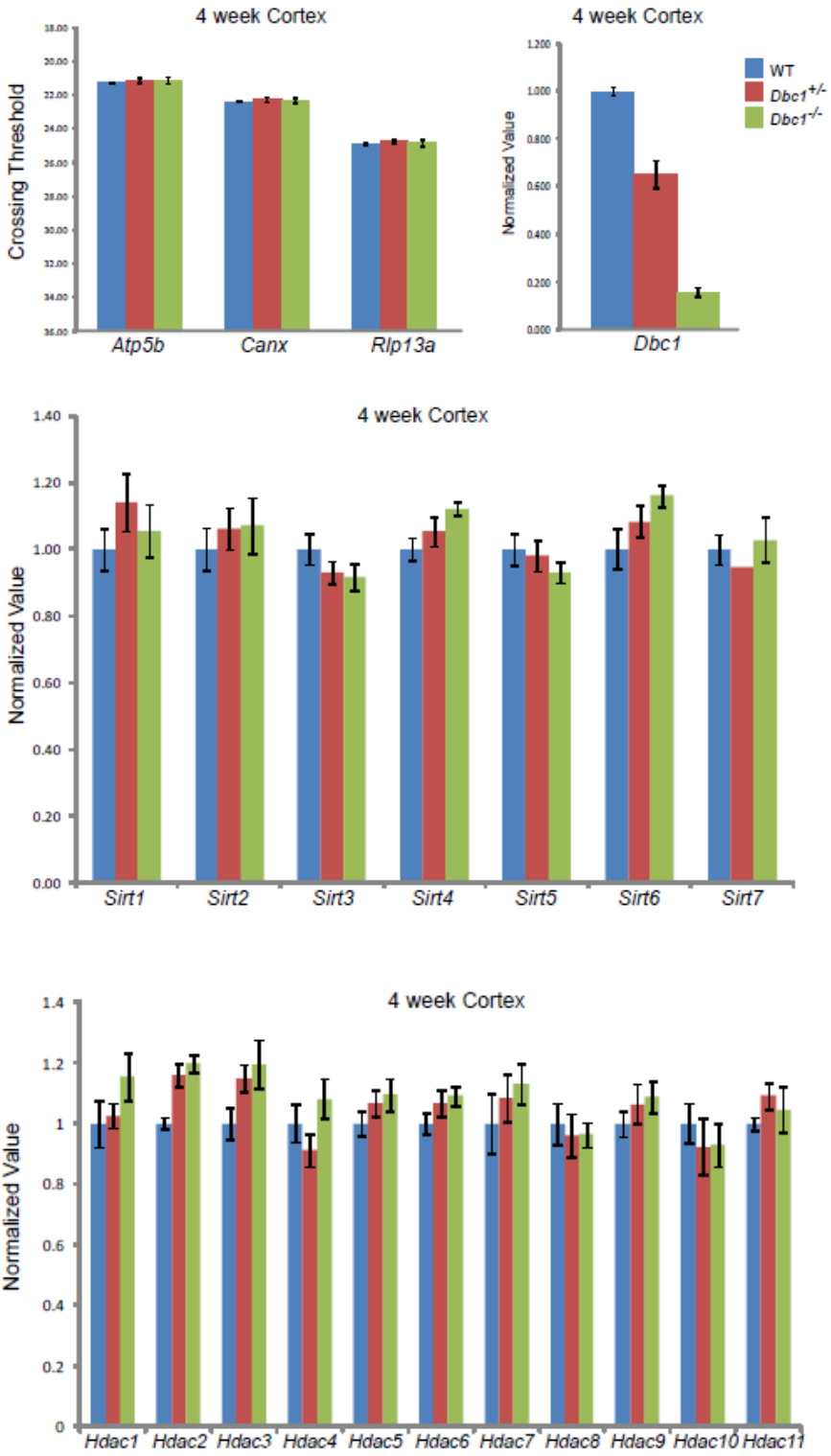

Figure 34. *Sirtuin (1-7)* and *Hdac (1-11)* mRNA levels in 4 week old cortex from WT, *Dbc1*$^{+/-}$ and *Dbc1*$^{-/-}$ mice. Expression levels were normalised to the housekeeping genes *Atp5b*, *Canx* and *Rlp13a* and expressed as fold change of WT levels ± SEM. n = 8 / genotype.

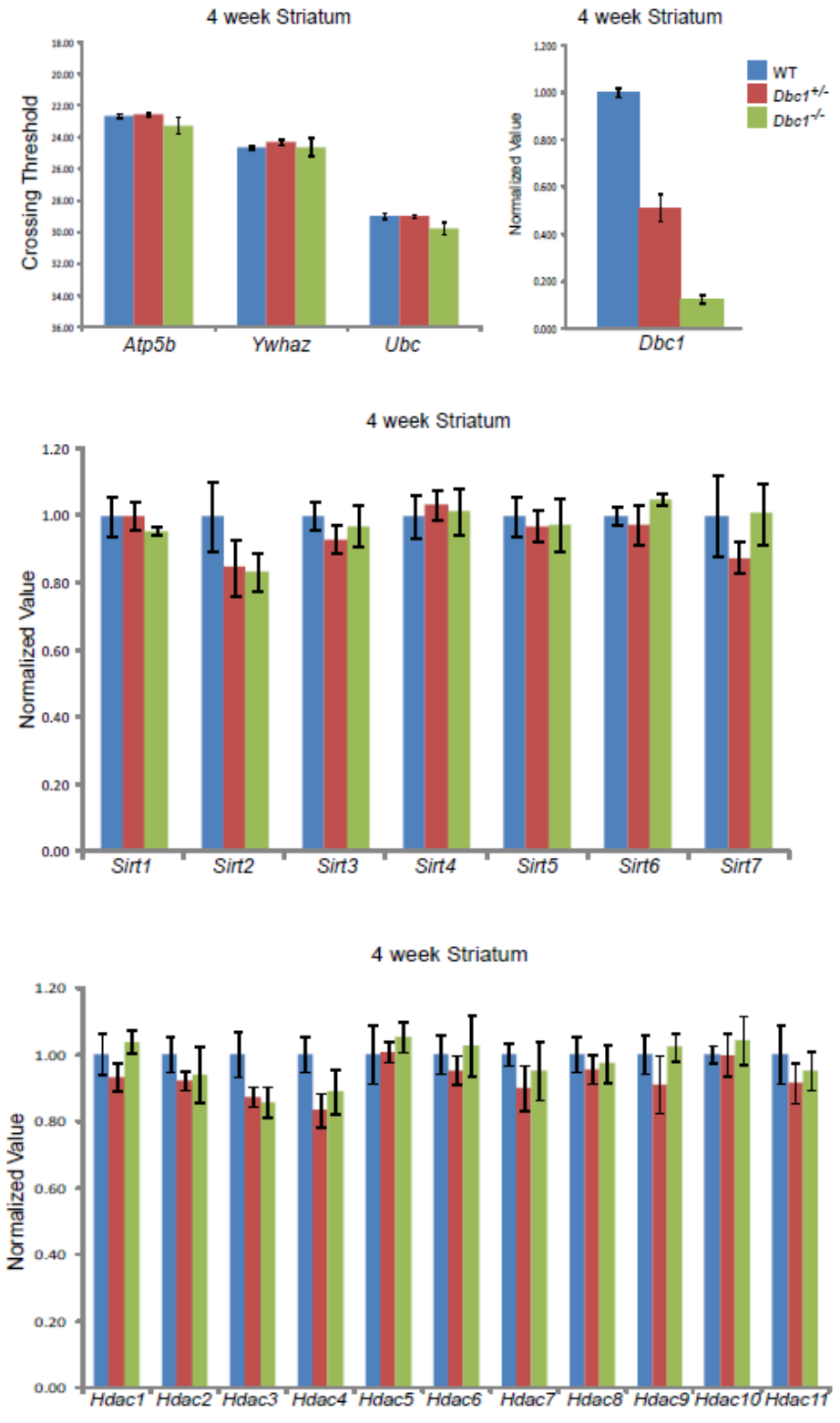

Figure 35. *Sirtuin* (1-7) and *Hdac* (1-11) mRNA levels in 4 week old stritum from WT, *Dbc1*$^{+/-}$ and *Dbc1*$^{-/-}$ mice. Expression levels were normalised to the housekeeping genes *Atp5b*, *Ywhaz* and *Ubc* and expressed as fold change of WT levels ± SEM. n = 8 / genotype.

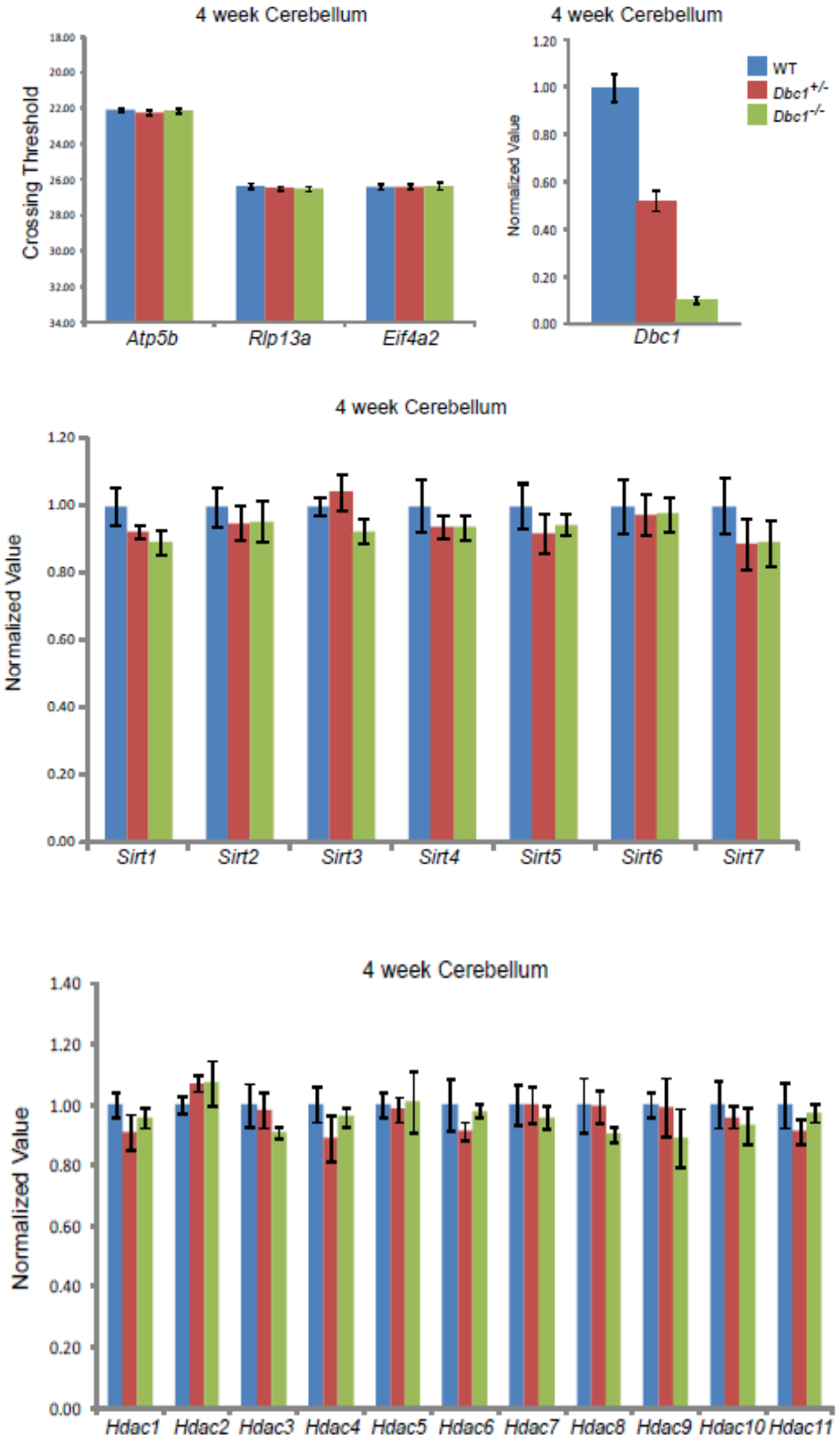

Figure 36. *Sirtuin* (1-7) and *Hdac* (1-11) mRNA levels in 4 week old cerebellum from WT, *Dbc1*$^{+/-}$ and *Dbc1*$^{-/-}$ mice. Expression levels were normalised to the housekeeping genes *Atp5b, Rlp13a* and *Eif4a2* and expressed as fold change of WT levels ± SEM. n = 8 / genotype.

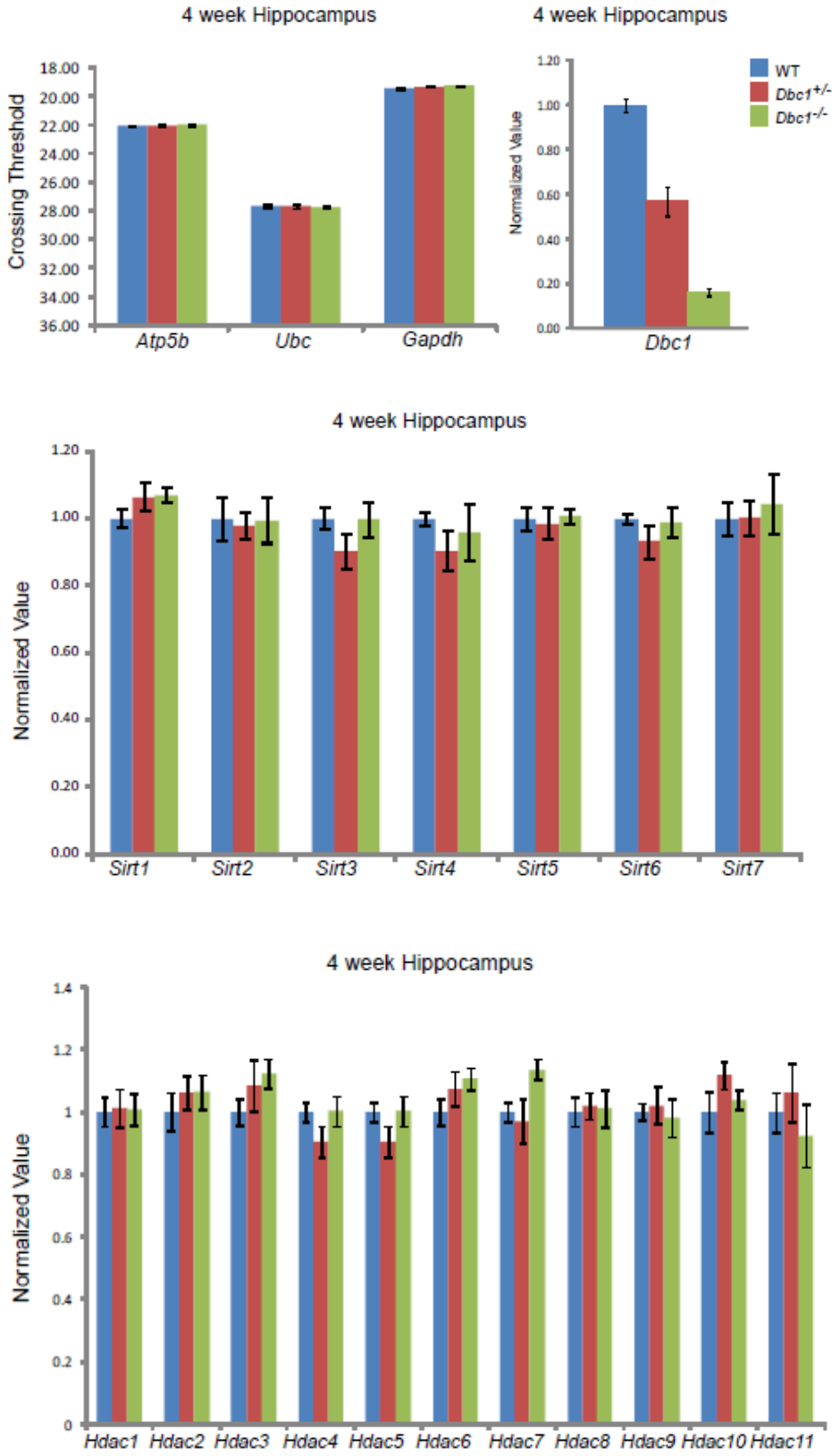

Figure 37. *Sirtuin* (1-7) and *Hdac* (1-11) mRNA levels in 4 week old hippocampus from WT, *Dbc1*$^{+/-}$ and *Dbc1*$^{-/-}$ mice. Expression levels were normalised to the housekeeping genes *Atp5b, Ubc* and *Gapdh* and expressed as fold change of WT levels ± SEM. n = 8 / genotype.

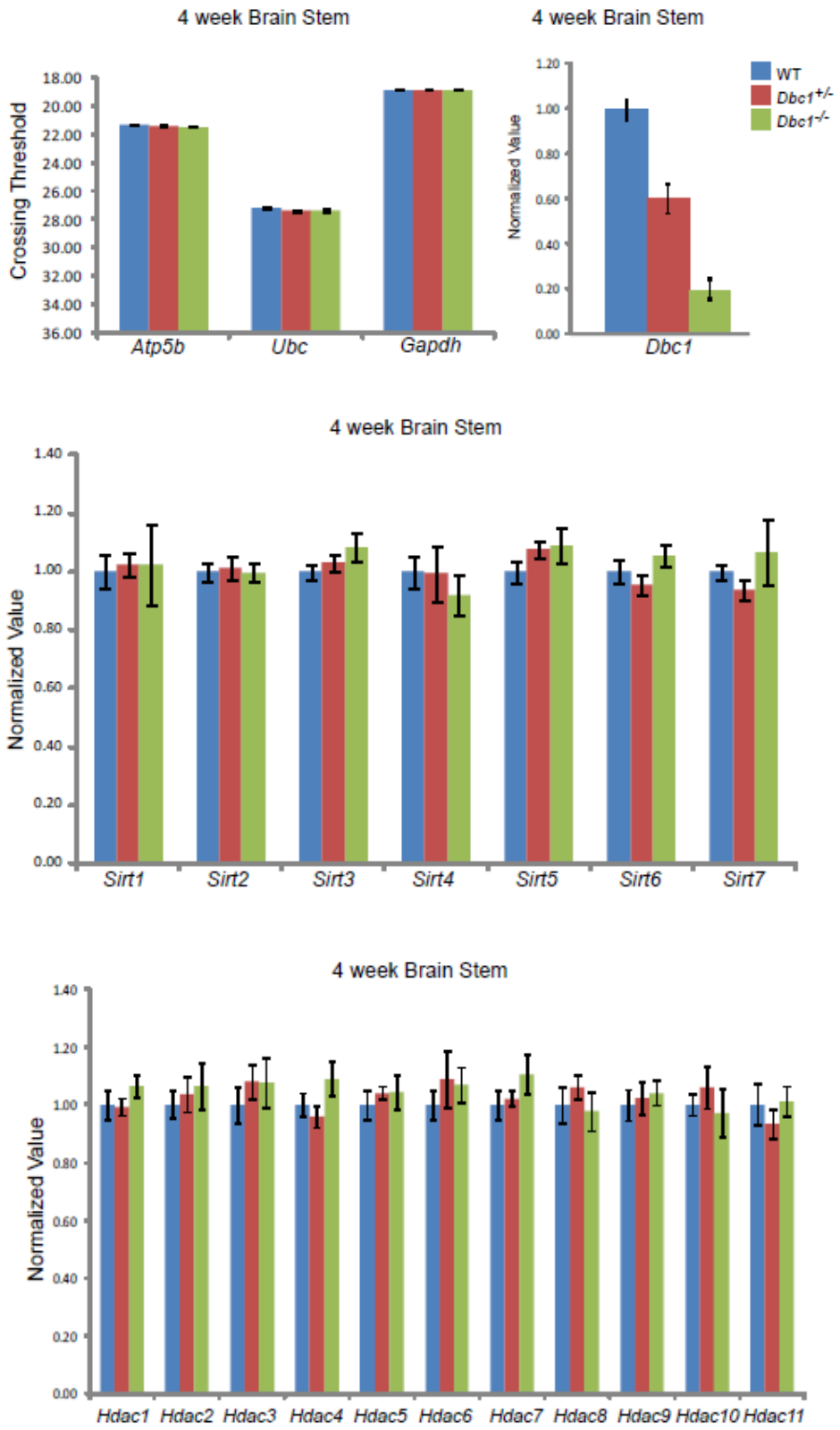

Figure 38. *Sirtuin* (1-7) and *Hdac* (1-11) mRNA levels in 4 week old brain stem from WT, *Dbc1*$^{+/-}$ and *Dbc1*$^{-/-}$ mice. Expression levels were normalised to the housekeeping genes *Atp5b, Ubc* and *Gapdh* and expressed as fold change of WT levels ± SEM. n = 8 / genotype.

4.2 *Dbc1* ablation does not improve HD-related phenotypes

The data presented so far indicate that SIRT1 function is altered in the brain of HD mice caused by the impairment of different cellular processes in specific brain regions. The phosphorylation status of SIRT1 is altered and we hypothesise that AMPK-α1 acts to rescue SIRT1 function. As DBC1 is a negative regulator of SIRT1 we decided to use a genetic approach to reduce DBC1 levels in R6/2 mice and investigate whether the dissociation between SIRT1 and DBC1 could increase striatal SIRT1 activity and improve HD phenotypes. We crossed R6/2 transgenic mice with *Dbc1* knock-out mice to obtain double transgenic mice (*Dbc1*$^{-/-}$::R6/2) (Fig. 39 and Table 7).

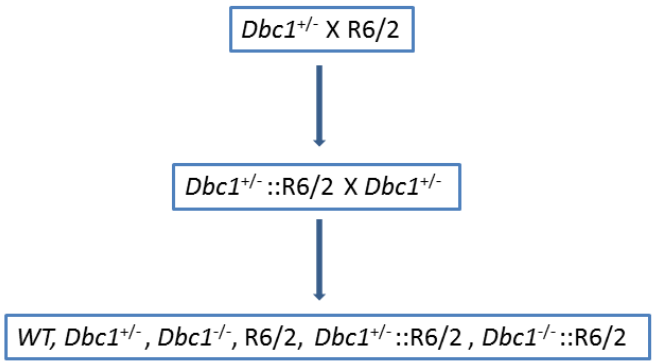

Figure 39. Breeding scheme used to reduce *Dbc1* levels in R6/2 mice.

Genotype	WT	*Dbc1*$^{+/-}$	*Dbc1*$^{-/-}$	R6/2	*Dbc1*$^{+/-}$*::R6/2*	*Dbc1*$^{-/-}$*:: R6/2*
Males	7	11	9	13	9	6
Females	15	8	9	9	9	13
Total	22	19	18	22	18	19

Table 7. Number of mice used in the phenotyping study.

R6/2 mice develop behavioural abnormalities such as rotarod, grip strength impairments, hypo-activity and deficiencies in learning and memory tasks by 8 weeks of age (Hockly et al., 2003). A concomitant loss of body and brain weight, as well as atrophy of skeletal muscle is also evident (Mangiarini et al., 1996).

The behavioural study was as follows:

- ✓ Body weight measured weekly from 4 until 14 weeks of age.
- ✓ Grip strength measured in mice at 4 weeks of age and then bi-weekly from 7 to 13 weeks of age.
- ✓ Rotarod performance was assessed at 4 weeks of age and then bi-weekly from 6 to 14 weeks.
- ✓ Spontaneous motor activity was measured bi-weekly from 5 to 13 weeks of age.

Mice were sacrificed at 15 weeks of age and the brains were weighed.

4.2.1 *Dbc1* ablation does not rescue SIRT1 activity in R6/2 mice

To confirm an increase of SIRT1 activity in the absence of DBC1, we immunostained nuclei extracted from half brains of WT, *Dbc1*$^{-/-}$, R6/2 and *Dbc1*$^{-/-}$::R6/2 mice at 9 weeks of age for SIRT1, P53, AcP53 and DBC1 and counterstained with DAPI. Notably, the absence of DBC1 did not affect the level and nuclear accumulation of SIRT1 and/or P53 (Fig. 41 A and B). As expected, the ablation of DBC1 in WT mice resulted in an increase of SIRT1 activity as reported by a significant reduction (≈65%) in signal intensity for AcP53 in *Dbc1*$^{-/-}$ as compared to WT mice. R6/2 mice showed a significantly higher level of AcP53 compared to WT samples, consistent with a decrease of SIRT1 activity (Fig. 41 A and B). Surprisingly, *Dbc1*$^{-/-}$::R6/2 mice showed the same SIRT1 impairment as R6/2 mice and the level of AcP53 was significantly higher than in WT mice (Fig. 41 A and B). Levels of *Dbc1* and R6/2 transgene have been confirmed by qPCR (Fig. 40). Taken together, these results suggest that the negative effect of mHTT on SIRT1 activity might be multifactorial and/or operate outside the inhibitory circuit controlled by DBC1. In line with these results, we did not detect any effect on the onset and progression of several behavioural and pathological HD-related phenotypes such as brain weight, body weight, grip strength, rotarod and activity (Fig. 42, 43, 44, 45, 46, 47, 48 and 49).

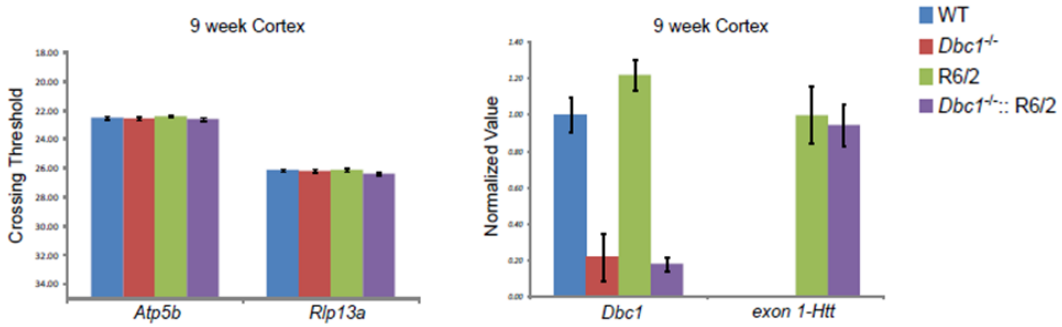

Figure 40. The mRNA expression levels of *Dbc1* and R6/2 transgene in 9 week old cortex from WT, *Dbc1*$^{-/-}$, R6/2 and *Dbc1*$^{-/-}$::R6/2 mice. Expression levels were normalised to the housekeeping genes *Atp5b* and *Rlp13a* and expressed as fold change of WT levels ± SEM. n = 8 / genotype.

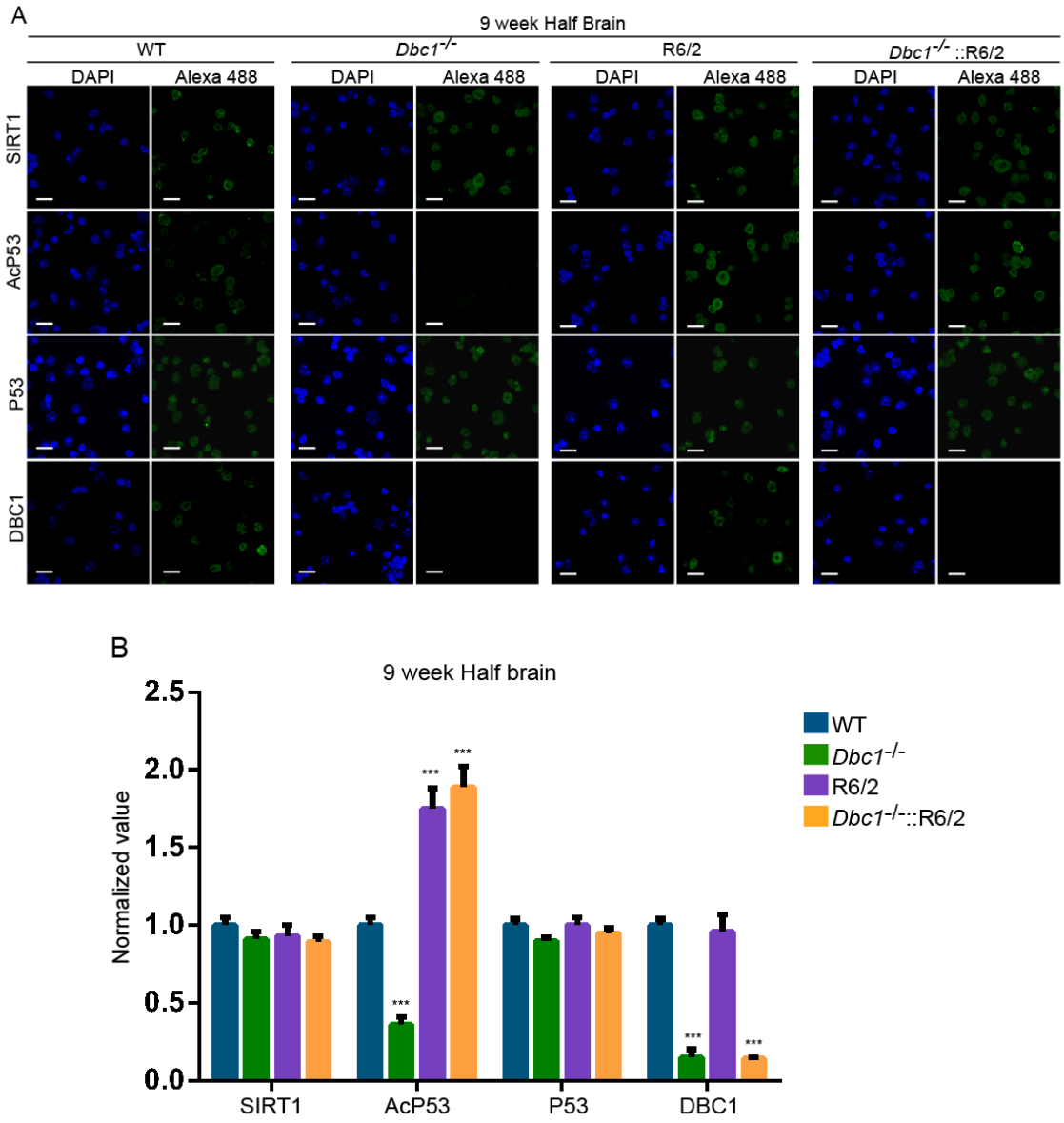

Figure 41. SIRT1 activity in 9 week half brain of WT, *Dbc1*$^{-/-}$ (*Dbc1* knock-out), R6/2 and *Dbc1*$^{-/-}$::R6/2 (Double transgenic) mice. (A) Representative immunofluorescence image of nuclei extracted from half brains of WT, *Dbc1*$^{-/-}$, R6/2 and *Dbc1*$^{-/-}$::R6/2 mice at 9 weeks of age immunostained for SIRT1, AcP53, P53 and DBC1 and counterstained with DAPI. (B) Relative intensity level of SIRT1, AcP53, P53 and DBC1 immunostaning in A. The quantification indicates that the level of acetylated P53 is lower in *Dbc1*$^{-/-}$ mice and higher in R6/2 as compared to WT, consistent with an increase and a decrease in SIRT1 activity, respectively. Scale bar: 10 µm. Data are mean ± SEM. ***p<0.001 statistically significant as compared to WT. n=4 / genotype.

4.2.2 DBC1 reduction does not improve the weight loss in R6/2 mice

Mice were weighed weekly from 4 until 14 weeks of age. As the gender significantly affected the weight ($p<0.0005$) and weight gain ($p<0.0005$), male and female weights were depicted separately (Fig. 42 and 43). R6/2 mice weighed significantly less than WT mice ($p<0.0005$) overall. Weight loss in R6/2 transgenic mice started at 11 weeks of age ($p=0.05$) and increased with disease progression ($p<0.0005$). The *Dbc1* mutation had no overall effect on R6/2 weight loss ($p=0.754$) or on the decrease in the weight of R6/2 over time ($p=0.694$)((Table 8).

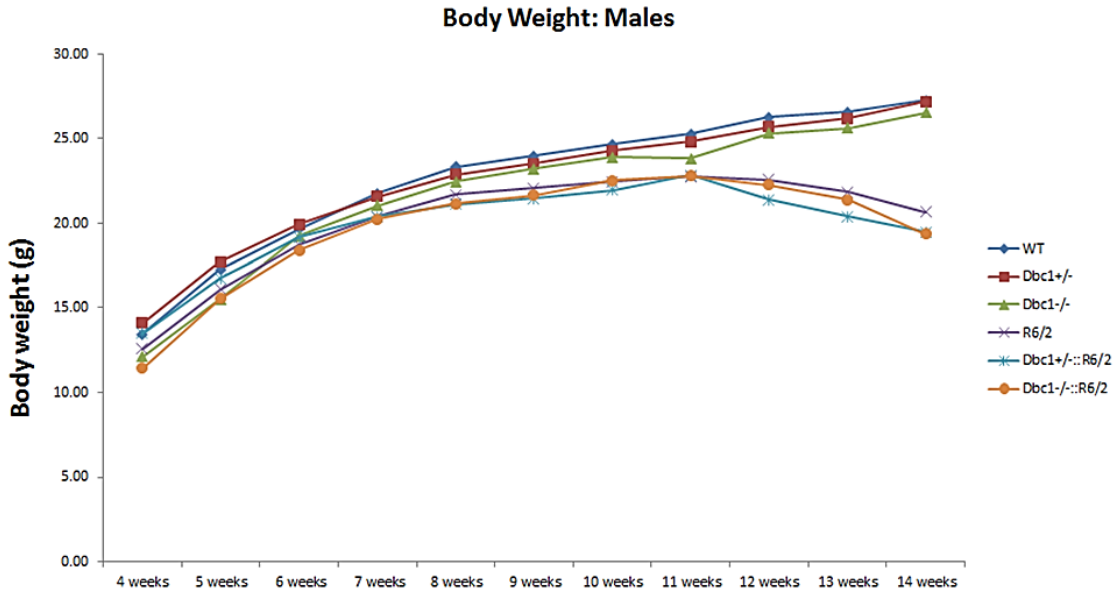

Figure 42. Effect of *Dbc1* knock-down and knock-out on body weight loss in R6/2 males mice. Mean body weight measured from 4 until 14 weeks of age in WT (22), *Dbc1*$^{+/-}$ (19), *Dbc1*$^{-/-}$ (18), R6/2 (22), *Dbc1*$^{+/-}$::R6/2 (18) and *Dbc1*$^{-/-}$::R6/2 (19) mice.

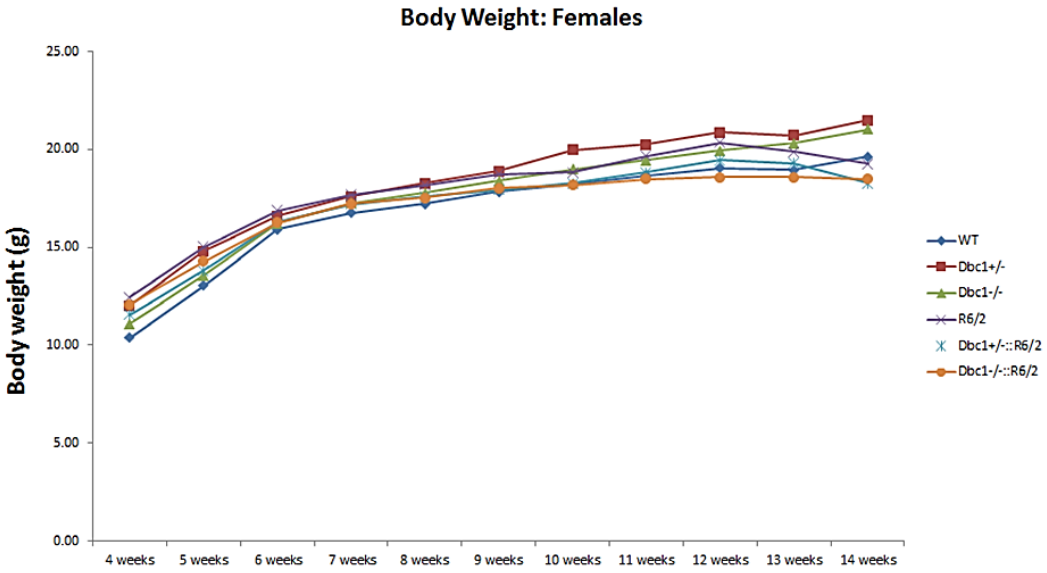

Figure 43. Effect of *Dbc1* knock-down and knock-out on body weight loss in R6/2 females mice. Mean body weight measured from 4 until 14 weeks of age in WT (22), *Dbc1*$^{+/-}$ (19), *Dbc1*$^{-/-}$ (18), R6/2 (22), *Dbc1*$^{+/-}$::R6/2 (18) and *Dbc1*$^{-/-}$::R6/2 (19) mice.

Comparison	*p-value*
Age*R6/2	$p<0.0005$
Age*Dbc1$^{-/-}$	$p=0.211$
Age*Dbc1$^{-/-}$*R6/2	$p=0.694$
R6/2	$p<0.0005$
Dbc1$^{-/-}$	$p=0.879$
Dbc1$^{-/-}$*R6/2	$p=0.754$

Table 8. Summary of *p*-values obtained from the statistical analysis of body weight measurements. Statistical analysis was performed by ANOVA-General Linear Model repeated measures.

4.2.3 Grip strength is not improved by the loss of DBC1 in R6/2 mice

Grip strength was measured in mice at 4 weeks of age and bi-weekly from 7 to 13 weeks of age. As there was a significant gender difference in over all grip strength performance ($p<0.0005$), the average grip strength of male and female mice is presented separately (Fig. 44 and 45). R6/2 mice had reduced grip strength compared to WT ($p<0.0005$). This deficit was apparent by 11 weeks of age ($p<0.0005$) and deteriorated over the time ($p<0.0005$). The *Dbc1* mutation had no overall effect on R6/2 grip strength ($p=0.261$) or with the time ($p=0.633$) (Table 9).

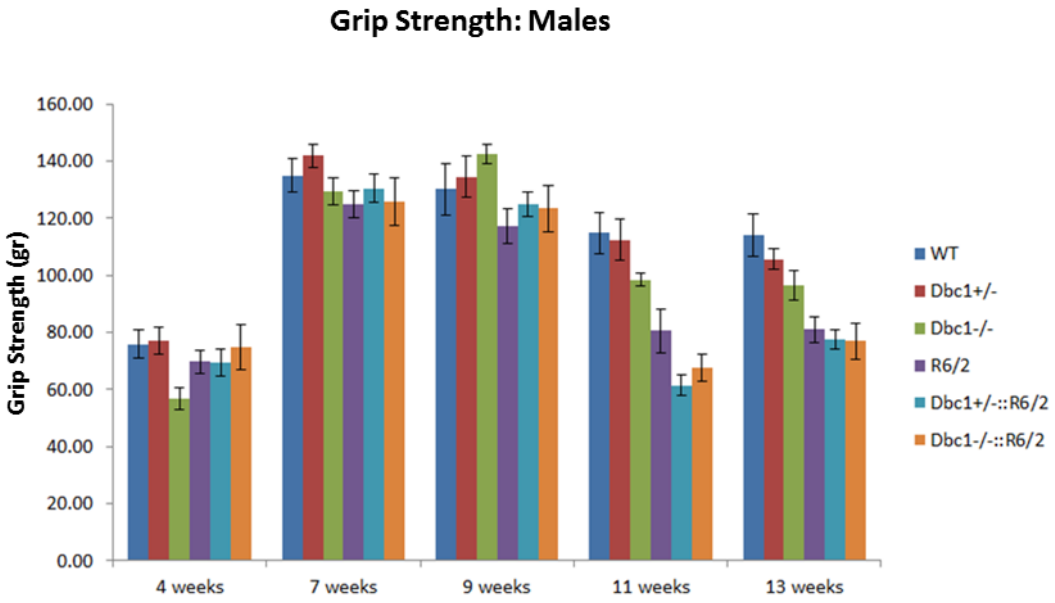

Figure 44. Effect of *Dbc1* knock-down and knock-out on grip strength performance in R6/2 females mice. Grip strength performance measured at 4 week and bi-weekly from 7 to 13 weeks of age in WT (22), *Dbc1*$^{+/-}$ (19), *Dbc1*$^{-/-}$ (18), R6/2 (22), *Dbc1*$^{+/-}$::R6/2 (18) and *Dbc1*$^{-/-}$::R6/2 (19) mice. Error bars represent ± SEM.

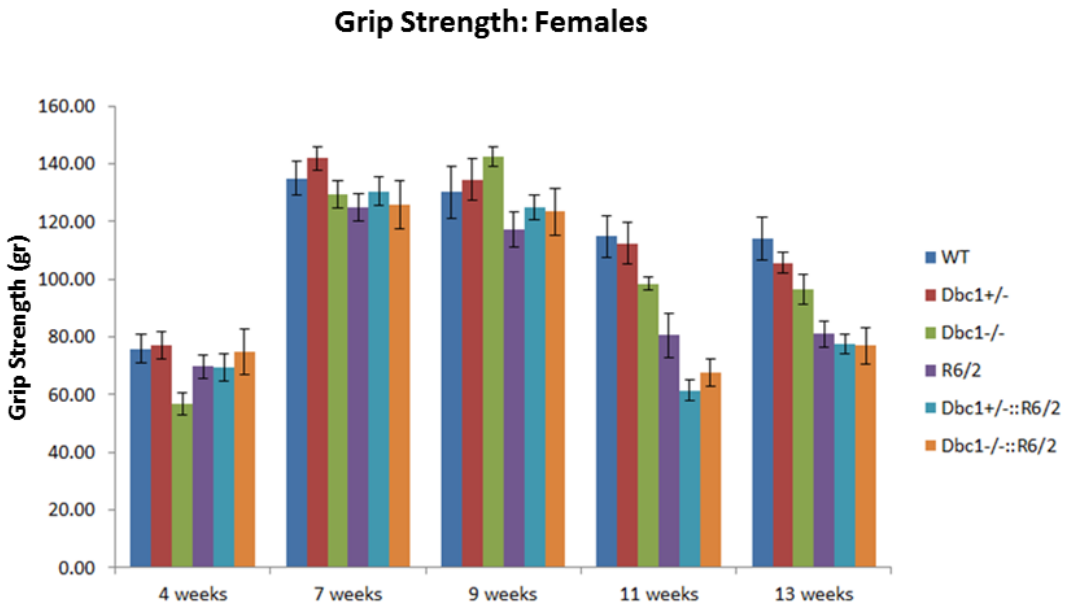

Figure 45. Effect of *Dbc1* knock-down and knock-out on grip strength performance in R6/2 females mice. Grip strength performance measured at 4 week and bi-weekly from 7 to 13 weeks of age in WT (22), *Dbc1*$^{+/-}$ (19), *Dbc1*$^{-/-}$ (18), R6/2 (22), *Dbc1*$^{+/-}$::R6/2 (18) and *Dbc1*$^{-/-}$::R6/2 (19) mice. Error bars represent ± SEM.

Comparison	*p-value*
Age*R6/2	$p<0.0005$
Age*Dbc1$^{-/-}$	$p=0.563$
Age*Dbc1$^{-/-}$*R6/2	$p=0.633$
R6/2	$p<0.0005$
Dbc1$^{-/-}$	$p=0.327$
Dbc1$^{-/-}$*R6/2	$p=0.261$

Table 9. Summary of *p*-values obtained from the statistical analysis of grip strenght measurements. Statistical analysis was performed by ANOVA-General Linear Model repeated measures.

4.2.4 Rotarod performance is not improved by the ablation of *Dbc1* gene in R6/2 mice

Rotarod performance was assessed at 4 weeks of age and measured bi-weekly from 6 to 14 weeks of age. No gender effects were observed (p=0.236). R6/2 mice were indistinguishable from WT littermates at 4 weeks of age (p=0.462) but their performance deteriorated over time (p<0.0005) starting at 8 weeks of age (p<0.0005). *Dbc1*$^{+/-}$ and *Dbc1*$^{-/-}$ mice did not perform differently from WT mice overall (p=0.584) or with time (p=0.384) and down-regulation or ablation of *Dbc1* had no effect on the rotarod performance of R6/2 mice (p=0.265) or its deterioration over the time (p=0.692) (Table 10). Therefore, it was concluded that neither DBC1 reduction nor depletion affected rotarod performance in WT or R6/2 mice (Figure 46).

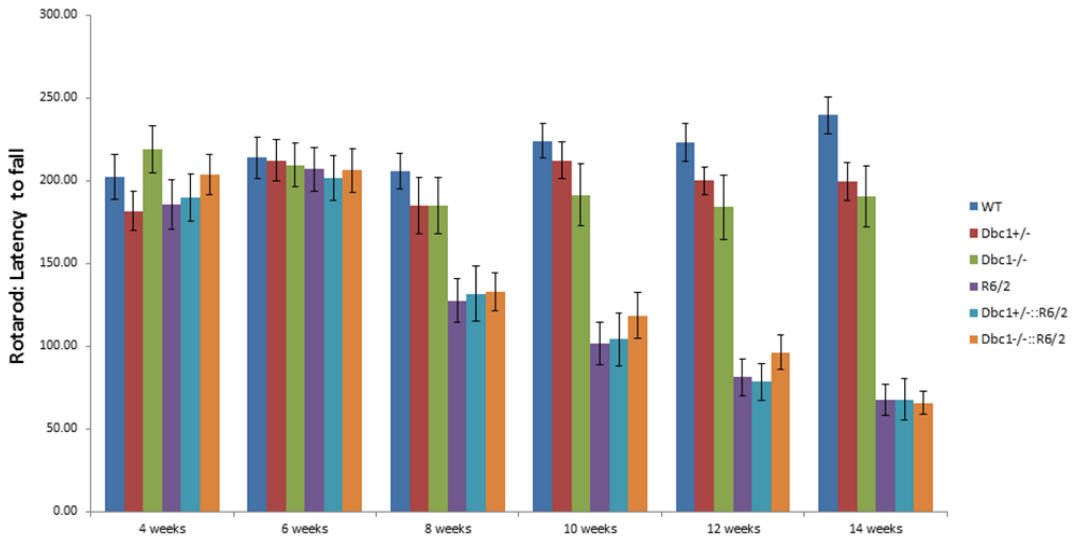

Figure 46. *Dbc1* knock-down and knock-out does not improve rotarod performance in R6/2 mice. Rotarod performance measured at 4 week and bi-weekly from 6 to 14 weeks of age in WT (22), *Dbc1*$^{+/-}$ (19), *Dbc1*$^{-/-}$ (18), R6/2 (22), *Dbc1*$^{+/-}$::R6/2 (18) and *Dbc1*$^{-/-}$::R6/2 (19) mice. Error bars represent ± SEM.

Comparison	*p-value*
Age*R6/2	$p<0.0005$
Age*$Dbc1^{-/-}$	$p=0.384$
Age*$Dbc1^{-/-}$*R6/2	$p=0.692$
R6/2	$p<0.0005$
$Dbc1^{-/-}$	$p=0.584$
$Dbc1^{-/-}$*R6/2	$p=0.265$

Table 10. Summary of *p*-values obtained from the statistical analysis of rotarod performance measurements. Statistical analysis was performed by ANOVA-General Linear Model repeated measures.

4.2.5 *Dbc1* genetic reduction does not influence hypo-activity of R6/2 mice

Spontaneous motor activity was recorded for each mouse for 30 min bi-weekly from 5 to 13 weeks of age. R6/2 mice exhibited significant hypo-activity with disease progression compared to wild type mice for all four parameters. Deficits in MOBILITY were already apparent in R6/2 transgenic mice at 5 weeks of age. HYPO-ACTIVITY became evident in R6/2 transgenic mice at 7 weeks of age. Decreased CENTRE REARING and REARING was detected at 9 and 11 weeks of age respectively. Reduction or ablation of DBC1 had no effect on any of these parameters at any age tested, and therefore did not modify the pattern of exploration over time and did not affect the hypo-activity of R6/2 mice (Fig. 47, 48, 49 and 50).

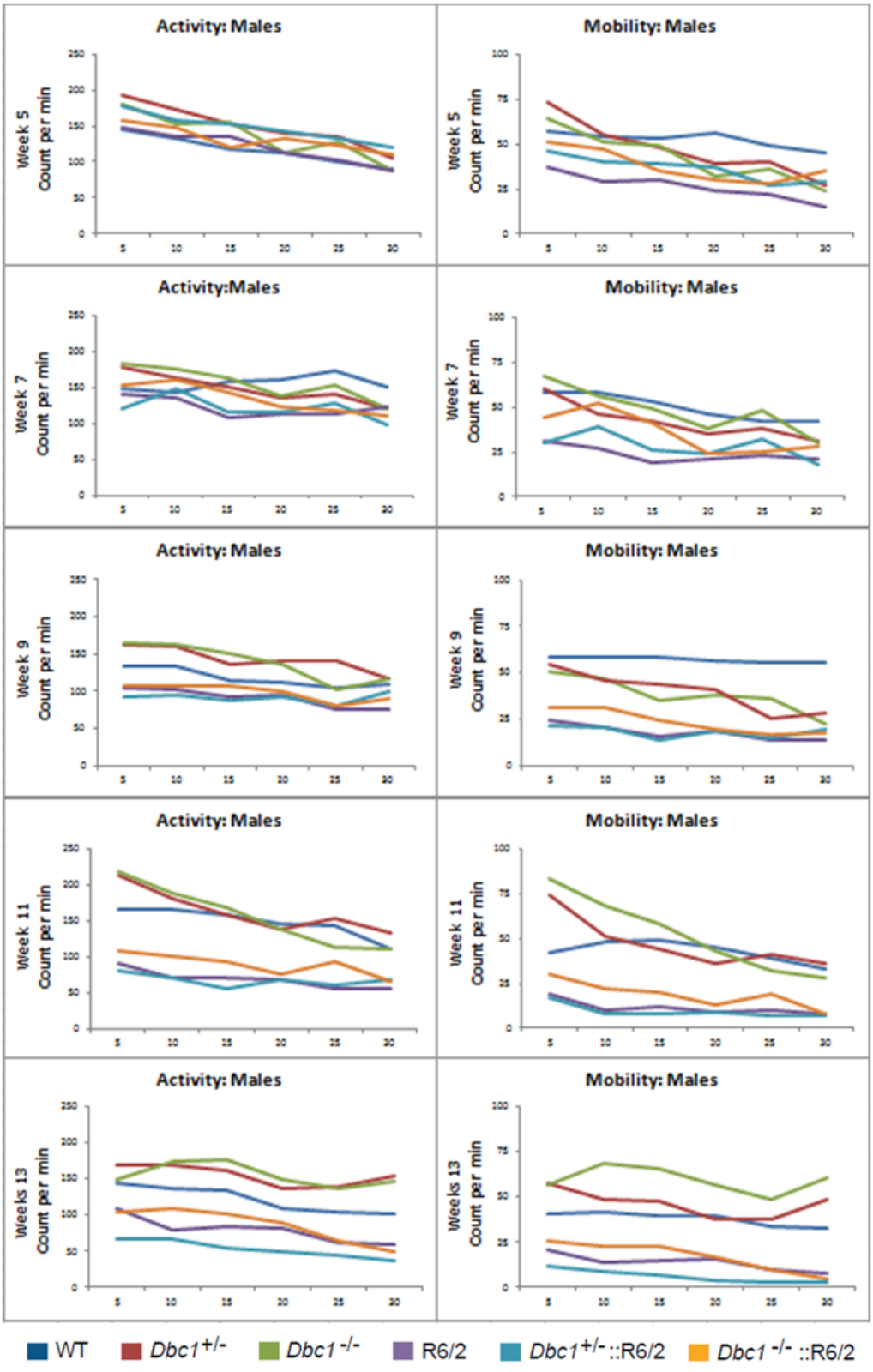

Figure 47. Spontaneous motor activity in R6/2 males. Activity and mobility were recorded in mice over the course of 30 min at 5, 7, 9, 11 and 13 weeks of age. Spontaneous motor activity parameter measurements were visualised by plotting 5 min moving averages.

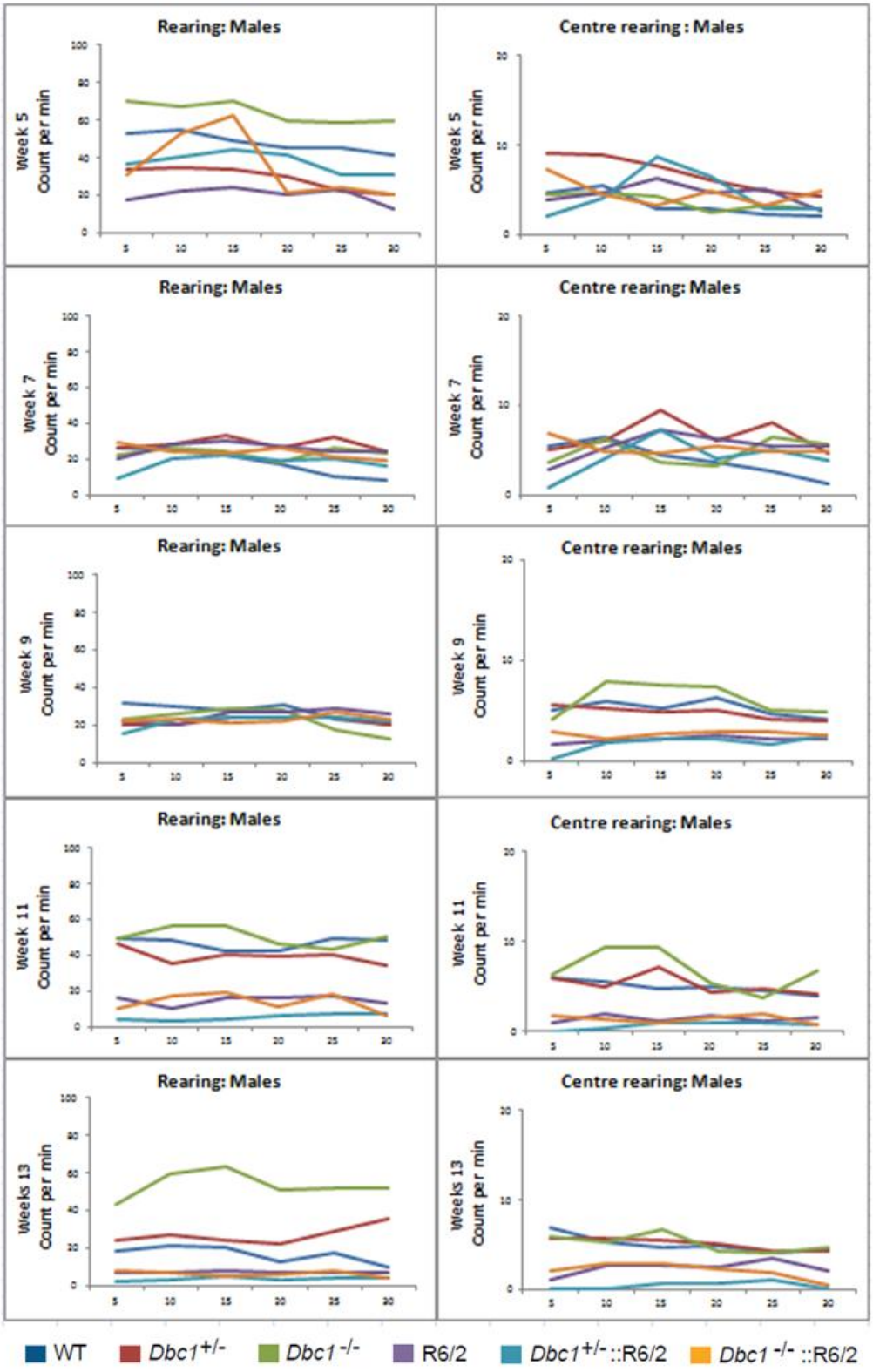

Figure 48. Spontaneous motor activity in R6/2 males. Rearing and centre rearing were recorded in mice over the course of 30 min at 5, 7, 9, 11 and 13 weeks of age. Spontaneous motor activity parameter measurements were visualised by plotting 5 min moving averages.

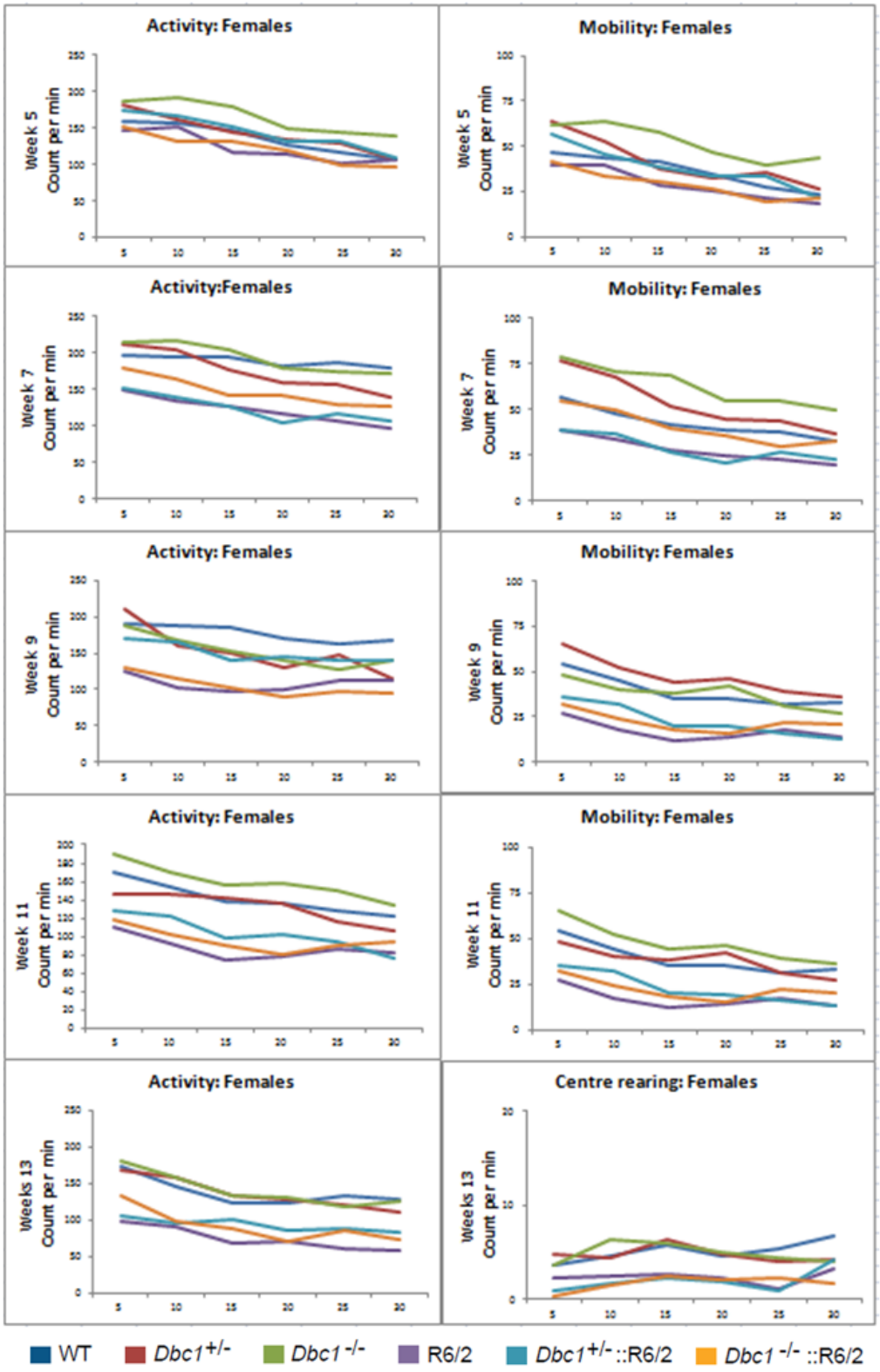

Figure 49. Spontaneous motor activity in R6/2 females. Activity and mobility were recorded in mice over the course of 30 min at 5, 7, 9, 11 and 13 weeks of age. Spontaneous motor activity parameter measurements were visualised by plotting 5 min moving averages.

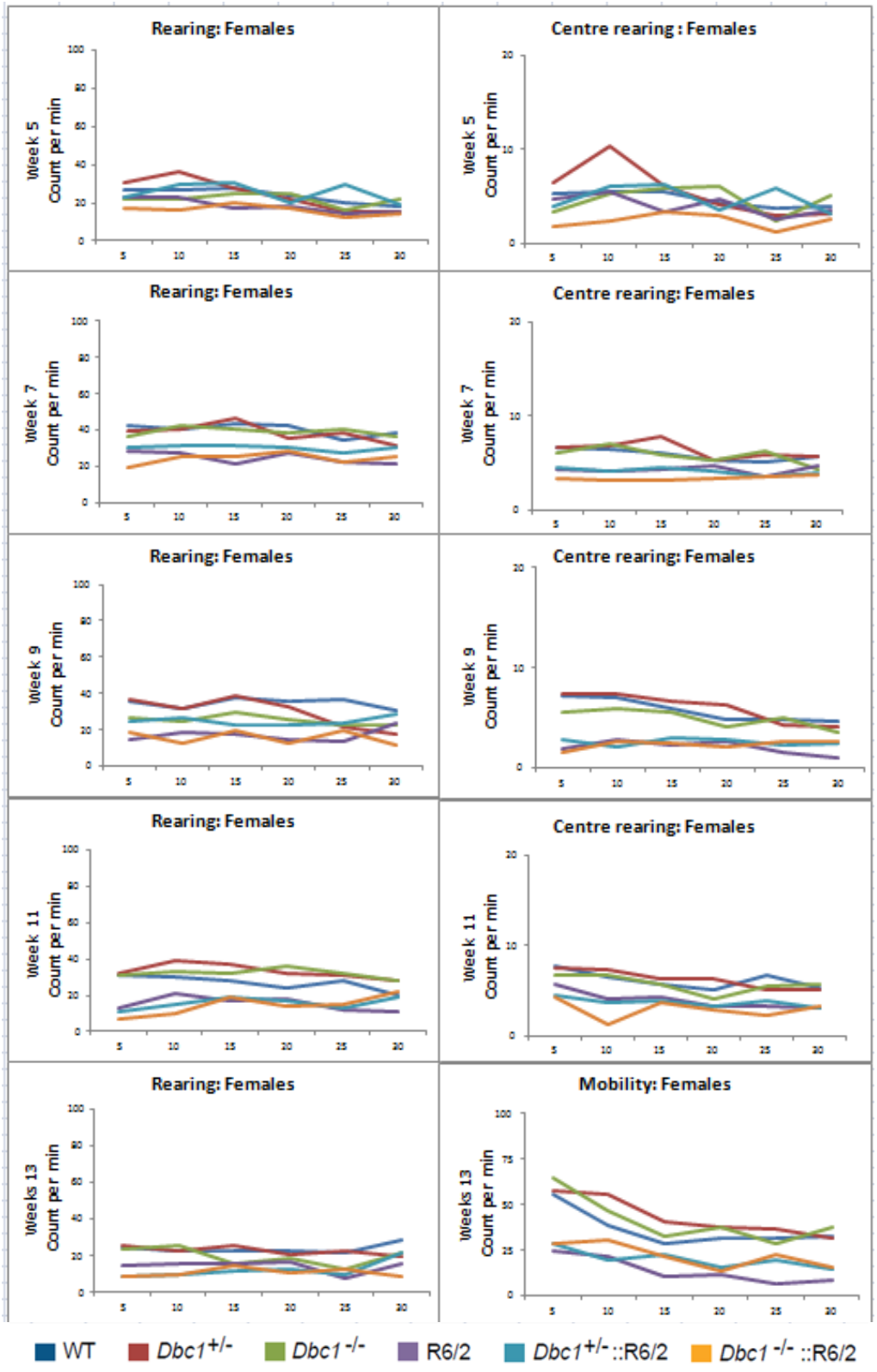

Figure 50. Spontaneous motor activity in R6/2 females. Rearing and centre rearing were recorded in mice over the course of 30 min at 5, 7, 9, 11 and 13 weeks of age. Spontaneous motor activity parameter measurements were visualised by plotting 5 min moving averages.

Comparison	Week	Activity	Mobility	Rearing	Centre rearing
Age*R6/2	5	=0.547	<0.001	=0.469	=0.642
	7	<0.001	<0.001	=0.358	=0.328
	9	<0.001	<0.001	<0.001	=0.219
	11	<0.001	<0.001	<0.001	<0.001
	13	<0.001	<0.001	<0.001	<0.001
Age*$Dbc1^{-/-}$	5	=0.643	=0.144	=0.664	=0.864
	7	=0.479	=0.241	=0.129	=0.267
	9	=0.246	=0.185	=0.678	=0.367
	11	=0.531	=0.598	=0.254	=0.120
	13	=0.798	=0.346	=0.146	=0.468
Age*$Dbc1^{-/-}$*R6/2	5	=0.380	=0.468	=0.498	=0.852
	7	=0.168	=0.216	=0.271	=0.216
	9	=0.243	=0.375	=0.117	=0.579
	11	=0.098	=0.598	=0.663	=0.865
	13	=0.735	=0.132	=0.749	=0.721
R6/2	5	=0.284	<0.001	=0.306	=0.845
	7	<0.001	<0.001	=0.097	=0.386
	9	<0.001	<0.001	<0.001	=0.124
	11	<0.001	<0.001	<0.001	<0.001
	13	<0.001	<0.001	<0.001	<0.001
$Dbc1^{-/-}$	5	=0.194	=0.846	=0.868	=0.276
	7	=0.635	=0.429	=0.531	=0.276
	9	=0.557	=0.647	=0.134	=0.236
	11	=0.118	=0.134	=0.465	=0.312
	13	=0.845	=0.921	=0.653	=0.364
$Dbc1^{-/-}$*R6/2	5	=0.538	=0.367	=0.184	=0.298
	7	=0.751	=0.287	=0.789	=0.309
	9	=0.251	=0.621	=0.472	=0.284
	11	=0.092	=0.391	=0.398	=0.361
	13	=0.120	=0.294	=0.524	=0.582

Table 12. Summary of *p*-values obtained from the statistical analysis of exploratory motor activity. Statistical analysis was performed by ANOVA-General Linear Model repeated measures.

4.2.6 The reduction in R6/2 brain weight is not increased by the genetic ablation of *Dbc1* gene

At the end of the behavioural study, the mice were sacrificed at 15 weeks of age and the brains weighed. As expected, R6/2 brains weighed significantly less than those of WT mice (p<0.0005). Unfortunately, the genetic ablation of *Dbc1* had no effect on R6/2 brain weight loss (p=0.11) (Fig. 51 and Table 11).

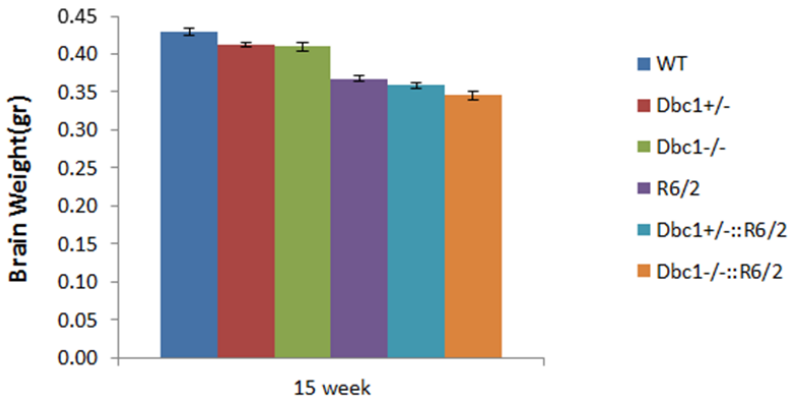

Figure 51. Effect of *Dbc1* knock-down and knock-out on brain weight in R6/2 mice. Brain weight measured at 15 weeks of age in WT (22), $Dbc1^{+/-}$ (19), $Dbc1^{-/-}$ (18), R6/2 (22), $Dbc1^{+/-}$::R6/2 (18) and $Dbc1^{-/-}$::R6/2 (19) mice. Error bars represent ± SEM.

Comparison	*p-value*
R6/2	p<0.0005
***Dbc1*$^{-/-}$**	p=0.43
***Dbc1*$^{-/-}$*R6/2**	p=0.11

Table 11. Summary of *p*-values obtained from the statistical analysis of brain weight measurements.

4.3 Cholesterogenic enzyme dys-homeostasis is not corrected by the ablation of *Dbc1* gene in R6/2 mice

Levels of cholesterol biosynthetic enzymes have been reported to be decreased in R6/2 mice (Valenza et al., 2007), and several studies have already shown a decrease in the expression of cholesterol synthesis enzymes in HD. It has been suggested that this is a result of mHTT perturbing the transcriptional activity of a master regulator of cholesterol synthesis SREBP-2 (Valenza et al., 2005; 2007; 2010).

The sterol regulatory element-binding protein (SREBP) transcription factor family is a regulator of lipid and sterol homeostasis in eukaryotes. In mammals, SREBPs are able to promote the expression of lipogenic and cholesterogenic genes and to facilitate fat storage. It has been demonstrated that SREBP is an *in vivo* target of SIRT1 (Ponugoti et al., 2010), and the interaction between SIRT1 and SREBP was increased during fasting and decreased upon feeding. Consistent with this, SREBP acetylation levels were decreased during fasting in mouse liver (Ponugoti et al., 2010). Interestingly, a modulation of SIRT1 activity results in changes in SREBP ubiquitination, protein stability, and target gene expression. In addition, chemical activators of SIRT1 inhibit SREBP target gene expression *in vitro* and *in vivo*, correlating with decreased hepatic lipid and cholesterol levels and attenuated liver steatosis in diet-induced and genetically obese mice (Walker et al. 2010).

Therefore, we checked if an increase of SIRT1 activity, due the ablation of *Dbc1* gene, might have an effect on the expression of cholesterol biosynthetic genes.

The expression of cholesterogenic enzymes was measure by Taqman qPCR assays.

DBC1 genetic ablation had no effect on the expression of cholesterogenic enzymes in

WT mice (Fig. 52), while the R6/2 genotype had a statistically significant effect on the expression of all cholesterogenic enzymes examined (Fig. 53)

Taken together, these results suggest that the expression of enzymes responsible for cholesterol synthesis is not affected in *Dbc1*$^{+/-}$ and *Dbc1*$^{-/-}$ mice. This may be because DBC1 and SIRT1 do not regulate cholesterol synthesis, or because a compensatory mechanism has acts to maintain the levels of cholesterol biosynthetic genes after DBC1 ablation.

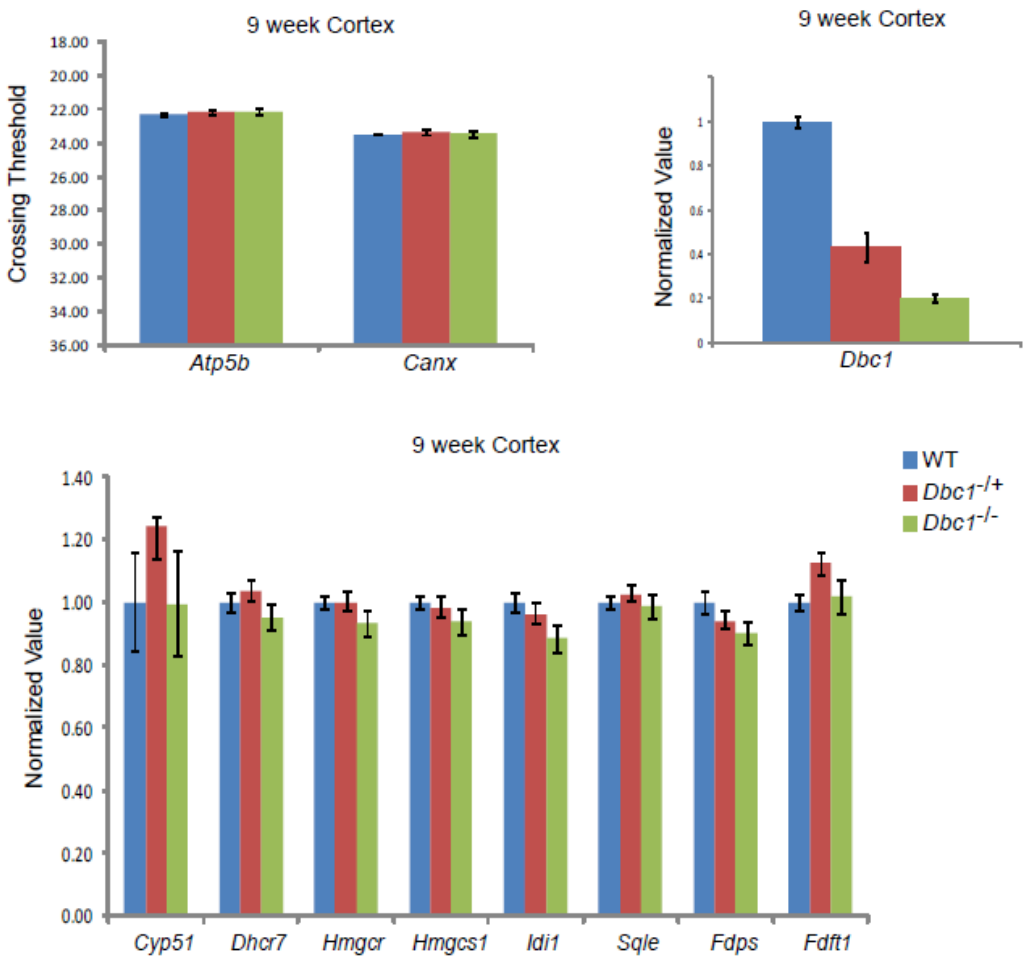

Figure 52. The mRNA expression levels of 7 cholesterogenic enzymes in 9 week old cortex from WT, *Dbc1*$^{+/-}$ and *Dbc1*$^{-/-}$ mice. Expression levels were normalised to the housekeeping genes *Atp5b* and *Canx* and expressed as fold change of WT levels ± SEM. n = 8 / genotype.

.

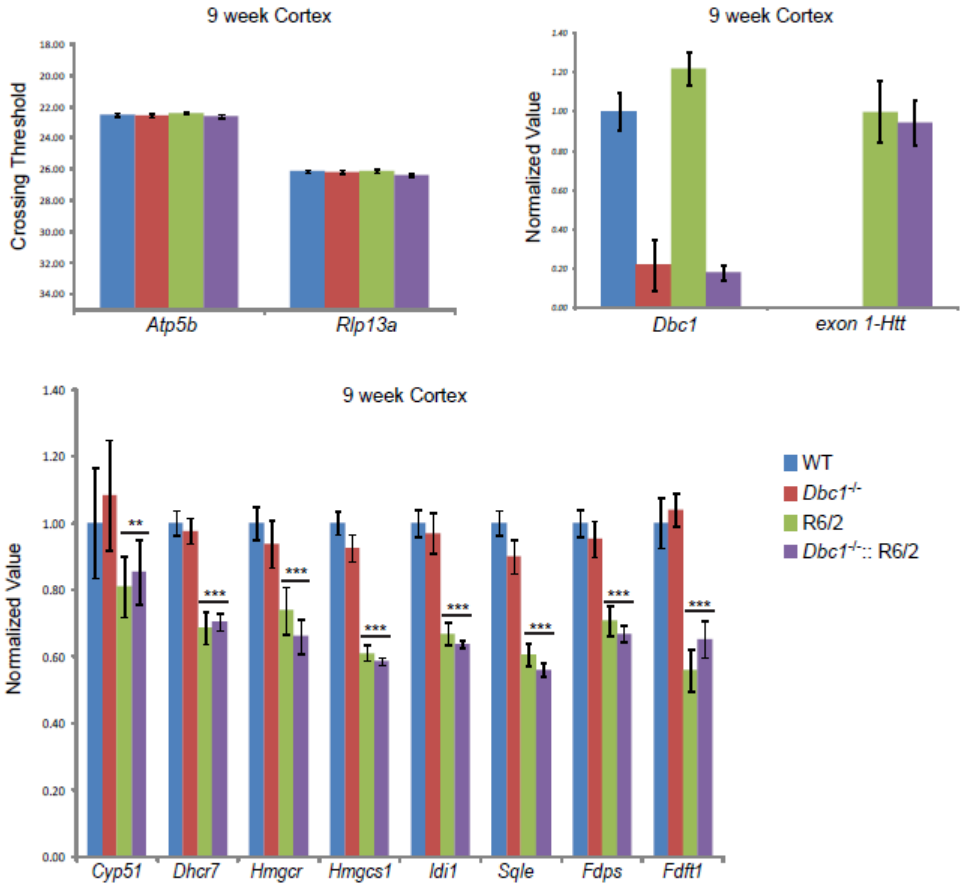

Figure 53. The mRNA expression levels of 7 cholesterogenic enzymes in 9 week old cortex from WT, *Dbc1*$^{-/-}$, R6/2 and *Dbc1*$^{-/-}$::R6/2 mice. Expression levels were normalised to the housekeeping genes *Atp5b* and *Rlp13a* and expressed as fold change of WT levels ± SEM. n = 8 / genotype.

4.4 General comments

Deleted in breast cancer 1 (DBC1) is a cellular factor that binds SIRT1 and regulates its deacetylase activity by directly interacting with the SIRT1 deacetylase domain. This interaction inhibits the ability of SIRT1 to deacetylate its specific substrates. Our objective was to explore the effect of *Dbc1* ablation on SIRT1 activity and to assess whether an increase in SIRT1 activity, resulting from *Dbc1* ablation, could improve HD-related phenotypes in a mouse model of HD. Therefore, we crossed R6/2 transgenic mice with mice in which DBC1 had been reduced or ablated to evaluate whether the increase in SIRT1 activity had a beneficial impact on disease progression in this HD mouse model.

A characterisation of *Dbc1* knock-out mice shows that the genetic ablation of DBC1 resulted in a significant decrease of DBC1 both at mRNA and protein level in the brain. Additionally, reduction or removal of DBC1 protein did not affect the expression of all *Hdacs* and *Sirtuins* or the expression of cholesterogenic enzymes in the brain. Moreover, loss of DBC1 on WT background resulted in a considerable increase in SIRT1 activity in the whole brain. Surprisingly, despite the ablation of DBC1, the SIRT1 function impairment remain unchanged in R6/2 mice. In line with these results, we did not detect any effect on the onset and progression of a wide range of behavioural, molecular and pathological HD-related phenotypes. Therefore, we conclude that DBC1 ablation does not modify disease progression in R6/2 mice.

Chapter 5 *Discussion*

5.1 Effect of Huntington's disease on SIRT1 function

The identification of SIRT1 and its involvement in lifespan extension and cellular protection from aggregation-prone proteins (Morley and Morimoto, 2004; Muchowski and Wacker, 2005; Douglas et al., 2009) has catalysed scientific attention as a promising therapeutic target for neurodegenerative disorders. Neurodegenerative disorders are complex diseases with many underlying pathways, and SIRT1 is a molecule with numerous different substrates in the cell. Therefore, it is not surprising that SIRT1 is involved in neurodegenerative disorders. The first study demonstrating the connection between SIRT1 and HD shows that the neuronal dysfunction phenotypes induced by mutant polyglutamine in Caenorhabditis elegans can be rescued by the overexpression of Sir2.1 (the homolog of SIRT1 in C. elegans) or treatment with an activator of SIRT1 (Parker et al., 2005).

Recent studies have shown that the overexpression of *Sirt1* can significantly reduce mHTT-induced toxicity in HD mouse models, improving motor function and reducing brain atrophy (Jeong et al., 2011; Jiang et al., 2011). These findings support a neuroprotective role of *Sirt1* overexpression in mouse models affected by Huntington's disease. However, the impact of this pathology on SIRT1 function has not been comprehensively investigated.

In the present study, we provide insight into the mechanisms behind the tissue-specific regulation of SIRT1 activity over time and in different brain regions in WT mice. Furthermore, we showed that a progressive impairment of SIRT1 activity in different brain regions of HD mice is linked to an altered phosphorylation profile of SIRT1. To

monitor SIRT1 activity in the brain, we analysed the acetylated status of P53 by performing immunohistochemistry on nuclei isolated from both R6/2 and *Hdh*Q150 mice together with their littermates. It is interesting to note that despite the different rate of disease progression that characterises these two models, we did not detect an alteration in SIRT1 function in the presymptomatic stages in both models. SIRT1 activity was overtly compromised by 9 weeks of age in the R6/2 mice and at 22 months in *Hdh*Q150 mice. This was not caused by SIRT1 sequestration into mHTT inclusions as we failed to detect any co-localization between SIRT1 and mHTT by immunohistochemistry. To further support this finding, we did not detect any variation in SIRT1 levels between HD and WT mice. These data suggest that mHTT can alter other mechanisms involved in the control of SIRT1 activity.

The role of post-translational modifications in the regulation of SIRT1 activity has been the subject of several studies and phosphorylation has been described as a major control PTM mechanism (Sasaki et al., 2008). It has been shown that kinases such as JNK1 and CK2 can phosphorylate SIRT1 thereby increasing its nuclear deacetylase activity (Nasrin et al., 2009; Zschoernig and Mahlknecht, 2009), as well as JNK1 phosphorylation has also been shown to induce SIRT1 ubiquitination and proteasomal degradation (Nasrin et al., 2009). Therefore, to understand the effect of mHTT on SIRT1 function, we monitored the phosphorylation status of SIRT1 in mice affected by Huntington's disease. Performing SIRT1 immunoprecipitation from half brains of R6/2 mice at 9 weeks and *Hdh*Q150 homozygous mice at 22 months of age, we detected an increased status of SIRT1 phosphorylation in HD mouse models. This might indicate that the impairment in SIRT1 function in the brain of HD mice may be related to an altered phosphorylation profile. As mentioned previously, MpM2 antibody (used to

detect the phosphorylation status of SIRT1) is able to detect only the phosphorylation on Serine and Threonine residues followed by Proline (S/T-P sites) present on any protein and it is not specific for any particular phosphorylation sites. Therefore, it cannot detect the activity of any specific kinase or phosphatase. Overall these results suggest that mHTT might, indirectly, affect SIRT1 activity. Indeed, we showed that the impairment of SIRT1 function in the brain of HD mice is not related to a sequestration into mHTT inclusions but we cannot exclude that several kinases or phosphates, that control the phosphorylation status of SIRT1, can be impaired from the interaction with mHTT aggregates.

Despite the huntingtin gene and protein is widely expressed in the human body, HD is largely restricted to the brain. As said previously, one of the neuropathological hallmarks of Huntington's disease is the striatum specificity and the disease progression can involve also other brain regions. Since, the results from half brain can mask the HD effects at the single brain regions level, we extended our analysis of SIRT1 phosphorylation status and SIRT1 function to the striatum, cerebellum and cortex. Consistent with the half brain data, we did not detect any difference in the phosphorylation status of SIRT1 in the early stage of the disease in the single brain regions between WT and HD mouse models. Interestingly, the levels of SIRT1 phosphorylation remain unchanged in the cortex with age. Analysing striatum and cerebellum, we found an opposite pattern of phosphorylation between them; surprisingly, we detected a reduction of phosphorylation status of SIRT1 in the striatum of both R6/2 (9 weeks) and *Hdh*Q150 homozygous (22 months) mice compared to WT, while cerebellum was characterized by an increase of SIRT1 phosphorylation in both HD mouse models as compared to WT littermates. These data

further confirm an altered status of SIRT1 phosphorylation in presence of mHTT and with disease progression; moreover is interesting to see how the alteration follows an opposite pattern between striatum and cerebellum.

To figure out if the altered pattern of SIRT1 phosphorylation in striatum and cerebellum of HD mice was related to an impairment of SIRT1 function, we isolated nuclei from both these brain regions of R6/2 and WT mice to perform an immunostaining and to monitor the acetylated status of P53. Interestingly, we detected a reduction in the level of AcP53 in striatum of WT mice from 4 to 14 weeks, consistent with an increase of SIRT1 activity with age. We did not detect the same increase in the striatum of R6/2 mice. When we analysed the acetylation status of P53 in the cerebellum, we could not find any change in WT mice but we found a significant increase of AcP53 in R6/2 mice from 4 to 14 weeks of age, corresponding to a progressive impairment of SIRT1 activity with age. Taken together, these data show for the first time the existence of different mechanisms to regulate SIRT1 activity in different brain regions of WT mice. The induction of SIRT1 activity in the striatum and the unchanged level of SIRT1 function in the cerebellum with age led us to monitor the phosphorylation status of SIRT1 in WT mice in both tissues at 4, 9 and 14 weeks. The SIRT1 immunoprecipitation from WT mice reveals a change in the phosphorylation status of SIRT1 in the striatum with age, suggesting that in the striatum the change in the phosphorylation status of SIRT1 with age can be related to an induction of SIRT1 activity. Cerebellum showed a constant phosphorylation status of SIRT1 in WT mice with age, consistent with an unchanged SIRT1 activity between 4 and 14 weeks of age.

The list of SIRT1 substrates and targets is continuously growing and many of them are located in the nucleus. We have already mentioned the ability of the

phosphorylation to induce the nuclear localization of SIRT1 promoting the interaction with its substrates (Nasrin et al., 2009). To check if the mis-regulation of SIRT1 phosphorylation could affect its nuclear localization, we performed a nuclear and cytoplasmic fractions from striatum and cerebellum of R6/2 and WT mice at 9 and 14 weeks of age. Interestingly, we did not detect any difference in the distribution of SIRT1 at any age between R6/2 and WT mice in both striatum and cerebellum. These results suggest that mHTT does not affect the subcellular distribution of SIRT1 and further support a link between regulation of SIRT1 activity and its phosphorylation levels.

Our finding that the phosphorylation status of SIRT1 is altered in HD mice further supports this central role for phosphorylation in the regulation of SIRT1 activity. Interestingly, despite the impairment in SIRT1 activity detected in both the striatum and cerebellum of HD mice, the phosphorylation level of SIRT1 was altered in opposing directions in these two brain regions, suggesting the existence of a tissue-specific regulation of SIRT1 via phosphorylation. This prompted us to further investigate the relationship between SIRT1 phosphorylation and its activity and this led to the identification of a striatum-specific phosphorylation-dependent induction of SIRT1 activity between 4 and 9 weeks of age in WT mice, which does not take place in the cerebellum. In light of these new findings, we can now interpret differential SIRT1 phosphorylation between the striatum and cerebellum of HD mice, suggesting that in physiological condition SIRT1 activity is induced in the striatum between 4 and 9 weeks (Fig. 53 A), whereas it remains constant in the cerebellum. The presence of mHTT can block this induction process in the striatum and cause a reduction in normal SIRT1

function in the cerebellum resulting in an impairment of SIRT1 activity in both brain regions.

In an attempt to rescue this SIRT1 deficiency, we crossed R6/2 mice with *Dbc1*KO mice, as DBC1 has been reported to be a negative regulator of SIRT1 via direct interaction with its deacetylase domain (Escande et al., 2010). Strikingly, despite a significant upregulation of SIRT1 activity in *Dbc1*KO mice, the *Dbc1*::R6/2 double transgenic mice showed the same SIRT1 impairment as R6/2 mice, suggesting that mHTT is altering key regulatory events that lie outside the inhibitory circuit controlled by DBC1. As a result of this, we did not detect any improvement on the onset and progression of several behavioural and pathological HD-related phenotypes.

In contrast to DBC1, AMPK-α1 has been reported to positively regulate the activity of SIRT1 by inducing SIRT1 activation through its dissociation from DBC1 (Escande et al., 2012; Lau et al., 2014). Interestingly, our co-immunoprecipitation experiments revealed an increased interaction between DBC1 and AMPK-α1 in the striatum of HD mice, which might point to a rescue attempt by the damaged system. Nevertheless, our immunohistochemical analysis on the cellular distribution of AMPK-α1 showed that AMPK-α1 is aberrantly distributed between the nucleus and the cytoplasm of R6/2 mice both in the striatum and the cerebellum, suggesting this event might be co-causal to the impairment of SIRT1 function (Fig. 53 A). In fact, we observed a delayed accumulation of AMPK-α1 in striatal nuclei of R6/2 mice that might impede SIRT1 activation, whereas AMPK-α1 nuclear accumulation in the cerebellum of R6/2 mice was anticipated by 9 weeks of age, maybe trying to reduce the inhibition dictated by mHTT. To support the existence of a striatum-specific regulatory circuit linking these 3 proteins in the induction of SIRT1 activity with age, our analysis of mRNA and

protein expression levels provided a complete picture in which it is possible to observe that in normal WT conditions the mRNA expression levels of *Sirt1*, *Dbc1* and *Ampk-α1* are downregulated between 4 and 9 weeks of age and remain such through to 14 weeks of age. Consistently, the protein level of AMPK-α1 is increased during the same time frame, suggesting that the protein might be stabilised, and that this could then lead to the induction of SIRT1. As a consequence of this induced activity with age, the level of SIRT1 could become stabilised, hence providing a negative feedback for *Sirt1* transcription. Interestingly, in the striatum of R6/2 mice, the stabilization/upregulation of AMPK-α1 does not take place, maybe due to an increased interaction with DBC1, and consequently this may lead to a failure in the induction of SIRT1. Therefore, SIRT1 activity is not stabilised and the feedback to lower the transcription level of SIRT1 is not transmitted. In the cerebellum the expression analysis also supports our hypothesis of an impairment in SIRT1 activity in R6/2 mice which is under the control of a different regulatory mechanism, that is not age-dependent and does not require the induction of SIRT1, as the protein would already be fully functional. We propose a model whereby disease progression leads to altered SIRT1 phosphorylation status. As a consequence, SIRT1 activity is reduced and P53 cannot be deacetylated thereby resulting in neuronal dysfunction (Fig. 53 B).

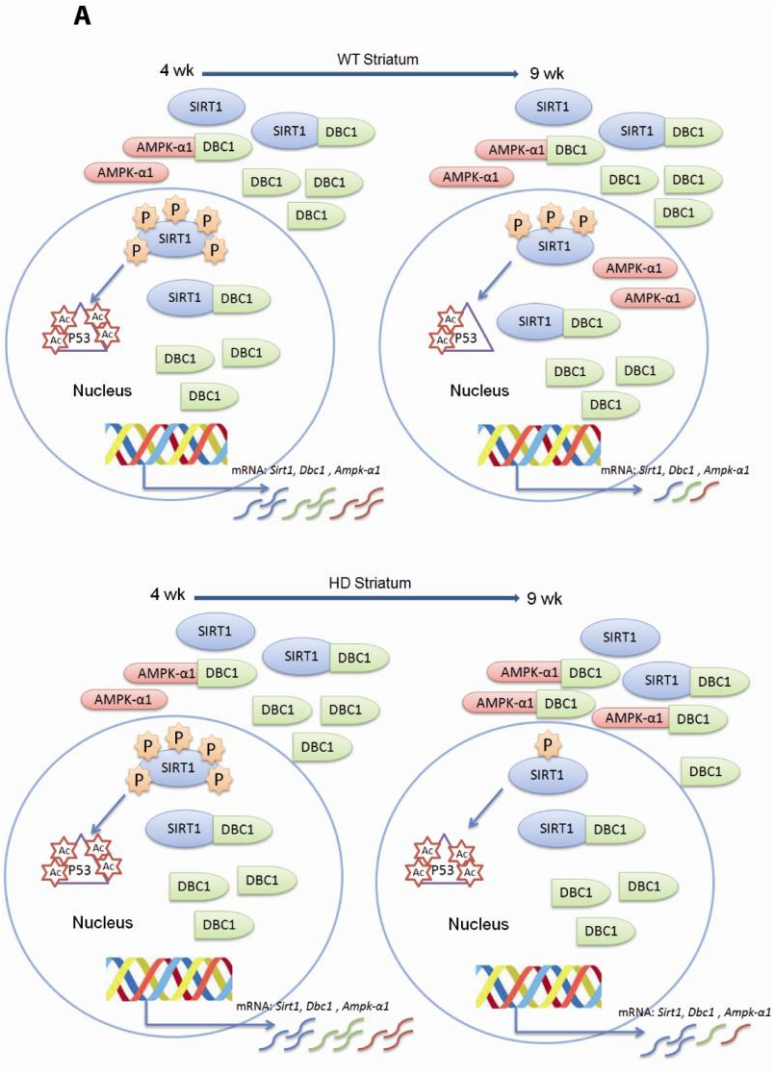

Figure 54 A. Proposed model for the striatum-specific regulation of SIRT1 via phosphorylation in WT mice and for the impairment in SIRT1 activity in HD brain. (A) In WT striatum the change in SIRT1 phosphorylation status between 4 and 9 weeks of age induces an increase in SIRT1 activity followed by a reduction of acetylated P53. WT striatum show a nuclear accumulation of AMPK-α1 at 9 weeks supporting a role for this kinase in the activation process of SIRT1 (AMPK-α1 is not the kinase involved in the change in SIRT1 phosphorylation status detected here, as the MpM2 antibody can recognise only the Ser/Thr-Pro residues and AMPK-α1 is able to phosphorylate only Ser/Thr residues not followed by proline). AMPK-α1 is present in the nucleus at 9 weeks and is proposed to activate SIRT1 through a mechanism independent of DBC1. The down-regulation of the mRNA level of *Sirt1*, *Dbc1* and *Ampk-α1* from 4 to 9 weeks of age is consistent with these three proteins being partners in the same regulatory circuit. In the HD condition the strong reduction in SIRT1 phosphorylation impedes the induction of SIRT1 activity. There is a greater interaction between AMPK-α1 and DBC1 which may result in the cytoplasmic retention of AMPK-α1, inhibiting the activation of SIRT1, and/or promoting a futile rescue attempt by preventing DBC1 from binding to SIRT1.

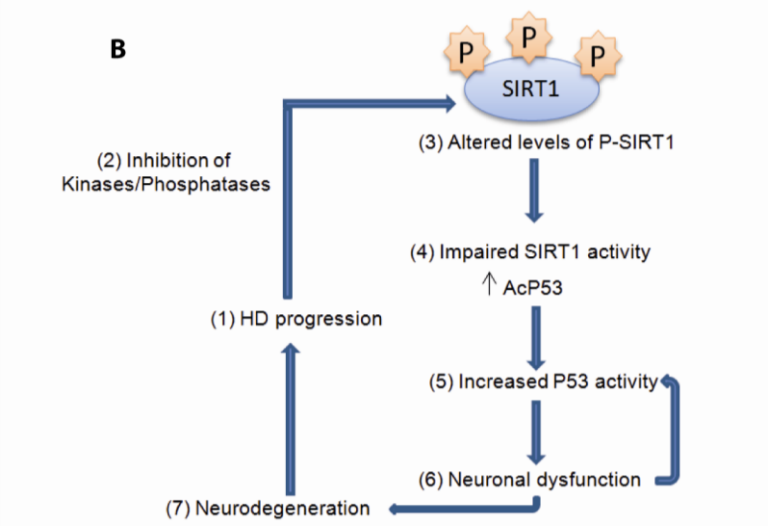

Figure 54 B. Proposed mechanisms of the striatum-specific regulation of SIRT1 via phosphorylation in WT mice and its impairment in R6/2 mice, and model for the impairment of SIRT1 activity in HD brain Disease progression in HD leads to a progressive alteration in SIRT1 phosphorylation. An altered phosphorylation status causes an impairment in SIRT1 function, which results in an increase in P53 activity which may contribute to neuronal dysfunction and ultimately cell death.

In conclusion, our data provide two major new findings. First, we showed that the mechanisms behind the tissue-specific regulation of SIRT1 activity are different between brain regions e.g. striatum and cerebellum. For the first time, we were able to describe a striatum-specific phosphorylation dependent mechanism of induction of SIRT1 activity with age in WT mice.

Second, we provide the first evidence of a progressive impairment of SIRT1 activity in two different HD mouse models. Given that SIRT1 has been proposed to play a central role in metabolism and longevity, loss of SIRT1 activity may contribute significantly to disease progression in HD.

5.2 Future work

Recent studies have shown that the overexpression of *Sirt1* can reduce mHTT-induced toxicity in HD mouse models, improving motor function and reducing brain atrophy (Jeong et al., 2011; Jiang et al., 2011). Moreover, we provide the first evidence of a progressive impairment of SIRT1 activity in two different HD mouse models and that the loss of SIRT1 activity may contribute significantly to disease progression in HD.

Taken together, these results suggest that the pharmacological targeting of SIRT1 to enhance its activity may provide a new therapeutic opportunity for Huntington's disease. The development of SIRT1 activators with high specificity for SIRT1 may be a promising approach for the treatment of Huntington's disease. The high homology of SIRT1 with all the other sirtuins makes the development of specific compounds for SIRT1 very difficult.

Several rational strategies based on the available protein structure and the catalytic pathways have been designed to develop small molecules (Sauve et al., 2009). One strategy involves designing resveratrol-like molecules, which has not yielded successful

results as the *in vivo* mechanisms that control the activation of SIRT1 is not fully understood. Another approach aims to increase the cellular levels of NAD^+ in order to activate SIRT1 function. This approach has the advantage of harnessing a natural metabolic pathway to enhance SIRT1 functions. Moreover, naturally occurring metabolites present the least risk of toxicity. The efficacies of agents that have been used to enhance NAD^+ are still questionable. Indeed, NAD^+ enhancement affects a host of other physiological pathways, hence the approach is not specific to SIRT1. A third strategy currently in the proof-of-principle stage designated nicotinamide derepression is based on countering the inhibitory effect of nicotinamide on sirtuins by designing molecules that are antagonistic to nicotinamide. This approach is still in its infancy and has not provided compounds with desired potency.

In the present study, we also showed that a progressive impairment of SIRT1 activity in different brain regions of HD mice is linked to an altered phosphorylation profile of SIRT1. As consequence, in the future work will be important to determine the kinases/phosphatases involved in the regulation of SIRT1 activity in different brain regions in order to develop compounds that can act synergistically with SIRT1 activators, act as novel SIRT1 inducers that bypass the impairment or restore this process by as-yet unidentified mechanisms.

5.3 Validity of SIRT1 as therapeutic target in HD: strengths and weaknesses

An exciting aspect is that SIRT1 mediates neuroprotection against both acute and chronic neurological diseases. Several studies have shown that the activation of SIRT1 can have beneficial effects in HD and also in many other neurodegenerative disorders, such as Alzheimer's disease, Parkinson's disease, amyotrophic lateral sclerosis, multiple sclerosis and cerebral ischemia.

The pathological hallmarks of Alzheimer's disease (AD) are the intracellular tangles and extracellular plaques in brain. The tangles, also known as neurofibrillary tangles, are formed by accumulation of insoluble tau proteins, and the plaques are deposits of β-amyloid (Aβ) peptides. The protective effect of SIRT1 against AD was initially observed in caloric restriction studies, where caloric restriction reduced Aβ and plaque generation in the brains of transgenic AD mice (Patel et al., 2005; Wang et al., 2005a). Moreover, recent studies show that either administration of resveratrol or overexpression of *Sirt1* reduces Aβ levels both *in vitro* and *in vivo* (Chen et al., 2005b; Qin et al., 2006b; Donmez et al., 2010). *Sirt1* overexpression stimulates the production of α-secretase in neurons and mice (Donmez et al., 2010; Qin et al., 2006b). Increased levels of α-secretase enhance normal process of Amyloid precursor protein (APP), leading to decreased generation of toxic Aβ. In addition, SIRT1 also reduces the NF-kappaB pathway in microglia and decreases Aβ level (Chen et al., 2005b). Parkinson's disease (PD) is a common neurodegenerative disease caused by the death of dopaminergic neurons of the substantia nigra in the midbrain. *Sirt1* overexpression (Wareski et al., 2009) or activation by resveratrol (Okawara et al., 2007; Chao et al., 2008; Albani et al., 2009) slows neuronal death as well as neurodegeneration in PD models both *in vivo* and *in vitro* (Donmez et al., 2012), indicating a neuroprotective role of SIRT1 against PD.

Amyotrophic lateral sclerosis (ALS) is a chronic, fatal neurodegenerative disease, characterized pathologically by the death of motor neurons in the spinal cord and cortex, possibly induced by a deficiency in the enzyme superoxide dismutase 1 (SOD1) (Rosen et al., 1993). In the animal model of ALS where a mutant form of SOD1 is expressed, SIRT1 levels are upregulated in motor neurons (Kim et al., 2007). *Sirt1*

overexpression protects neurons against toxicity induced by the mutant SOD1 in both cultured neurons and mouse brain (Kim et al., 2007). This protection corresponds to the increased deacetylation of p53. Resveratrol also enhances the protective effect of SIRT1 in a mouse model of ALS (Kim et al., 2007; Markert et al., 2010).

Multiple sclerosis (MS) is a myelin sheath disease with lesions typically located in the brain, spinal cord or cranial nerves, and, most commonly, in the optic nerve. The causes of multiple sclerosis are not fully identified but likely arise from an autoimmune etiology; therefore, it is traditionally treated as an inflammatory disease. In a mouse model of multiple sclerosis, experimental autoimmune encephalomyelitis (EAE), SIRT1 activation by SRT501 or SRT1720 maintains axonal density, prevents neuronal loss, and improves neuronal dysfunction (Shindler et al., 2007, 2010). SIRT1 inhibition with Sirtinol attenuates the neuroprotective effects of SRT501 (Shindler et al., 2010), suggesting a protective role of SIRT1 in multiple sclerosis.

Ischemic stroke is a common neurological disease caused by the sudden reduction or cessation of blood flow to the brain, leading to infarction. The neuroprotective effect of SIRT1 was first reported in ischemic preconditioning and the SIRT1 activating compound resveratrol reduced neuronal injury of the hippocampus in ischemia in rats (Raval et al., 2006; Morris et al., 2011). Sirtinol, an inhibitor of SIRT1 activity, abolished the neuroprotection of preconditioning and resveratrol (Raval et al., 2006), indicating that SIRT1 plays a key role in mediating neuroprotection. This neuroprotective role is further supported by two studies (Chong and Maiese, 2008; Della-Morte et al., 2009) showing that SIRT1 activation reduces ischemic neuronal injuries. Another study showed that, in primary neuronal culture, pretreatment with NAD^+ reduces neuronal death induced by oxygen-glucose deprivation, an *in vitro* model of ischemia (Wang et

al., 2008). SIRT1 is necessary for NAD^+ neuroprotection, as NAD^+ treatment upregulates SIRT1 activity, and *Sirt1* knockdown attenuates the protection mediated by NAD^+ (Wang et al., 2008).

Although exciting discoveries have been made in SIRT1 neurobiology, important questions still remain to be answered. Indeed, we cannot exclude that the administration of compounds able to increase the activity of SIRT1 could show some limits. It's known that SIRT1 is involved in different cellular processes and it can behave differently in different tissues (Fig. 54). Moreover, the number of SIRT1 substrates grows daily, making the situation more difficult because the pathways involved overlap with other proteins (Fig. 54).

As SIRT1 elicits multiple divergent effects in the central nervous system and periphery, different outcomes might occur, depending on how, when, and where SIRT1 is activated. Although pharmacological or genetic activation of SIRT1 show many beneficial effects, making it an attractive drug target, we should not forget that SIRT1 acts on many different downstream targets, which are involved in numerous biological activities. Drugs that can specifically activate SIRT1 need to be tested in HD mammalian models, in order to identify whether the benefits of these drugs are sustained. If so, clinical trials will be necessary to follow up and to address whether SIRT1 modulators have beneficial effects in HD patients.

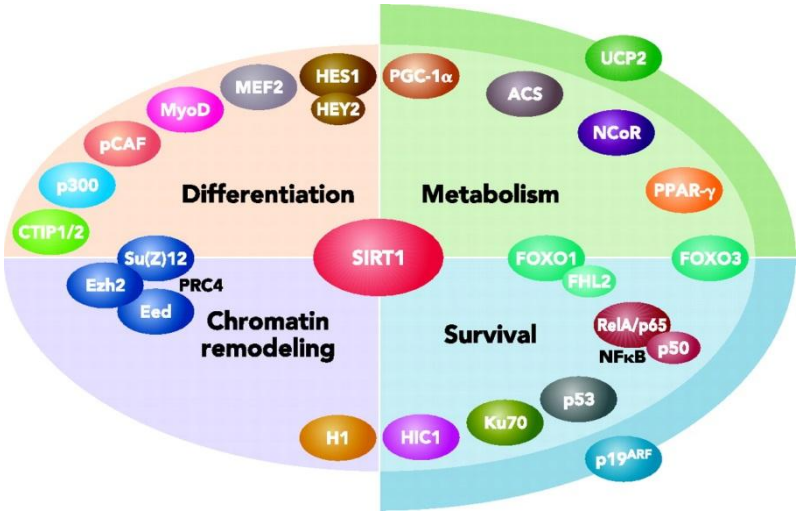

Figure 55. Interacting partners, substrates and downstream effectors of SIRT1. (Reproduced from Dimitrios and Wilhelm, 2006).

Bibliography

Ahringer J (2000) NuRD and SIN3 histone deacetylase complexes in development. Trends Genet 16: 351-356.

Albani D, Polito L, Batelli S, De Mauro S, Fracasso C, et al. (2009) The SIRT1 activator resveratrol protects SK-N-BE cells from oxidative stress and against toxicity caused by alpha-synuclein or amyloid-beta (1-42) peptide. J Neurochem 110: 1445-1456.

Albin RL, Qin Y, Young AB, Penney JB, Chesselet MF (1991) Preproenkephalin messenger RNA-containing neurons in striatum of patients with symptomatic and presymptomatic Huntington's disease: an in situ hybridization study. Ann Neurol 30: 542-549.

Albin RL, Young AB, Penney JB (1989) The functional anatomy of basal ganglia disorders. Trends Neurosci 12: 366-375.

Allen JA, Halverson-Tamboli RA, Rasenick MM (2007) Lipid raft microdomains and neurotransmitter signalling. Nat Rev Neurosci 8: 128-140.

Altar CA, Cai N, Bliven T, Juhasz M, Conner JM, et al. (1997) Anterograde transport of brain-derived neurotrophic factor and its role in the brain. Nature 389: 856-860.

Arrasate M, Mitra S, Schweitzer ES, Segal MR, Finkbeiner S (2004) Inclusion body formation reduces levels of mutant huntingtin and the risk of neuronal death. Nature 431: 805-810.

Augood SJ, Faull RL, Love DR, Emson PC (1996) Reduction in enkephalin and substance P messenger RNA in the striatum of early grade Huntington's disease: a detailed cellular in situ hybridization study. Neuroscience 72: 1023-1036.

Bacos K, Bjorkqvist M, Petersen A, Luts L, Maat-Schieman ML, et al. (2008) Islet beta-cell area and hormone expression are unaltered in Huntington's disease. Histochem Cell Biol 129: 623-629.

Bae BI, Xu H, Igarashi S, Fujimuro M, Agrawal N, et al. (2005) p53 mediates cellular dysfunction and behavioral abnormalities in Huntington's disease. Neuron 47: 29-41.

Bates, Tabrizi, and Jones (2014). Huntington's disease, 4rd ed. (Oxford, Oxford University Press).

Bence NF, Sampat RM, Kopito RR (2001) Impairment of the ubiquitin-proteasome system by protein aggregation. Science 292: 1552-1555.

Bennett EJ, Bence NF, Jayakumar R, Kopito RR (2005) Global impairment of the ubiquitin-proteasome system by nuclear or cytoplasmic protein aggregates precedes inclusion body formation. Mol Cell 17: 351-365.

Bibb JA, Yan Z, Svenningsson P, Snyder GL, Pieribone VA, et al. (2000) Severe deficiencies in dopamine signaling in presymptomatic Huntington's disease mice. Proc Natl Acad Sci U S A 97: 6809-6814.

Bizat N, Hermel JM, Humbert S, Jacquard C, Creminon C, et al. (2003) In vivo calpain/caspase cross-talk during 3-nitropropionic acid-induced striatal degeneration:

implication of a calpain-mediated cleavage of active caspase-3. J Biol Chem 278: 43245-43253.

Bjorkqvist M, Fex M, Renstrom E, Wierup N, Petersen A, et al. (2005) The R6/2 transgenic mouse model of Huntington's disease develops diabetes due to deficient beta-cell mass and exocytosis. Hum Mol Genet 14: 565-574.

Bloch J, Bachoud-Levi AC, Deglon N, Lefaucheur JP, Winkel L, et al. (2004) Neuroprotective gene therapy for Huntington's disease, using polymer-encapsulated cells engineered to secrete human ciliary neurotrophic factor: results of a phase I study. Hum Gene Ther 15: 968-975.

Boutell JM, Thomas P, Neal JW, Weston VJ, Duce J, et al. (1999) Aberrant interactions of transcriptional repressor proteins with the Huntington's disease gene product, huntingtin. Hum Mol Genet 8: 1647-1655.

Canals JM, Pineda JR, Torres-Peraza JF, Bosch M, Martin-Ibanez R, et al. (2004) Brain-derived neurotrophic factor regulates the onset and severity of motor dysfunction associated with enkephalinergic neuronal degeneration in Huntington's disease. J Neurosci 24: 7727-7739.

Canto C, Gerhart-Hines Z, Feige JN, Lagouge M, Noriega L, et al. (2009) AMPK regulates energy expenditure by modulating NAD+ metabolism and SIRT1 activity. Nature 458: 1056-1060.

Carter RJ, Lione LA, Humby T, Mangiarini L, Mahal A, et al. (1999) Characterization of progressive motor deficits in mice transgenic for the human Huntington's disease mutation. J Neurosci 19: 3248-3257.

Caviston JP, Ross JL, Antony SM, Tokito M, Holzbaur EL (2007) Huntingtin facilitates dynein/dynactin-mediated vesicle transport. Proc Natl Acad Sci U S A 104: 10045-10050.

Cepeda C, Ariano MA, Calvert CR, Flores-Hernandez J, Chandler SH, et al. (2001) NMDA receptor function in mouse models of Huntington disease. J Neurosci Res 66: 525-539.

Cha JH, Frey AS, Alsdorf SA, Kerner JA, Kosinski CM, et al. (1999) Altered neurotransmitter receptor expression in transgenic mouse models of Huntington's disease. Philos Trans R Soc Lond B Biol Sci 354: 981-989.

Cha JH, Kosinski CM, Kerner JA, Alsdorf SA, Mangiarini L, et al. (1998) Altered brain neurotransmitter receptors in transgenic mice expressing a portion of an abnormal human huntington disease gene. Proc Natl Acad Sci U S A 95: 6480-6485.

Chalkiadaki A, Guarente L (2012) Sirtuins mediate mammalian metabolic responses to nutrient availability. Nat Rev Endocrinol 8: 287-296.

Chao J, Yu MS, Ho YS, Wang M, Chang RC (2008) Dietary oxyresveratrol prevents parkinsonian mimetic 6-hydroxydopamine neurotoxicity. Free Radic Biol Med 45: 1019-1026.

Chen D, Steele AD, Hutter G, Bruno J, Govindarajan A, et al. (2008) The role of calorie restriction and SIRT1 in prion-mediated neurodegeneration. Exp Gerontol 43: 1086-1093.

Chen J, Zhou Y, Mueller-Steiner S, Chen LF, Kwon H, et al. (2005) SIRT1 protects against microglia-dependent amyloid-beta toxicity through inhibiting NF-kappaB signaling. J Biol Chem 280: 40364-40374.

Chen M, Ona VO, Li M, Ferrante RJ, Fink KB, et al. (2000) Minocycline inhibits caspase-1 and caspase-3 expression and delays mortality in a transgenic mouse model of Huntington disease. Nat Med 6: 797-801.

Cheng HL, Mostoslavsky R, Saito S, Manis JP, Gu Y, et al. (2003) Developmental defects and p53 hyperacetylation in Sir2 homolog (SIRT1)-deficient mice. Proc Natl Acad Sci U S A 100: 10794-10799.

Chong ZZ, Maiese K (2008) Enhanced tolerance against early and late apoptotic oxidative stress in mammalian neurons through nicotinamidase and sirtuin mediated pathways. Curr Neurovasc Res 5: 159-170.

Choo YS, Johnson GV, MacDonald M, Detloff PJ, Lesort M (2004) Mutant huntingtin directly increases susceptibility of mitochondria to the calcium-induced permeability transition and cytochrome c release. Hum Mol Genet 13: 1407-1420.

Ciechanover A, Brundin P (2003) The ubiquitin proteasome system in neurodegenerative diseases: sometimes the chicken, sometimes the egg. Neuron 40: 427-446.

Colin E, Zala D, Liot G, Rangone H, Borrell-Pages M, et al. (2008) Huntingtin phosphorylation acts as a molecular switch for anterograde/retrograde transport in neurons. EMBO J 27: 2124-2134.

Cong X, Held JM, DeGiacomo F, Bonner A, Chen JM, et al. (2011) Mass spectrometric identification of novel lysine acetylation sites in huntingtin. Mol Cell Proteomics 10: M111 009829.

Conner JM, Lauterborn JC, Yan Q, Gall CM, Varon S (1997) Distribution of brain-derived neurotrophic factor (BDNF) protein and mRNA in the normal adult rat CNS: evidence for anterograde axonal transport. J Neurosci 17: 2295-2313.

Crook ZR, Housman D (2011) Huntington's disease: can mice lead the way to treatment? Neuron 69: 423-435.

Davies SW, Turmaine M, Cozens BA, DiFiglia M, Sharp AH, et al. (1997) Formation of neuronal intranuclear inclusions underlies the neurological dysfunction in mice transgenic for the HD mutation. Cell 90: 537-548.

de la Monte SM, Vonsattel JP, Richardson EP, Jr. (1988) Morphometric demonstration of atrophic changes in the cerebral cortex, white matter, and neostriatum in Huntington's disease. J Neuropathol Exp Neurol 47: 516-525.

de Ruijter AJ, van Gennip AH, Caron HN, Kemp S, van Kuilenburg AB (2003) Histone deacetylases (HDACs): characterization of the classical HDAC family. Biochem J 370: 737-749.

Della-Morte D, Dave KR, DeFazio RA, Bao YC, Raval AP, et al. (2009) Resveratrol pretreatment protects rat brain from cerebral ischemic damage via a sirtuin 1-uncoupling protein 2 pathway. Neuroscience 159: 993-1002.

DiFiglia M, Sapp E, Chase K, Schwarz C, Meloni A, et al. (1995) Huntingtin is a cytoplasmic protein associated with vesicles in human and rat brain neurons. Neuron 14: 1075-1081.

DiFiglia M, Sapp E, Chase KO, Davies SW, Bates GP, et al. (1997) Aggregation of huntingtin in neuronal intranuclear inclusions and dystrophic neurites in brain. Science 277: 1990-1993.

DiProspero NA, Chen EY, Charles V, Plomann M, Kordower JH, et al. (2004) Early changes in Huntington's disease patient brains involve alterations in cytoskeletal and synaptic elements. J Neurocytol 33: 517-533.

Donmez G, Arun A, Chung CY, McLean PJ, Lindquist S, et al. (2012) SIRT1 protects against alpha-synuclein aggregation by activating molecular chaperones. J Neurosci 32: 124-132.

Donmez G, Wang D, Cohen DE, Guarente L (2010) SIRT1 suppresses beta-amyloid production by activating the alpha-secretase gene ADAM10. Cell 142: 320-332.

Douglas PM, Summers DW, Cyr DM (2009) Molecular chaperones antagonize proteotoxicity by differentially modulating protein aggregation pathways. Prion 3: 51-58.

Dragatsis I, Levine MS, Zeitlin S (2000) Inactivation of Hdh in the brain and testis results in progressive neurodegeneration and sterility in mice. Nat Genet 26: 300-306.

Duan W, Guo Z, Jiang H, Ladenheim B, Xu X, et al. (2004) Paroxetine retards disease onset and progression in Huntingtin mutant mice. Ann Neurol 55: 590-594.

Duan W, Guo Z, Jiang H, Ware M, Li XJ, et al. (2003) Dietary restriction normalizes glucose metabolism and BDNF levels, slows disease progression, and increases survival in huntingtin mutant mice. Proc Natl Acad Sci U S A 100: 2911-2916.

Dunah AW, Jeong H, Griffin A, Kim YM, Standaert DG, et al. (2002) Sp1 and TAFII130 transcriptional activity disrupted in early Huntington's disease. Science 296: 2238-2243.

Duyao MP, Auerbach AB, Ryan A, Persichetti F, Barnes GT, et al. (1995) Inactivation of the mouse Huntington's disease gene homolog Hdh. Science 269: 407-410.

Emiliani S, Fischle W, Van Lint C, Al-Abed Y, Verdin E (1998) Characterization of a human RPD3 ortholog, HDAC3. Proc Natl Acad Sci U S A 95: 2795-2800.

Escande C, Chini CC, Nin V, Dykhouse KM, Novak CM, et al. (2010) Deleted in breast cancer-1 regulates SIRT1 activity and contributes to high-fat diet-induced liver steatosis in mice. J Clin Invest 120: 545-558.

Farrer LA, Meaney FJ (1985) An anthropometric assessment of Huntington's disease patients and families. Am J Phys Anthropol 67: 185-194.

Ferrante RJ, Andreassen OA, Dedeoglu A, Ferrante KL, Jenkins BG, et al. (2002) Therapeutic effects of coenzyme Q10 and remacemide in transgenic mouse models of Huntington's disease. J Neurosci 22: 1592-1599.

Ferrante RJ, Kubilus JK, Lee J, Ryu H, Beesen A, et al. (2003) Histone deacetylase inhibition by sodium butyrate chemotherapy ameliorates the neurodegenerative phenotype in Huntington's disease mice. J Neurosci 23: 9418-9427.

Finkel T, Deng CX, Mostoslavsky R (2009) Recent progress in the biology and physiology of sirtuins. Nature 460: 587-591.

Finnin MS, Donigian JR, Cohen A, Richon VM, Rifkind RA, et al. (1999) Structures of a histone deacetylase homologue bound to the TSA and SAHA inhibitors. Nature 401: 188-193.

Fischle W, Dequiedt F, Hendzel MJ, Guenther MG, Lazar MA, et al. (2002) Enzymatic activity associated with class II HDACs is dependent on a multiprotein complex containing HDAC3 and SMRT/N-CoR. Mol Cell 9: 45-57.

Flick F, Luscher B (2012) Regulation of sirtuin function by posttranslational modifications. Front Pharmacol 3: 29.

Ford E, Voit R, Liszt G, Magin C, Grummt I, et al. (2006) Mammalian Sir2 homolog SIRT7 is an activator of RNA polymerase I transcription. Genes Dev 20: 1075-1080.

Fox JH, Barber DS, Singh B, Zucker B, Swindell MK, et al. (2004) Cystamine increases L-cysteine levels in Huntington's disease transgenic mouse brain and in a PC12 model of polyglutamine aggregation. J Neurochem 91: 413-422.

Gafni J, Hermel E, Young JE, Wellington CL, Hayden MR, et al. (2004) Inhibition of calpain cleavage of huntingtin reduces toxicity: accumulation of calpain/caspase fragments in the nucleus. J Biol Chem 279: 20211-20220.

Gao L, Cueto MA, Asselbergs F, Atadja P (2002) Cloning and functional characterization of HDAC11, a novel member of the human histone deacetylase family. J Biol Chem 277: 25748-25755.

Gauthier LR, Charrin BC, Borrell-Pages M, Dompierre JP, Rangone H, et al. (2004) Huntingtin controls neurotrophic support and survival of neurons by enhancing BDNF vesicular transport along microtubules. Cell 118: 127-138.

Gerhart-Hines Z, Dominy JE, Jr., Blattler SM, Jedrychowski MP, Banks AS, et al. (2011) The cAMP/PKA pathway rapidly activates SIRT1 to promote fatty acid oxidation independently of changes in NAD(+). Mol Cell 44: 851-863.

Gervais FG, Singaraja R, Xanthoudakis S, Gutekunst CA, Leavitt BR, et al. (2002) Recruitment and activation of caspase-8 by the Huntingtin-interacting protein Hip-1 and a novel partner Hippi. Nat Cell Biol 4: 95-105.

Gines S, Seong IS, Fossale E, Ivanova E, Trettel F, et al. (2003) Specific progressive cAMP reduction implicates energy deficit in presymptomatic Huntington's disease knock-in mice. Hum Mol Genet 12: 497-508.

Giuliano P, De Cristofaro T, Affaitati A, Pizzulo GM, Feliciello A, et al. (2003) DNA damage induced by polyglutamine-expanded proteins. Hum Mol Genet 12: 2301-2309.

Graham RK, Deng Y, Slow EJ, Haigh B, Bissada N, et al. (2006) Cleavage at the caspase-6 site is required for neuronal dysfunction and degeneration due to mutant huntingtin. Cell 125: 1179-1191.

Gray M, Shirasaki DI, Cepeda C, Andre VM, Wilburn B, et al. (2008) Full-length human mutant huntingtin with a stable polyglutamine repeat can elicit progressive and selective neuropathogenesis in BACHD mice. J Neurosci 28: 6182-6195.

Gu X, Andre VM, Cepeda C, Li SH, Li XJ, et al. (2007) Pathological cell-cell interactions are necessary for striatal pathogenesis in a conditional mouse model of Huntington's disease. Mol Neurodegener 2: 8.

Gu X, Li C, Wei W, Lo V, Gong S, et al. (2005) Pathological cell-cell interactions elicited by a neuropathogenic form of mutant Huntingtin contribute to cortical pathogenesis in HD mice. Neuron 46: 433-444.

Gunawardena S, Her LS, Brusch RG, Laymon RA, Niesman IR, et al. (2003) Disruption of axonal transport by loss of huntingtin or expression of pathogenic polyQ proteins in Drosophila. Neuron 40: 25-40.

Guo X, Williams JG, Schug TT, Li X (2010) DYRK1A and DYRK3 promote cell survival through phosphorylation and activation of SIRT1. J Biol Chem 285: 13223-13232.

Gutekunst CA, Li SH, Yi H, Mulroy JS, Kuemmerle S, et al. (1999) Nuclear and neuropil aggregates in Huntington's disease: relationship to neuropathology. J Neurosci 19: 2522-2534.

Haigis MC, Guarente LP (2006) Mammalian sirtuins--emerging roles in physiology, aging, and calorie restriction. Genes Dev 20: 2913-2921.

Haigis MC, Mostoslavsky R, Haigis KM, Fahie K, Christodoulou DC, et al. (2006) SIRT4 inhibits glutamate dehydrogenase and opposes the effects of calorie restriction in pancreatic beta cells. Cell 126: 941-954.

Hallows WC, Lee S, Denu JM (2006) Sirtuins deacetylate and activate mammalian acetyl-CoA synthetases. Proc Natl Acad Sci USA 103: 10230-10235.

Harjes P, Wanker EE (2003) The hunt for huntingtin function: interaction partners tell many different stories. Trends Biochem Sci 28: 425-433.

Hay DG, Sathasivam K, Tobaben S, Stahl B, Marber M, et al. (2004) Progressive decrease in chaperone protein levels in a mouse model of Huntington's disease and induction of stress proteins as a therapeutic approach. Hum Mol Genet 13: 1389-1405.

Heng MY, Duong DK, Albin RL, Tallaksen-Greene SJ, Hunter JM, et al. (2010) Early autophagic response in a novel knock-in model of Huntington disease. Hum Mol Genet 19: 3702-3720.

Hermel E, Gafni J, Propp SS, Leavitt BR, Wellington CL, et al. (2004) Specific caspase interactions and amplification are involved in selective neuronal vulnerability in Huntington's disease. Cell Death Differ 11: 424-438.

Hickey MA, Kosmalska A, Enayati J, Cohen R, Zeitlin S, et al. (2008) Extensive early motor and non-motor behavioral deficits are followed by striatal neuronal loss in knock-in Huntington's disease mice. Neuroscience 157: 280-295.

Hilditch-Maguire P, Trettel F, Passani LA, Auerbach A, Persichetti F, et al. (2000) Huntingtin: an iron-regulated protein essential for normal nuclear and perinuclear organelles. Hum Mol Genet 9: 2789-2797.

Hockly E, Cordery PM, Woodman B, Mahal A, van Dellen A, et al. (2002) Environmental enrichment slows disease progression in R6/2 Huntington's disease mice. Ann Neurol 51: 235-242.

Hockly E, Woodman B, Mahal A, Lewis CM, Bates G (2003) Standardization and statistical approaches to therapeutic trials in the R6/2 mouse. Brain Res Bull 61: 469-479.

Hodgson JG, Agopyan N, Gutekunst CA, Leavitt BR, LePiane F, et al. (1999) A YAC mouse model for Huntington's disease with full-length mutant huntingtin, cytoplasmic toxicity, and selective striatal neurodegeneration. Neuron 23: 181-192.

Holbert S, Denghien I, Kiechle T, Rosenblatt A, Wellington C, et al. (2001) The Gln-Ala repeat transcriptional activator CA150 interacts with huntingtin: neuropathologic and genetic evidence for a role in Huntington's disease pathogenesis. Proc Natl Acad Sci U S A 98: 1811-1816.

Hoyer-Hansen M, Bastholm L, Szyniarowski P, Campanella M, Szabadkai G, et al. (2007) Control of macroautophagy by calcium, calmodulin-dependent kinase kinase-beta, and Bcl-2. Mol Cell 25: 193-205.

Hoyer-Hansen M, Jaattela M (2007) Connecting endoplasmic reticulum stress to autophagy by unfolded protein response and calcium. Cell Death Differ 14: 1576-1582.

Humphrey GW, Wang Y, Russanova VR, Hirai T, Qin J, et al. (2001) Stable histone deacetylase complexes distinguished by the presence of SANT domain proteins CoREST/kiaa0071 and Mta-L1. J Biol Chem 276: 6817-6824.

Huntington G (1872) On Chorea. Medical and Surgical Reporter XXVI:317-321.

Huntington's disease Collaborative Research Group (1993) A Novel Gene Containing a Trinucleotide Repeat that is Expanded and Unstable on Huntington's Disease Chromosomes. Cell, vol. 72, p. 971-983 (1993)

Ivkovic S, Ehrlich ME (1999) Expression of the striatal DARPP-32/ARPP-21 phenotype in GABAergic neurons requires neurotrophins in vivo and in vitro. J Neurosci 19: 5409-5419.

Jeong H, Cohen DE, Cui L, Supinski A, Savas JN, et al. (2012) Sirt1 mediates neuroprotection from mutant huntingtin by activation of the TORC1 and CREB transcriptional pathway. Nat Med 18: 159-165.

Jeong H, Then F, Melia TJ, Jr., Mazzulli JR, Cui L, et al. (2009) Acetylation targets mutant huntingtin to autophagosomes for degradation. Cell 137: 60-72.

Jiang H, Nucifora FC, Jr., Ross CA, DeFranco DB (2003) Cell death triggered by polyglutamine-expanded huntingtin in a neuronal cell line is associated with degradation of CREB-binding protein. Hum Mol Genet 12: 1-12.

Jiang M, Wang J, Fu J, Du L, Jeong H, et al. (2012) Neuroprotective role of Sirt1 in mammalian models of Huntington's disease through activation of multiple Sirt1 targets. Nat Med 18: 153-15

Johnson MA, Villanueva M, Haynes CL, Seipel AT, Buhler LA, et al. (2007) Catecholamine exocytosis is diminished in R6/2 Huntington's disease model mice. J Neurochem 103: 2102-2110.

Johnston JA, Illing ME, Kopito RR (2002) Cytoplasmic dynein/dynactin mediates the assembly of aggresomes. Cell Motil Cytoskeleton 53: 26-38.

Kaeberlein M, McVey M, Guarente L (1999) The SIR2/3/4 complex and SIR2 alone promote longevity in Saccharomyces cerevisiae by two different mechanisms. Genes Dev 13: 2570-2580.

Kahn BB, Alquier T, Carling D, Hardie DG (2005) AMP-activated protein kinase: ancient energy gauge provides clues to modern understanding of metabolism. Cell Metab 1: 15-25.

Kaltenbach LS, Romero E, Becklin RR, Chettier R, Bell R, et al. (2007) Huntingtin interacting proteins are genetic modifiers of neurodegeneration. PLoS Genet 3: e82.

Karpuj MV, Garren H, Slunt H, Price DL, Gusella J, et al. (1999) Transglutaminase aggregates huntingtin into nonamyloidogenic polymers, and its enzymatic activity increases in Huntington's disease brain nuclei. Proc Natl Acad Sci U S A 96: 7388-7393.

Kegel KB, Kim M, Sapp E, McIntyre C, Castano JG, et al. (2000) Huntingtin expression stimulates endosomal-lysosomal activity, endosome tubulation, and autophagy. J Neurosci 20: 7268-7278.

Kegel KB, Meloni AR, Yi Y, Kim YJ, Doyle E, et al. (2002) Huntingtin is present in the nucleus, interacts with the transcriptional corepressor C-terminal binding protein, and represses transcription. J Biol Chem 277: 7466-7476.

Kegel KB, Sapp E, Yoder J, Cuiffo B, Sobin L, et al. (2005) Huntingtin associates with acidic phospholipids at the plasma membrane. J Biol Chem 280: 36464-36473.

Kim D, Nguyen MD, Dobbin MM, Fischer A, Sananbenesi F, et al. (2007) SIRT1 deacetylase protects against neurodegeneration in models for Alzheimer's disease and amyotrophic lateral sclerosis. EMBO J 26: 3169-3179.

Kim JE, Chen J, Lou Z (2008) DBC1 is a negative regulator of SIRT1. Nature 451: 583-586.

Kotian S, Liyanarachchi S, Zelent A, Parvin JD (2011) Histone deacetylases 9 and 10 are required for homologous recombination. J Biol Chem 286: 7722-7726.

Kouroku Y, Fujita E, Jimbo A, Kikuchi T, Yamagata T, et al. (2002) Polyglutamine aggregates stimulate ER stress signals and caspase-12 activation. Hum Mol Genet 11: 1505-1515.

Kouroku Y, Fujita E, Tanida I, Ueno T, Isoai A, et al. (2007) ER stress (PERK/eIF2alpha phosphorylation) mediates the polyglutamine-induced LC3 conversion, an essential step for autophagy formation. Cell Death Differ 14: 230-239.

Labbadia J, Cunliffe H, Weiss A, Katsyuba E, Sathasivam K, et al. (2011) Altered chromatin architecture underlies progressive impairment of the heat shock response in mouse models of Huntington disease. J Clin Invest 121: 3306-3319.

Labbadia J, Novoselov SS, Bett JS, Weiss A, Paganetti P, et al. (2012) Suppression of protein aggregation by chaperone modification of high molecular weight complexes. Brain 135: 1180-1196.

Lalic NM, Maric J, Svetel M, Jotic A, Stefanova E, et al. (2008) Glucose homeostasis in Huntington disease: abnormalities in insulin sensitivity and early-phase insulin secretion. Arch Neurol 65: 476-480.

Lanska DJ, Lavine L, Lanska MJ, Schoenberg BS (1988) Huntington's disease mortality in the United States. Neurology 38: 769-772.

Larsen KE, Fon EA, Hastings TG, Edwards RH, Sulzer D (2002) Methamphetamine-induced degeneration of dopaminergic neurons involves autophagy and upregulation of dopamine synthesis. J Neurosci 22: 8951-8960.

Lau AW, Liu P, Inuzuka H, Gao D (2014) SIRT1 phosphorylation by AMP-activated protein kinase regulates p53 acetylation. Am J Cancer Res 4: 245-255.

Lesort M, Lee M, Tucholski J, Johnson GV (2003) Cystamine inhibits caspase activity. Implications for the treatment of polyglutamine disorders. J Biol Chem 278: 3825-3830.

Levine MS, Klapstein GJ, Koppel A, Gruen E, Cepeda C, et al. (1999) Enhanced sensitivity to N-methyl-D-aspartate receptor activation in transgenic and knockin mouse models of Huntington's disease. J Neurosci Res 58: 515-532.

Li SH, Cheng AL, Zhou H, Lam S, Rao M, et al. (2002) Interaction of Huntington disease protein with transcriptional activator Sp1. Mol Cell Biol 22: 1277-1287.

Li SH, Li XJ (2004) Huntingtin-protein interactions and the pathogenesis of Huntington's disease. Trends Genet 20: 146-154.

Li Z, Chen L, Kabra N, Wang C, Fang J, et al. (2009) Inhibition of SUV39H1 methyltransferase activity by DBC1. J Biol Chem 284: 10361-10366.

Liang Z, Shi T, Ouyang S, Li H, Yu K, et al. (2010) Investigation of the catalytic mechanism of Sir2 enzyme with QM/MM approach: SN1 vs SN2? J Phys Chem B 114: 11927-11933.

Lin CH, Tallaksen-Greene S, Chien WM, Cearley JA, Jackson WS, et al. (2001) Neurological abnormalities in a knock-in mouse model of Huntington's disease. Hum Mol Genet 10: 137-144.

Lione LA, Carter RJ, Hunt MJ, Bates GP, Morton AJ, et al. (1999) Selective discrimination learning impairments in mice expressing the human Huntington's disease mutation. J Neurosci 19: 10428-10437.

Luo J, Nikolaev AY, Imai S, Chen D, Su F, et al. (2001) Negative control of p53 by Sir2alpha promotes cell survival under stress. Cell 107: 137-148.

Luo S, Vacher C, Davies JE, Rubinsztein DC (2005) Cdk5 phosphorylation of huntingtin reduces its cleavage by caspases: implications for mutant huntingtin toxicity. J Cell Biol 169: 647-656.

Luthi-Carter R, Strand A, Peters NL, Solano SM, Hollingsworth ZR, et al. (2000) Decreased expression of striatal signaling genes in a mouse model of Huntington's disease. Hum Mol Genet 9: 1259-1271.

Mangiarini L, Sathasivam K, Seller M, Cozens B, Harper A, et al. (1996) Exon 1 of the HD gene with an expanded CAG repeat is sufficient to cause a progressive neurological phenotype in transgenic mice. Cell 87: 493-506.

Mantamadiotis T, Lemberger T, Bleckmann SC, Kern H, Kretz O, et al. (2002) Disruption of CREB function in brain leads to neurodegeneration. Nat Genet 31: 47-54.

Mao Z, Choo YS, Lesort M (2006) Cystamine and cysteamine prevent 3-NP-induced mitochondrial depolarization of Huntington's disease knock-in striatal cells. Eur J Neurosci 23: 1701-1710.

Markert CD, Kim E, Gifondorwa DJ, Childers MK, Milligan CE (2010) A single-dose resveratrol treatment in a mouse model of amyotrophic lateral sclerosis. J Med Food 13: 1081-1085.

Markianos M, Panas M, Kalfakis N, Vassilopoulos D (2005) Plasma testosterone in male patients with Huntington's disease: relations to severity of illness and dementia. Ann Neurol 57: 520-525.

McKinsey TA, Zhang CL, Olson EN (2000) Activation of the myocyte enhancer factor-2 transcription factor by calcium/calmodulin-dependent protein kinase-stimulated binding of 14-3-3 to histone deacetylase 5. Proc Natl Acad Sci U S A 97: 14400-14405.

Menalled L, El-Khodor BF, Patry M, Suarez-Farinas M, Orenstein SJ, et al. (2009) Systematic behavioral evaluation of Huntington's disease transgenic and knock-in mouse models. Neurobiol Dis 35: 319-336.

Menalled LB, Sison JD, Dragatsis I, Zeitlin S, Chesselet MF (2003) Time course of early motor and neuropathological anomalies in a knock-in mouse model of Huntington's disease with 140 CAG repeats. J Comp Neurol 465: 11-26.

Miller J, Arrasate M, Brooks E, Libeu CP, Legleiter J, et al. (2011) Identifying polyglutamine protein species in situ that best predict neurodegeneration. Nat Chem Biol 7: 925-934.

Milnerwood AJ, Gladding CM, Pouladi MA, Kaufman AM, Hines RM, et al. (2010) Early increase in extrasynaptic NMDA receptor signaling and expression contributes to phenotype onset in Huntington's disease mice. Neuron 65: 178-190.

Mizuno K, Carnahan J, Nawa H (1994) Brain-derived neurotrophic factor promotes differentiation of striatal GABAergic neurons. Dev Biol 165: 243-256.

Modregger J, DiProspero NA, Charles V, Tagle DA, Plomann M (2002) PACSIN 1 interacts with huntingtin and is absent from synaptic varicosities in presymptomatic Huntington's disease brains. Hum Mol Genet 11: 2547-2558.

Moffitt H, McPhail GD, Woodman B, Hobbs C, Bates GP (2009) Formation of polyglutamine inclusions in a wide range of non-CNS tissues in the *Hdh*Q150 knock-in mouse model of Huntington's disease. PLoS One 4: e8025.

Morley JF, Morimoto RI (2004) Regulation of longevity in Caenorhabditis elegans by heat shock factor and molecular chaperones. Mol Biol Cell 15: 657-664.

Morris KC, Lin HW, Thompson JW, Perez-Pinzon MA (2011) Pathways for ischemic cytoprotection: role of sirtuins in caloric restriction, resveratrol, and ischemic preconditioning. J Cereb Blood Flow Metab 31: 1003-1019.

Morton AJ, Edwardson JM (2001) Progressive depletion of complexin II in a transgenic mouse model of Huntington's disease. J Neurochem 76: 166-172.

Mostoslavsky R, Chua KF, Lombard DB, Pang WW, Fischer MR, et al. (2006) Genomic instability and aging-like phenotype in the absence of mammalian SIRT6. Cell 124: 315-329.

Muchowski PJ, Wacker JL (2005) Modulation of neurodegeneration by molecular chaperones. Nat Rev Neurosci 6: 11-22.

Nasir J, Floresco SB, O'Kusky JR, Diewert VM, Richman JM, et al. (1995) Targeted disruption of the Huntington's disease gene results in embryonic lethality and behavioral and morphological changes in heterozygotes. Cell 81: 811-823.

Nasrin N, Kaushik VK, Fortier E, Wall D, Pearson KJ, et al. (2009) JNK1 phosphorylates SIRT1 and promotes its enzymatic activity. PLoS One 4: e8414.

Nicholls DG (2009) Mitochondrial calcium function and dysfunction in the central nervous system. Biochim Biophys Acta 1787: 1416-1424.

Nin V, Escande C, Chini CC, Giri S, Camacho-Pereira J, et al. (2012) Role of deleted in breast cancer 1 (DBC1) protein in SIRT1 deacetylase activation induced by protein kinase A and AMP-activated protein kinase. J Biol Chem 287: 23489-23501.

Nisoli E, Tonello C, Cardile A, Cozzi V, Bracale R, et al. (2005) Calorie restriction promotes mitochondrial biogenesis by inducing the expression of eNOS. Science 310: 314-317.

Novak MJ, Tabrizi SJ (2010) Huntington's disease. BMJ 340: c3109.

Nucifora FC, Jr., Sasaki M, Peters MF, Huang H, Cooper JK, et al. (2001) Interference by huntingtin and atrophin-1 with cbp-mediated transcription leading to cellular toxicity. Science 291: 2423-2428

Ogura M, Nakamura Y, Tanaka D, Zhuang X, Fujita Y, et al. (2010) Overexpression of SIRT5 confirms its involvement in deacetylation and activation of carbamoyl phosphate synthetase 1. Biochem Biophys Res Commun 393: 73-78.

Okawara M, Katsuki H, Kurimoto E, Shibata H, Kume T, et al. (2007) Resveratrol protects dopaminergic neurons in midbrain slice culture from multiple insults. Biochem Pharmacol 73: 550-560.

Omi K, Hachiya NS, Tokunaga K, Kaneko K (2005) siRNA-mediated inhibition of endogenous Huntington disease gene expression induces an aberrant configuration of the ER network in vitro. Biochem Biophys Res Commun 338: 1229-1235.

Orr HT, Zoghbi HY (2007) Trinucleotide repeat disorders. Annu Rev Neurosci 30: 575-621.

Pallos J, Bodai L, Lukacsovich T, Purcell JM, Steffan JS, et al. (2008) Inhibition of specific HDACs and sirtuins suppresses pathogenesis in a Drosophila model of Huntington's disease. Hum Mol Genet 17: 3767-3775.

Pang TY, Stam NC, Nithianantharajah J, Howard ML, Hannan AJ (2006) Differential effects of voluntary physical exercise on behavioral and brain-derived neurotrophic factor expression deficits in Huntington's disease transgenic mice. Neuroscience 141: 569-584.

Panov AV, Gutekunst CA, Leavitt BR, Hayden MR, Burke JR, et al. (2002) Early mitochondrial calcium defects in Huntington's disease are a direct effect of polyglutamines. Nat Neurosci 5: 731-736.

Parker JA, Arango M, Abderrahmane S, Lambert E, Tourette C, et al. (2005) Resveratrol rescues mutant polyglutamine cytotoxicity in nematode and mammalian neurons. Nat Genet 37: 349-350.

Pasinetti GM, Wang J, Marambaud P, Ferruzzi M, Gregor P, et al. (2011) Neuroprotective and metabolic effects of resveratrol: therapeutic implications for Huntington's disease and other neurodegenerative disorders. Exp Neurol 232: 1-6.

Patel NV, Gordon MN, Connor KE, Good RA, Engelman RW, et al. (2005) Caloric restriction attenuates Abeta-deposition in Alzheimer transgenic models. Neurobiol Aging 26: 995-1000.

Persichetti F, Ambrose CM, Ge P, McNeil SM, Srinidhi J, et al. (1995) Normal and expanded Huntington's disease gene alleles produce distinguishable proteins due to translation across the CAG repeat. Mol Med 1: 374-383.

Petersen A, Larsen KE, Behr GG, Romero N, Przedborski S, et al. (2001) Expanded CAG repeats in exon 1 of the Huntington's disease gene stimulate dopamine-mediated striatal neuron autophagy and degeneration. Hum Mol Genet 10: 1243-1254.

Ponugoti B, Kim DH, Xiao Z, Smith Z, Miao J, et al. (2010) SIRT1 deacetylates and inhibits SREBP-1C activity in regulation of hepatic lipid metabolism. J Biol Chem 285: 33959-33970.

Purushotham A, Schug TT, Xu Q, Surapureddi S, Guo X, et al. (2009) Hepatocyte-specific deletion of SIRT1 alters fatty acid metabolism and results in hepatic steatosis and inflammation. Cell Metab 9: 327-338.

Qin W, Yang T, Ho L, Zhao Z, Wang J, et al. (2006) Neuronal SIRT1 activation as a novel mechanism underlying the prevention of Alzheimer disease amyloid neuropathology by calorie restriction. J Biol Chem 281: 21745-21754.

Rajendran R, Garva R, Krstic-Demonacos M, Demonacos C (2011) Sirtuins: molecular traffic lights in the crossroad of oxidative stress, chromatin remodeling, and transcription. J Biomed Biotechnol 2011: 368276.

Raval AP, Dave KR, Perez-Pinzon MA (2006) Resveratrol mimics ischemic preconditioning in the brain. J Cereb Blood Flow Metab 26: 1141-1147.

Ravikumar B, Berger Z, Vacher C, O'Kane CJ, Rubinsztein DC (2006) Rapamycin pre-treatment protects against apoptosis. Hum Mol Genet 15: 1209-1216.

Ravikumar B, Duden R, Rubinsztein DC (2002) Aggregate-prone proteins with polyglutamine and polyalanine expansions are degraded by autophagy. Hum Mol Genet 11: 1107-1117.

Reijonen S, Putkonen N, Norremolle A, Lindholm D, Korhonen L (2008) Inhibition of endoplasmic reticulum stress counteracts neuronal cell death and protein aggregation caused by N-terminal mutant huntingtin proteins. Exp Cell Res 314: 950-960.

Reiner A, Albin RL, Anderson KD, D'Amato CJ, Penney JB, et al. (1988) Differential loss of striatal projection neurons in Huntington disease. Proc Natl Acad Sci U S A 85: 5733-5737.

Richfield EK, Maguire-Zeiss KA, Cox C, Gilmore J, Voorn P (1995) Reduced expression of preproenkephalin in striatal neurons from Huntington's disease patients. Ann Neurol 37: 335-343.

Rigamonti D, Bauer JH, De-Fraja C, Conti L, Sipione S, et al. (2000) Wild-type huntingtin protects from apoptosis upstream of caspase-3. J Neurosci 20: 3705-3713.

Rockabrand E, Slepko N, Pantalone A, Nukala VN, Kazantsev A, et al. (2007) The first 17 amino acids of Huntingtin modulate its sub-cellular localization, aggregation and effects on calcium homeostasis. Hum Mol Genet 16: 61-77.

Rodgers JT, Lerin C, Haas W, Gygi SP, Spiegelman BM, et al. (2005) Nutrient control of glucose homeostasis through a complex of PGC-1alpha and SIRT1. Nature 434: 113-118.

Rosen DR, Siddique T, Patterson D, Figlewicz DA, Sapp P, et al. (1993) Mutations in Cu/Zn superoxide dismutase gene are associated with familial amyotrophic lateral sclerosis. Nature 362: 59-62.

Rubinsztein DC (2006) The roles of intracellular protein-degradation pathways in neurodegeneration. Nature 443: 780-786.

Ruderman NB, Xu XJ, Nelson L, Cacicedo JM, Saha AK, et al. (2010) AMPK and SIRT1: a long-standing partnership? Am J Physiol Endocrinol Metab 298: E751-760.

Ryu H, Lee J, Hagerty SW, Soh BY, McAlpin SE, et al. (2006) ESET/SETDB1 gene expression and histone H3 (K9) trimethylation in Huntington's disease. Proc Natl Acad Sci U S A 103: 19176-19181.

Sanberg PR, Fibiger HC, Mark RF (1981) Body weight and dietary factors in Huntington's disease patients compared with matched controls. Med J Aust 1: 407-409.

Sapp E, Ge P, Aizawa H, Bird E, Penney J, et al. (1995) Evidence for a preferential loss of enkephalin immunoreactivity in the external globus pallidus in low grade Huntington's disease using high resolution image analysis. Neuroscience 64: 397-404.

Sasaki T, Maier B, Koclega KD, Chruszcz M, Gluba W, et al. (2008) Phosphorylation regulates SIRT1 function. PLoS One 3: e4020.

Sathasivam K, Hobbs C, Turmaine M, Mangiarini L, Mahal A, et al. (1999) Formation of polyglutamine inclusions in non-CNS tissue. Hum Mol Genet 8: 813-822.

Sathasivam K, Neueder A, Gipson TA, Landles C, Benjamin AC, et al. (2013) Aberrant splicing of HTT generates the pathogenic exon 1 protein in Huntington disease. Proc Natl Acad Sci U S A 110: 2366-2370.

Sathasivam K, Woodman B, Mahal A, Bertaux F, Wanker EE, et al. (2001) Centrosome disorganization in fibroblast cultures derived from R6/2 Huntington's disease (HD) transgenic mice and HD patients. Hum Mol Genet 10: 2425-2435.

Saudou F, Finkbeiner S, Devys D, Greenberg ME (1998) Huntingtin acts in the nucleus to induce apoptosis but death does not correlate with the formation of intranuclear inclusions. Cell 95: 55-66.

Sauve (2009) Pharmaceuti- cal strategiesforactivatingsirtuins. Curr.Pharm.Des. 15, 45–56.doi: 10.2174/138161209787185797

Schilling B, Gafni J, Torcassi C, Cong X, Row RH, et al. (2006) Huntingtin phosphorylation sites mapped by mass spectrometry. Modulation of cleavage and toxicity. J Biol Chem 281: 23686-23697.

Schilling BK, Stone MH, Utter A, Kearney JT, Johnson M, et al. (2001) Creatine supplementation and health variables: a retrospective study. Med Sci Sports Exerc 33: 183-188.

Schilling G, Becher MW, Sharp AH, Jinnah HA, Duan K, et al. (1999) Intranuclear inclusions and neuritic aggregates in transgenic mice expressing a mutant N-terminal fragment of huntingtin. Hum Mol Genet 8: 397-407.

Schmitt I, Bachner D, Megow D, Henklein P, Hameister H, et al. (1995) Expression of the Huntington disease gene in rodents: cloning the rat homologue and evidence for downregulation in non-neuronal tissues during development. Hum Mol Genet 4: 1173-1182.

Seo H, Sonntag KC, Isacson O (2004) Generalized brain and skin proteasome inhibition in Huntington's disease. Ann Neurol 56: 319-328.

Settembre C, Fraldi A, Jahreiss L, Spampanato C, Venturi C, et al. (2008) A block of autophagy in lysosomal storage disorders. Hum Mol Genet 17: 119-129.

Shimazu T, Horinouchi S, Yoshida M (2007) Multiple histone deacetylases and the CREB-binding protein regulate pre-mRNA 3'-end processing. J Biol Chem 282: 4470-4478.

Shimokawa I, Trindade LS (2010) Dietary restriction and aging in rodents: a current view on its molecular mechanisms. Aging Dis 1: 89-107.

Shindler KS, Ventura E, Dutt M, Elliott P, Fitzgerald DC, et al. (2010) Oral resveratrol reduces neuronal damage in a model of multiple sclerosis. J Neuroophthalmol 30: 328-339.

Shindler KS, Ventura E, Rex TS, Elliott P, Rostami A (2007) SIRT1 activation confers neuroprotection in experimental optic neuritis. Invest Ophthalmol Vis Sci 48: 3602-3609.

Sieradzan KA, Mechan AO, Jones L, Wanker EE, Nukina N, et al. (1999) Huntington's disease intranuclear inclusions contain truncated, ubiquitinated huntingtin protein. Exp Neurol 156: 92-99.

Sittler A, Lurz R, Lueder G, Priller J, Lehrach H, et al. (2001) Geldanamycin activates a heat shock response and inhibits huntingtin aggregation in a cell culture model of Huntington's disease. Hum Mol Genet 10: 1307-1315.

Slow EJ, van Raamsdonk J, Rogers D, Coleman SH, Graham RK, et al. (2003) Selective striatal neuronal loss in a YAC128 mouse model of Huntington disease. Hum Mol Genet 12: 1555-1567.

Smith R, Klein P, Koc-Schmitz Y, Waldvogel HJ, Faull RL, et al. (2007) Loss of SNAP-25 and rabphilin 3a in sensory-motor cortex in Huntington's disease. J Neurochem 103: 115-123.

Spires TL, Grote HE, Varshney NK, Cordery PM, van Dellen A, et al. (2004) Environmental enrichment rescues protein deficits in a mouse model of Huntington's disease, indicating a possible disease mechanism. J Neurosci 24: 2270-2276.

Steffan JS, Agrawal N, Pallos J, Rockabrand E, Trotman LC, et al. (2004) SUMO modification of Huntingtin and Huntington's disease pathology. Science 304: 100-104.

Steffan JS, Bodai L, Pallos J, Poelman M, McCampbell A, et al. (2001) Histone deacetylase inhibitors arrest polyglutamine-dependent neurodegeneration in Drosophila. Nature 413: 739-743.

Steffan JS, Kazantsev A, Spasic-Boskovic O, Greenwald M, Zhu YZ, et al. (2000) The Huntington's disease protein interacts with p53 and CREB-binding protein and represses transcription. Proc Natl Acad Sci U S A 97: 6763-6768.

Strehlow AN, Li JZ, Myers RM (2007) Wild-type huntingtin participates in protein trafficking between the Golgi and the extracellular space. Hum Mol Genet 16: 391-409.

Stunkel W, Peh BK, Tan YC, Nayagam VM, Wang X, et al. (2007) Function of the SIRT1 protein deacetylase in cancer. Biotechnol J 2: 1360-1368.

Sun Y, Savanenin A, Reddy PH, Liu YF (2001) Polyglutamine-expanded huntingtin promotes sensitization of N-methyl-D-aspartate receptors via post-synaptic density 95. J Biol Chem 276: 24713-24718.

Sun Z, Wang HB, Deng YP, Lei WL, Xie JP, et al. (2005) Increased calbindin-D28k immunoreactivity in striatal projection neurons of R6/2 Huntington's disease transgenic mice. Neurobiol Dis 20: 907-917.

Sundararajan R, Chen G, Mukherjee C, White E (2005) Caspase-dependent processing activates the proapoptotic activity of deleted in breast cancer-1 during tumor necrosis factor-alpha-mediated death signaling. Oncogene 24: 4908-4920.

Takano H, Gusella JF (2002) The predominantly HEAT-like motif structure of huntingtin and its association and coincident nuclear entry with dorsal, an NF-kB/Rel/dorsal family transcription factor. BMC Neurosci 3: 15.

Thompson LM, Aiken CT, Kaltenbach LS, Agrawal N, Illes K, et al. (2009) IKK phosphorylates Huntingtin and targets it for degradation by the proteasome and lysosome. J Cell Biol 187: 1083-1099.

Tissenbaum HA, Guarente L (2001) Increased dosage of a sir-2 gene extends lifespan in Caenorhabditis elegans. Nature 410: 227-230.

Trottier Y, Devys D, Imbert G, Saudou F, An I, et al. (1995) Cellular localization of the Huntington's disease protein and discrimination of the normal and mutated form. Nat Genet 10: 104-110.

Valenza M, Carroll JB, Leoni V, Bertram LN, Bjorkhem I, et al. (2007) Cholesterol biosynthesis pathway is disturbed in YAC128 mice and is modulated by huntingtin mutation. Hum Mol Genet 16: 2187-2198.

Valenza M, Cattaneo E (2011) Emerging roles for cholesterol in Huntington's disease. Trends Neurosci 34: 474-486.

Valenza M, Leoni V, Karasinska JM, Petricca L, Fan J, et al. (2010) Cholesterol defect is marked across multiple rodent models of Huntington's disease and is manifest in astrocytes. J Neurosci 30: 10844-10850.

Valenza M, Leoni V, Tarditi A, Mariotti C, Bjorkhem I, et al. (2007) Progressive dysfunction of the cholesterol biosynthesis pathway in the R6/2 mouse model of Huntington's disease. Neurobiol Dis 28: 133-142.

Valenza M, Rigamonti D, Goffredo D, Zuccato C, Fenu S, et al. (2005) Dysfunction of the cholesterol biosynthetic pathway in Huntington's disease. J Neurosci 25: 9932-9939.

Van Raamsdonk JM, Murphy Z, Selva DM, Hamidizadeh R, Pearson J, et al. (2007) Testicular degeneration in Huntington disease. Neurobiol Dis 26: 512-520.

Van Raamsdonk JM, Murphy Z, Slow EJ, Leavitt BR, Hayden MR (2005) Selective degeneration and nuclear localization of mutant huntingtin in the YAC128 mouse model of Huntington disease. Hum Mol Genet 14: 3823-3835.

Van Raamsdonk JM, Pearson J, Slow EJ, Hossain SM, Leavitt BR, et al. (2005) Cognitive dysfunction precedes neuropathology and motor abnormalities in the YAC128 mouse model of Huntington's disease. J Neurosci 25: 4169-4180.

Vaziri H, Dessain SK, Ng Eaton E, Imai SI, Frye RA, et al. (2001) hSIR2(SIRT1) functions as an NAD-dependent p53 deacetylase. Cell 107: 149-159.

Ventimiglia R, Mather PE, Jones BE, Lindsay RM (1995) The neurotrophins BDNF, NT-3 and NT-4/5 promote survival and morphological and biochemical differentiation of striatal neurons in vitro. Eur J Neurosci 7: 213-222.

Verbessem P, Lemiere J, Eijnde BO, Swinnen S, Vanhees L, et al. (2003) Creatine supplementation in Huntington's disease: a placebo-controlled pilot trial. Neurology

Verdin E, Dequiedt F, Kasler HG (2003) Class II histone deacetylases: versatile regulators. Trends Genet 19: 286-293.

Wakeling LA, Ions LJ, Ford D (2009) Could Sirt1-mediated epigenetic effects contribute to the longevity response to dietary restriction and be mimicked by other dietary interventions? Age (Dordr) 31: 327-341.

Walker AK, Yang F, Jiang K, Ji JY, Watts JL, et al. (2010) Conserved role of SIRT1 orthologs in fasting-dependent inhibition of the lipid/cholesterol regulator SREBP. Genes Dev 24: 1403-1417.

Walker, F.O. (2007). Huntington's disease. The Lancet 369, 218-228.

Wang CE, Tydlacka S, Orr AL, Yang SH, Graham RK, et al. (2008) Accumulation of N-terminal mutant huntingtin in mouse and monkey models implicated as a pathogenic mechanism in Huntington's disease. Hum Mol Genet 17: 2738-2751.

Wang J, Ho L, Qin W, Rocher AB, Seror I, et al. (2005) Caloric restriction attenuates beta-amyloid neuropathology in a mouse model of Alzheimer's disease. FASEB J 19: 659-661.

Wang RH, Sengupta K, Li C, Kim HS, Cao L, et al. (2008) Impaired DNA damage response, genome instability, and tumorigenesis in SIRT1 mutant mice. Cancer Cell 14: 312-323.

Wang S, Xing Z, Vosler PS, Yin H, Li W, et al. (2008) Cellular NAD replenishment confers marked neuroprotection against ischemic cell death: role of enhanced DNA repair. Stroke 39: 2587-2595.

Warby SC, Doty CN, Graham RK, Shively J, Singaraja RR, et al. (2009) Phosphorylation of huntingtin reduces the accumulation of its nuclear fragments. Mol Cell Neurosci 40: 121-127.

Warby SC, Visscher H, Collins JA, Doty CN, Carter C, et al. (2011) HTT haplotypes contribute to differences in Huntington disease prevalence between Europe and East Asia. Eur J Hum Genet 19: 561-566.

Wareski P, Vaarmann A, Choubey V, Safiulina D, Liiv J, et al. (2009) PGC-1{alpha} and PGC-1{beta} regulate mitochondrial density in neurons. J Biol Chem 284: 21379-21385.

Westerheide SD, Anckar J, Stevens SM, Jr., Sistonen L, Morimoto RI (2009) Stress-inducible regulation of heat shock factor 1 by the deacetylase SIRT1. Science 323: 1063-1066.

Wheeler VC, Auerbach W, White JK, Srinidhi J, Auerbach A, et al. (1999) Length-dependent gametic CAG repeat instability in the Huntington's disease knock-in mouse. Hum Mol Genet 8: 115-122.

Wheeler VC, White JK, Gutekunst CA, Vrbanac V, Weaver M, et al. (2000) Long glutamine tracts cause nuclear localization of a novel form of huntingtin in medium spiny striatal neurons in HdhQ92 and HdhQ111 knock-in mice. Hum Mol Genet 9: 503-513.

Woodman B, Butler R, Landles C, Lupton MK, Tse J, et al. (2007) The Hdh(Q150/Q150) knock-in mouse model of HD and the R6/2 exon 1 model develop comparable and widespread molecular phenotypes. Brain Res Bull 72: 83-97.

Wyttenbach A, Carmichael J, Swartz J, Furlong RA, Narain Y, et al. (2000) Effects of heat shock, heat shock protein 40 (HDJ-2), and proteasome inhibition on protein aggregation in cellular models of Huntington's disease. Proc Natl Acad Sci U S A 97: 2898-2903.

Yamanaka T, Miyazaki H, Oyama F, Kurosawa M, Washizu C, et al. (2008) Mutant Huntingtin reduces HSP70 expression through the sequestration of NF-Y transcription factor. EMBO J 27: 827-839.

Yanai A, Huang K, Kang R, Singaraja RR, Arstikaitis P, et al. (2006) Palmitoylation of huntingtin by HIP14 is essential for its trafficking and function. Nat Neurosci 9: 824-831.

Yang WM, Tsai SC, Wen YD, Fejer G, Seto E (2002) Functional domains of histone deacetylase-3. J Biol Chem 277: 9447-9454.

Yang XJ, Gregoire S (2005) Class II histone deacetylases: from sequence to function, regulation, and clinical implication. Mol Cell Biol 25: 2873-2884.

Yang XJ, Seto E (2008) The Rpd3/Hda1 family of lysine deacetylases: from bacteria and yeast to mice and men. Nat Rev Mol Cell Biol 9: 206-218.

Yu J, Auwerx J (2010) Protein deacetylation by SIRT1: an emerging key post-translational modification in metabolic regulation. Pharmacol Res 62: 35-41.

Yuan Z, Zhang X, Sengupta N, Lane WS, Seto E (2007) SIRT1 regulates the function of the Nijmegen breakage syndrome protein. Mol Cell 27: 149-162.

Zala D, Colin E, Rangone H, Liot G, Humbert S, et al. (2008) Phosphorylation of mutant huntingtin at S421 restores anterograde and retrograde transport in neurons. Hum Mol Genet 17: 3837-3846.

Zeitlin S, Liu JP, Chapman DL, Papaioannou VE, Efstratiadis A (1995) Increased apoptosis and early embryonic lethality in mice nullizygous for the Huntington's disease gene homologue. Nat Genet 11: 155-163.

Zeron MM, Hansson O, Chen N, Wellington CL, Leavitt BR, et al. (2002) Increased sensitivity to N-methyl-D-aspartate receptor-mediated excitotoxicity in a mouse model of Huntington's disease. Neuron 33: 849-860.

Zhang Y, Gilquin B, Khochbin S, Matthias P (2006) Two catalytic domains are required for protein deacetylation. J Biol Chem 281: 2401-2404.

Zhao W, Kruse JP, Tang Y, Jung SY, Qin J, et al. (2008) Negative regulation of the deacetylase SIRT1 by DBC1. Nature 451: 587-590.

Zschoernig B, Mahlknecht U (2009) Carboxy-terminal phosphorylation of SIRT1 by protein kinase CK2. Biochem Biophys Res Commun 381: 372-377.

Zuccato C, Ciammola A, Rigamonti D, Leavitt BR, Goffredo D, et al. (2001) Loss of huntingtin-mediated BDNF gene transcription in Huntington's disease. Science 293: 493-498.

Zuccato C, Liber D, Ramos C, Tarditi A, Rigamonti D, et al. (2005) Progressive loss of BDNF in a mouse model of Huntington's disease and rescue by BDNF delivery. Pharmacol Res 52: 133-139.

Zuccato C, Valenza M, Cattaneo E (2010) Molecular mechanisms and potential therapeutical targets in Huntington's disease. Physiol Rev 90: 905-981.

Appendix

Appendix 1

Sequence of SIRT1 protein with relative Ser-Pro and Thr-Pro residues detected by the MpM2 antibody.

```
  1 madevalalq aagspsaaaa meaasqpade plrkrprrdg pglgrspgep saavapaaag
 61 ceaasaaapa alwreaagaa asaereapat avagdgdngs glrrepraad dfdddegeee
121 deaaaaaaaa aigyrdnlll tdglltngfh scesddddrt shasssdwtp rprigpytfv
181 qqhlmigtdp rtilkdllpe tipppelddm tlwqivinil seppkrkkrk dintiedavk
241 llqeckkiiv ltgagvsvsc gipdfrsrdg iyarlavdfp dlpdpqamfd ieyfrkdprp
301 ffkfakeiyp gqfqpslchk fialsdkegk llrnytqnid tleqvagiqr ilqchgsfat
361 asclickykv dceavrgdif nqvvprcprc padeplaimk peivffgenl peqfhramky
421 dkdevdlliv igsslkvrpv alipssiphe vpqilinrep lphlhfdvel lgdcdviine
481 lchrlggeya klccnpvkls eitekpprpq kelvhlselp ptplhiseds sspertvpqd
541 ssviatlvdq atnnnvndle vsesscveek pqevqtsrnv eninvenpdf kavgsstadk
601 nertsvaetv rkcwpnrlak eqiskrlegn qylfvppnry ifhgaevysd seddvlssss
661 cgsnsdsgtc qspsleeple deseieefyn gleddterpe caggsgfgad ggdqevvnea
721 iatrqeltdv nypsdks
```